ADA 038266

IN-MISSILE CALCULATIONS OF SILICON DOSE-A COMPARISON WITH EXPERIMENT

Science Applications, Inc.

P.O. Box 2351

La Jolla, California 92038

September 1975

Final Report for Period 4 June 1973—30 August 1975

CONTRACT No. DNA 001-73-C-0258

Prepared for

Director

DEFENSE NUCLEAR AGENCY

Washington, D. C. 20305

DDC

APR 12 1977

A

Final rept. 4 Jun 73 — 30 Aug 75,

REPORT DOCUMENTATION PAGE		READ INSTRUCTIONS BEFORE COMPLETING FORM
1. REPORT NUMBER DNA 3830F	2. GOVT ACCESSION NO.	3. RECIPIENT'S CATALOG NUMBER
4. TITLE (and Subtitle) IN-MISSILE CALCULATIONS OF SILICON DOSE—A COMPARISON WITH EXPERIMENT.		5. TYPE OF REPORT & PERIOD COVERED Final Report for Period 4 Jun 73—30 Aug 75
		6. PERFORMING ORG. REPORT NUMBER SAI-75-639-LJ
7. AUTHOR(s) William H. Scott, Jr., Dean C. Kaul Phil A. Read, Ron E. Dietz		8. CONTRACT OR GRANT NUMBER(s) DNA 001-73-C-0258
9. PERFORMING ORGANIZATION NAME AND ADDRESS Science Applications, Inc. P.O. Box 2351 La Jolla, California 92038		10. PROGRAM ELEMENT, PROJECT, TASK AREA & WORK UNIT NUMBERS NWED Subtask W99QAXPE083-08
11. CONTROLLING OFFICE NAME AND ADDRESS Director Defense Nuclear Agency Washington, D.C. 20305		12. REPORT DATE September 1975
		13. NUMBER OF PAGES 108
14. MONITORING AGENCY NAME & ADDRESS(if different from Controlling Office)		15. SECURITY CLASS. (of this report) UNCLASSIFIED
		15a. DECLASSIFICATION/DOWNGRADING SCHEDULE

16. DISTRIBUTION STATEMENT (of this Report)

Approved for public release; distribution unlimited.

17. DISTRIBUTION STATEMENT (of the abstract entered in Block 20, if different from Report)

18. SUPPLEMENTARY NOTES

This work sponsored by the Defense Nuclear Agency under Subtask W99QAXPE083-08.

19. KEY WORDS (Continue on reverse side if necessary and identify by block number)

Adjoint Monte Carlo	Neutrons and Gamma Rays	Measurement
In-Missile Dose	Combinatorial Geometry	Complex Geometry
Silicon Dose	MORSE	Multigroup Cross Sections

20. ABSTRACT (Continue on reverse side if necessary and identify by block number)

Adjoint Monte Carlo calculations of the neutron induced silicon dose rate measured in the guidance section of a Sprint missile are presented. The Sprint in-missile measurements and a similar measurement inside a simple steel-styrofoam sample were performed by the Intelcom Radiation Technology Corporation. Forward and adjoint Monte Carlo calculations were performed of the time dependent dose rate in the steel-styrofoam sample giving a time dependent benchmark comparison → next page

DD FORM 1 JAN 73 1473   EDITION OF 1 NOV 65 IS OBSOLETE

388862

cont.

20. ABSTRACT (Continued)

of two calculations and an experiment. A complete description of the three dimensional complex Sprint missile radiation transport model is given. Adjoint Monte Carlo calculations of the Sprint in-missile measurements show that neutron induced doses are accurately calculated for all neutron energies except from 1 to .1 MeV where the contribution to the total dose is negligible. Thus the comparison of calculation and experiment demonstrates that neutron induced missile doses are accurately calculated. Further, there is evidence that neutron radiation response functions can be calculated with simpler geometry models which should reduce their cost in the future.

SUMMARY

Adjoint Monte Carlo calculations of the neutron induced silicon dose rate measured in the guidance section of a Sprint missile are presented. The Sprint in-missile measurements and a similar measurement inside a simple steel-styrofoam sample were performed by the Intelcom Radiation Technology Corporation. Forward and adjoint Monte Carlo calculations were performed of the time dependent dose rate in the steel-styrofoam sample giving a time dependent benchmark comparison of two calculations and an experiment. A complete description of the three dimensional complex Sprint missile radiation transport model is given. Adjoint Monte Carlo calculations of the Sprint in-missile measurements show that neutron induced doses are accurately calculated for all neutron energies except from 1 to .1 MeV where the contribution to the total dose is negligible. Thus the comparison of calculation and experiment demonstrates that neutron induced missile doses are accurately calculated. Further, there is evidence that neutron radiation response functions can be calculated with simpler geometry models which should reduce their cost in the future.

1

TABLE OF CONTENTS

2

LIST OF ILLUSTRATIONS

LIST OF TABLES

1. INTRODUCTION

Through the decade of the sixties, computation of radiation environments from nuclear weapons was limited by computer technology and the paucity of basic data in the form of reaction cross sections. These limitations resulted in high degrees of uncertainty, i.e. factors of 3 and more, in the results of all radiation transport calculations, including those for weapons radiation output and subsequent transport. In fact confidence in calculated weapons output was so low that experimentally determined values were preferred as sources in weapons radiation environment problems, while in the case of radiation transport in the atmosphere gross experiments such as HENRE[1-3] were attempted in order to gain confidence in the then state-of-the-art of transport technology. The lack of success in instilling confidence in results was due not only to limitations in calculational capabilities but also to the ambitious nature of these experiments, which, when combined with the then state-of-the-art in experimental technique, produced measured results which were difficult to reproduce or interpret in the context of radiation transport calculations. The rather large uncertainties in radiation environments led the Defense Nuclear Agency (DNA) to support two major technology programs, one to improve the calculation of weapon radiation output and the other to improve radiation transport in the environment, with special emphasis on transport in the atmosphere.

By 1971 these programs had made considerable progress, reducing the uncertainties in particular calculated values such as integrated dose, to on the order of a factor of two.[4] Also at this time the United States was heavily involved in the design and deployment of an anti-ballistic

missile (ABM) system. The Safeguard ABM system consisted of two missiles, Spartan, an exoatmospheric interceptor, and Sprint, which intercepted reentry vehicles which had penetrated the atmosphere.

Given the mission of the latter it was possible to conceive of the deployment of several such systems in close proximity in time and space, with the resulting possibility of mutual destruction or as it is termed, fratricide. This scenario gave rise to an analytical problem in which the source, intervening media and target were all known more or less exactly. Therefore, the only uncertainties in analyzing the response of one Sprint missile to the nearby detonation of another lay in the accuracy to which each radiation component could be calculated and the effect of each component on the target vehicle.

Based on related studies, SAI suggested to DNA that neutron interactions within the target missile could conceivably produce gamma radiation which was of the same order of intensity as the gamma environment impinging on the missile. Because of improvements in source definition and radiation transport prediction capabilities resulting from the DNA programs, it was both feasible and desirable to calculate this (n, missile γ) component. Further, SAI proposed that the n, γ calculations be made in the adjoint mode to produce a missile radiation response data base which could be used to generate internal doses from any incident neutron or gamma ray source. The data base would also generate internal doses based on any response function.

This effort was supported by DNA and led to results[5] which were of great interest to the designers of the Sprint system, particularly because for the first time precise definitions of the internal radiation environment had been determined. This new interest led to a reassessment of the response of various key missile components to the newly

8

calculated radiation environments. In 1973 at a meeting of the Basic Mechanisms Panel of the Transient Effects on Electronic Systems (TREES) Working Group, several programs to study various aspects of the response of missile components to the new environments were proposed. Because of the expense of these programs and because of the past shortcomings of radiation transport calculations, the panel members were skeptical of both the new radiation environments and the proposed studies. A particular aspect of concern was the adequacy of the cross sections and geometric representation of the Sprint which were used in the radiation transport calculations.

As a result of this concern a program to verify techniques of calculating the in-missile radiation environment was developed. This program consisted of experimental measurements of a section of a Sprint missile and an analytical program to calculate the measured data. Four groups were involved in the program. Martin Marietta, the developer and manufacturer of the Sprint supplied a detailed description of the Sprint missile section including blueprints, parts lists and elemental compositions. Intelcom Radiation Technology Corporation performed the LINAC radiation experiments which were calculated by Science Applications, Inc. and Oak Ridge National Laboratory.

The entire program was formulated as a single coordinated effort with each phase planned jointly by both experimenters and analysts. In this way it was hoped that the program goal could be accomplished within the state-of-the-art constraints of both experimental and analytical capabilities. A major problem with the analysis of past experiments had been in the definition of detector response as a function of radiation type and energy and, perhaps more important, the communication of this

information to the analyst. This was seen as a particularly difficult problem for this project since space limitations dictated the fabrication of an entirely new detector for the experimental task. As a result of these considerations a preliminary experiment was designed which subjected the detector to an environment similar to that which it might see in the missile but in a very simplified geometry. This was intended to give analysts an opportunity to refine their representation of the detector in the absence of other complicating factors.

It was also felt that, aside from uncertainties in the cross section information to be used, the greatest source of calculational error would probably be inaccurate geometric representation of the complex components of the missile system. To ensure maximum reliability of that computational model another preliminary experiment was planned. In this one, the detectors were placed in the missile which was then exposed to a Cs-137 photon source. This was intended to give analysts an opportunity to check their model with a relatively simple photon only transport problem utilizing cross sections more certain and far less complex than is the case for neutrons.

Detector placement and missile orientation in the final experiment were based on the internal radiation environments of the previous SAI calculations. Detectors were placed in the missile guidance set (MGS) and the autopilot, and the missile and detectors were exposed to neutrons from the IRT Linac facility in a side-on and nearly head-on configuration. In addition, to obtain information on low energy as well as high energy neutrons, the missile was exposed at two flight path stations, 17.59 meters for the low energy neutron flux and 53.09 meters for the high energy neutron flux. Budget considerations dictated that the final

10

analyses of the experiments be accomplished by one organization only. Therefore, SAI analyzed both the preliminary experiments and the final experiments while ORNL calculated only the preliminary experiment. The results of the SAI analysis are presented in the following sections.

The quality of both the experimental and calculational results of this project cannot be fully appreciated without a knowledge of the dramatic change in the state-of-the-art of predicting radiation environments occurring over the decade from 1965 - 1975. For more detailed discussions of previous experimental attempts to determine radiation environments a review of the literature is required. For example during the 1960's two projects, Bare Reactor Experiment-Nevada (BREN) and High Energy Neutron Reactions Experiment (HENRE) were designed to obtain dose versus range for various source heights. The reactor (BREN) and accelerator (HENRE) were placed on a tower in Nevada and various measurements were made on the ground and in the air by suspending detectors from helicopters. Also other experiments were designed by Gulf General Atomic to verify the time dependent radiation transport in concrete[6-8] and by Lawrence Livermore Laboratory to verify cross sections (pulsed sphere experiments[9]). Finally it should be noted that the techniques reported here are the result of the use of what is now off-the-shelf technology and not merely that of a special effort designed to solve a single problem. Thus, these results are an indication of the degree of excellence which the state-of-the-art of radiation transport prediction has attained.

2. STEEL-STYROFOAM DESIGN EFFORT

Because of the geometrical complexities of the Sprint missile, it was decided early in the program that a simpler geometry should also be measured and calculated. This "simple" experiment would allow the experimeters and calculaters to compare some results not clouded by geometry or cross section complexities. In order for the simple experiment to be a useful comparison, it had to meet several criteria. First its total and time dependent response should be as much like the Sprint missile as possible. Second its geometry should be well defined and its cross sections well known. Third calculation or measurement of the simple experiment should not present any additional difficulties not expected in the Sprint experiment. The fourth and final criteria was that the sample be constructed at a reasonable cost.

With these guidelines in mind, SAI was given the task of designing the simple experiment. Initially a sphere design was considered as the simplest possible geometry. Previous adjoint Monte Carlo calculations by SAI of the Sprint missile response function were folded with a point silicon flux-to-dose response for neutrons and gamma rays to approximate the response of the silicon surface barrier detector inside the missile. The units of this missile response are rads(Si)/(incident neutron/cm^2). Thus a neutron flux on the missile surface is converted to dose in silicon which includes all radiation transport effects such as neutron attenuation, inelastic and capture gamma-ray production, and neutron and gamma-ray scattering.

In order to design the one-dimensional spherical model of the Sprint, an initial geometry was selected similar in size, density and composition to the Sprint Autopilot section. Starting with this initial configuration, adjoint Monte Carlo calculations with the MORSE code[11, 12] of the silicon dose of several similar sphere configurations were compared with the desired missile response. The initial geometry configuration was composed of H, C, Al and Fe so that the number of atoms of each matched the number of similar elements in the combinatorial geometry model of the Autopilot section. The Autopilot section was found to have a volume of $1.04 \times 10^4 cm^3$ excluding voids and containing the following number of atom types:

H	1.640(+26)
C	2.041(+26)
Al ($11 \leq z \leq 20$)	1.090(+26)
Fe ($z > 20$)	.534(+26)

In order to use polystyrene C_1H_1 as the source of hydrogen and carbon, the excess carbon was included as aluminum so that the assumed number of atoms were

CH	1.640(+26)
Al	1.490(+26)
Fe	.534(+26)

From the total volume of 1.04(+4) cm^3, the number of atoms and assuming natural densities for Al and Fe, radii for the Fe, Al and CH and the CH density were calculated as

	r(cm)	ρ (gm/cm^3)
CH	12.04	.484
Fe	12.38	7.86
Al	13.54	2.7

Adjoint Monte Carlo calculations of the silicon response to this and other similar spheres were performed with the Monte Carlo code MORSE. During these preliminary calculations, possible estimators for the final Sprint calculations were investigated. For the one dimensional sphere, the most efficient estimator was boundary crossing on the outer surface. However a next flight estimator to an infinite monodirectional beam worked almost as well as the boundary crossing estimator, and thus was selected for the three dimensional Sprint calculations. The form of the adjoint next flight estimator to the monodirectional beam is

$$\text{score} = W \sum_j P_{ij} f_{ij} (\vec{\Omega} \cdot \vec{\Omega}') e^{-\tau_j}$$

where scoring is performed before each collision and source generation where

W = the particle weight

$\vec{\Omega} \cdot \vec{\Omega}'$ = the scattering cosine to the beam direction

P_{ij} = the downscatter probability but is not normalized as it includes effects of absorption or secondary generation

f_{ij} = the normalized scattering angular distribution, and

τ_j = the mean free paths to the outside surface.

This equation is like a flux-at-a-point estimator without the $1/4\pi R^2$ factor.

A forward calculation with next flight estimation to the sphere center was also performed. The results agreed with the adjoint calculations but because of the infinite variance nature of the estimator, the statistics were poorer. Thus at this time it appeared that the adjoint calculation with next

14

flight estimation to neutron beam would be the most efficient technique for the final Sprint experiment calculations.

The first adjoint calculations of the initial sphere showed that thermal neutron buildup in the CH sphere was greater than similar calculations of the Sprint Autopilot, most likely because the materials are more homogeneous in the Sprint. However reducing the density of the CH to .34 gm/cc or .01575 atoms/barn-cm each of H and C and changing the CH radius to 12.4 cm gave a similar number of scatterings as the Sprint Autopilot calculations. Even so with this new geometry, buildup caused enough statistical fluctuation that calculations of less than one minute of the CDC 7600 were not adequate to optimize the design of the outer metal shell.

In order to optimize the design calculations of the outer material, a simple correlated sampling version MORSE was developed so that several thicknesses of the outer material could be investigated with the same random walks. Several particle weights were kept for each history, each weight corresponding to a different thickness of the outer material, and the outer material was modeled as several concentric spheres. Whenever a history crossed one of these spheres in an outward direction, the corresponding weight was scored in a leakage estimator and then that weight was set to zero so that if the same history later recrossed the same surface it would score zero. This simple correlated sampling trick allowed several outer-layer thicknesses to be investigated on a single calculation, and because they used the same random histories the results were correlated. This means that differences between thicknesses are not related to the absolute uncertainties in the Monte Carlo results and thus are a better measure of the effect of the additional thickness than would be obtained by several independent calculations.

Outer materials that were investigated were Al, Fe, and Cu. It was found that all three compared adequately with the Sprint response for high energy neutrons, but at energies below 500 keV both Al and Fe were much lower than the desired response. Table 1 compares the responses of Al, Cu, and Fe at three radii to the desired response. Apparently the missile response at low energies is high because of the large eV capture resonance in tantalum which is located close to the calculation point in the missile. Copper has a similar resonance at 229 eV, although not as strong as tantalum, and thus the 2.1 cm thickness of copper gives the response closest to the desired response. However at an early meeting of experimenters and calculators, it was decided to construct the experiment with iron instead of copper because the energy spectra of the epithermal capture gamma rays are better known for iron. Also copper activation posed possible experimental difficulties. Dr. Larry Harris of IRT also requested that the sample be rectangular or cylindrical rather than spherical to facilitate fabrication.

At this point several steel-styrofoam configurations were calculated to find an easily fabricated design that would not have any calculation or experimental difficulties. Each of these calculations had approximately the same volume, iron mass and CH mass, the main differences being geometry. Rather than documenting each of these calculations separately, they are listed in Table 2 along with the reason for the calculation and a brief conclusion. Because these geometries did not have spherical symmetry, the leakage estimator used in the previous correlated sampling sphere calculations was no longer valid. Each of these calculations used the adjoint next flight estimator to the parallel beam which was briefly discussed earlier in this chapter. When a next flight estimator is used to compute

TABLE 1. COMPARISONS OF 1-D MODEL RESPONSES WITH THREE OUTER MATERIALS AND THREE THICKNESSES. INNER MATERIAL IS 12.4 CM of CH OF DENSITY 0.340 GM/CC. RECOMMENDED OUTER MATERIALS ARE CU 2.1 CM OR FE 1.6 CM IN THAT ORDER

Group	E_{max}	Desired Response	Cu			Fe			Al		
			1.1 cm	1.6 cm	2.1 cm	1.1 cm	1.6 cm	2.1 cm	1.1 cm	1.6 cm	2.1 cm
35	17.00 MeV	8.51(-10)	7.14(-10)	6.98(-10)	6.81(-10)	8.75(-10)	9.04(-10)	9.32(-10)	7.53	7.43	7.35
34	15.00	9.10	9.51	9.78	10.00	9.44	9.79	10.30	8.67	8.01	7.85
33	13.50	9.55	10.20	10.50	10.00	10.50	10.80	11.00	6.59	6.48	8.41
32	11.05	9.77	10.50	10.70	10.70	10.80	11.10	11.20	9.44	9.38	9.31
31	9.05	7.76	8.33	8.44	8.36	8.12	8.37	8.58	7.44	7.40	7.36
30	7.00	4.02	4.41	4.66	5.04	4.40	4.95	5.31	3.15	3.19	3.17
29	5.49	2.24	2.01	2.40	2.67	2.08	2.43	2.73	0.90	0.93	0.89
28	4.07	1.46	1.43	1.70	1.88	1.11	1.37	1.56	0.51	0.49	0.49
27	3.01	1.20	1.03	1.30	1.46	1.07	1.28	1.37	0.38	0.40	0.39
26	2.47	1.13	0.96	1.15	1.23	0.79	1.05	1.21	0.37	0.37	0.35
25	2.35	1.06	0.83	0.98	1.10	0.64	0.81	0.93	0.32	0.32	0.32
24	1.83	0.69	0.53	0.64	0.78	0.59	0.80	0.93	0.26	0.27	0.29
23	1.10	0.94	0.43	0.56	0.68	0.45	0.56	0.66	0.15	0.16	0.16
22	550.20 keV	1.24	0.56	0.71	0.84	0.40	0.51	0.62	0.16	0.16	0.17
21	111.10	1.90	0.60	0.76	0.87	0.47	0.56	0.58	0.19	0.20	0.22
20	19.30	2.65	0.75	0.84	0.94	0.63	0.72	0.73	0.25	0.25	0.26
19	3.36	3.25	1.10	1.25	1.28	0.71	0.72	0.75	0.36	0.35	0.36
18	582.90 eV	3.54	1.75	2.06	2.24	0.81	0.91	0.89	0.38	0.39	0.39
17	101.30	4.12	1.13	1.23	1.36	0.91	1.02	1.02	0.41	0.40	0.35
16	22.00	3.96	1.38	1.60	1.65	1.13	1.18	1.16	0.60	0.60	0.59
15	3.93	3.33	1.76	1.92	2.01	1.43	1.51	1.57	0.65	0.63	0.60
14	0.87	3.34	2.30	2.39	2.52	1.64	1.71	1.78	0.64	0.63	0.57
13	0.41	2.32	3.43	3.74	3.77	1.74	1.82	1.87	0.51	0.48	0.47

TABLE 2. STEEL-STYROFOAM DESIGN CALCULATIONS

Calculation	Description	Reason	Conclusion
1	Fe, Al, CH sphere. Replaced some Fe with Al	To see if the response was closer to the desired response than Fe alone	Response was lower than the Fe only sphere which was already low
2	Rectangular Fe box surrounding the CH, broad beam	This configuration should be the easiest to fabricate.	Response was similar to the Fe sphere
3	Same box, 22 cm incident beam diameter	To see if the beam missing the corners would have any effect	Response from neutrons below .1 MeV was 40% of 2 indicating that the beam edges cause significant effects
4	Waffer design (see Fig. 1)	Is the Fe on the sides necessary?	Results were much lower than Fe sphere. Fe or sides is important.
5	Double waffer design (see Fig. 2)	Will moving Fe closer to the detector improve the response?	No significant improvement from 4.
6	20.32 cm diameter Fe cylinder	Will fit entirely inside beam yet similar to the sphere	Response is same as the sphere. This became the cylinder standard.

18

TABLE 2. STEEL-STYROFOAM DESIGN CALCULATIONS (Cont'd.)

Calculation	Description	Reason	Conclusion
7	20.32 cylinder in a 19.5 diameter beam	Test the importance of the beam fringes for the cy-linder	Similar to 6 except 50% from .5 MeV to 3 keV
8	Same cylinder in a beam originating at a point 16 meters away	Test if beam divergence could be important	No difference from cy-linder standard
9	Cylinder with thicker edges	One last attempt to in-crease the response	Not significantly different from 6

CYLINDRICAL CROSS SECTION
(Dimensions in cm)
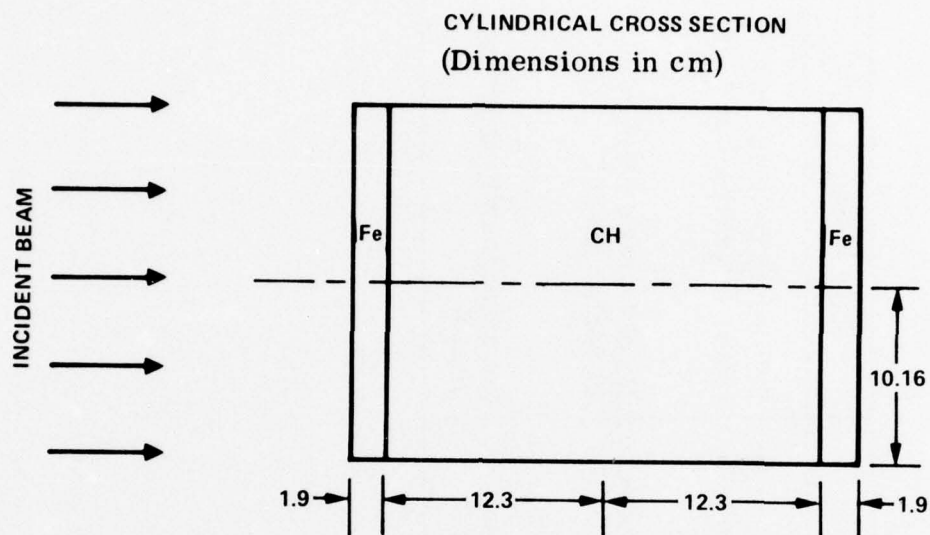
Figure 1. Wafer Design for Steel Styrofoam Sample
(Calculation 4 on Table 2)
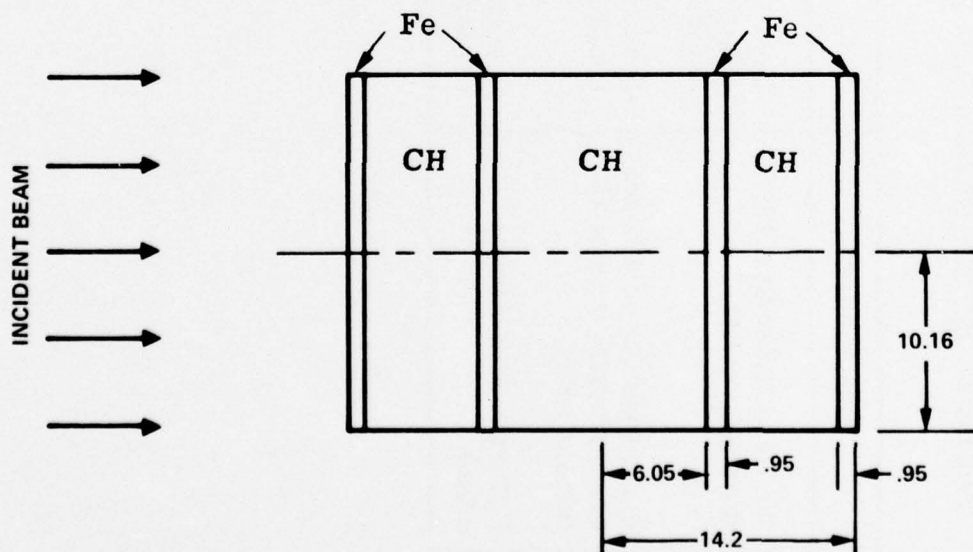
Figure 2. Double Wafer Design for Steel Styrofoam
Sample (Calculation 5 on Table 2)

20

the flux at a point in a forward calculation, an infinite variance condition often arises because of the $(1/4\pi r^2)$ factor in the score when particles scatter near the point, causing large variances that are not readily reduced by calculating more histories. This problem does not arise with the adjoint next flight estimator to a beam because the estimation to a beam has no $(1/4\pi r^2)$ factor and no scatterings near an estimation point.

From Table 2 the important features governing the design of the cylinder experiment can be seen. From 1, 2, and 6 compared with 4 and 5 it is important that the steel entirely surround the styrofoam in order to maximize leakage. Low energy neutrons are thermalizing in the CH and then being captured in the Fe with the detector seeing the capture gamma rays. To maximize the dose from low energy neutrons, they must not be able to leak out of the CH without entering the Fe. This is the reason that the waffer designs of 4 and 5 (Figs. 1 and 2) give such a low response. The box (calculation 2) gave good results and would be easiest to fabricate, but calculation 3 showed that the beam fringes acting on the corners would have significant effects. Because the beam edges cannot be exactly determined, the cylinder design was adopted to fit the entire sample into the beam. Even so, calculation 7 showed that .8 cm difference in the beam diameter could have 50% effects on the response to neutrons from .5 MeV to 3 keV. For this reason care was taken to assure that the entire steel cylinder fit safely into the beam. Calculation 8 showed no effects of the incident beam striking the cylinder walls at a small angle and calculation 9 showed that the steel thickness chosen by correlated sampling of the sphere sample was still correct for the cylinder.

The dimensions of the cylinder used in the above calculation were constrained so that (1) the total volume would be the same as the previous

correlated sphere calculation, (2) the cylinder diameter was 20.32 cm, and (3) the iron thickness was 1.6 cm. These constraints gave the cylinder a length of 35.44 cm. For final construction at Intelcom the length was reduced to the diameter to make a more regular sample. Figure 3 shows the final dimensions of the steel styrofoam cylinder constructed by Intelcom and used in their experiment.[10] The cylinder and end plates were made of slightly different steels.

(Dimensions in cm)
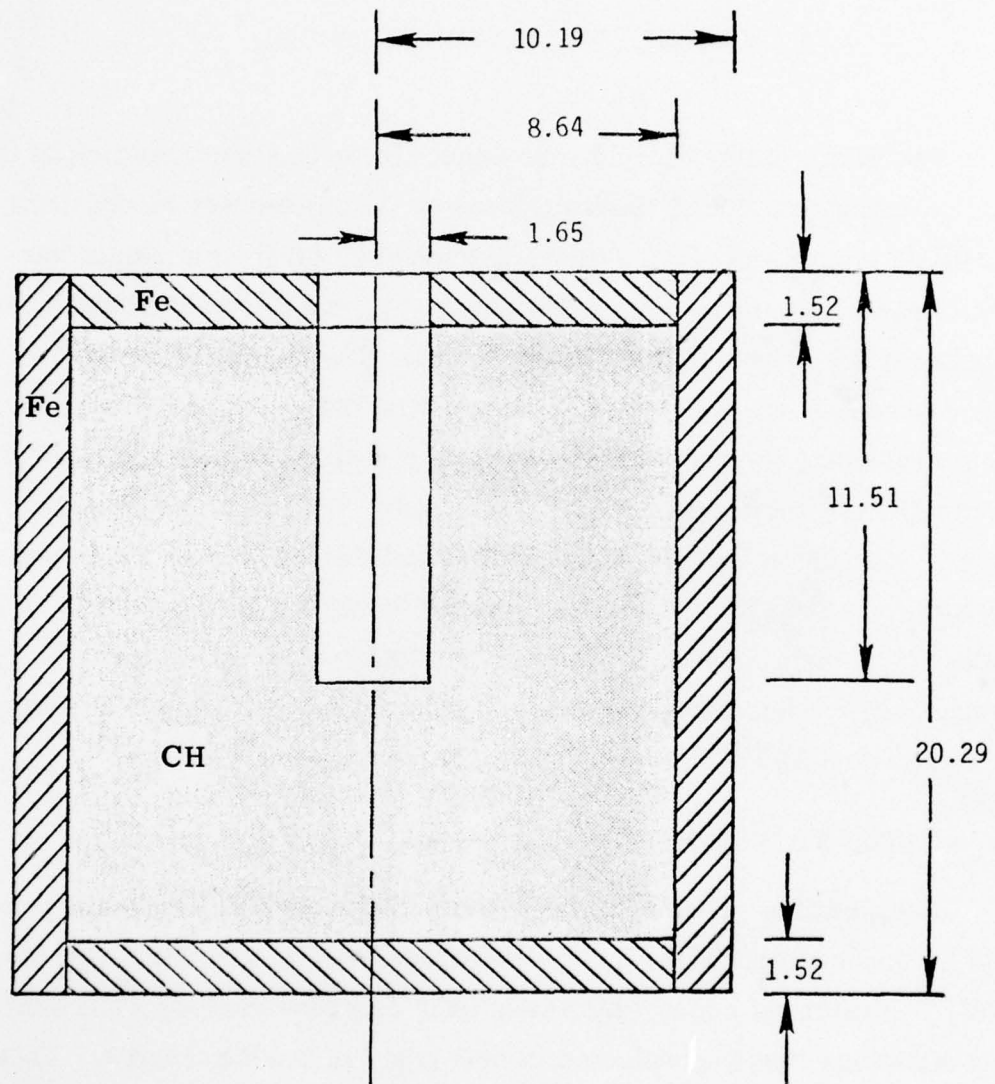
Figure 3. Sectional View of the Steel Styrofoam
Sample (Furnished by IRT)

3. RADIATION TRANSPORT MODEL

The heart of any three dimensional Monte Carlo calculation is the radiation transport model which consists of (1) a geometry model depicting the missile components to the desired accuracy, (2) the elemental densities of each region modeled in the geometry, and (3) the physical cross sections for the elements used in the model. The first section of this chapter presents our sources of cross section data, and describes our efforts necessary to process this data into a multigroup library compatible with the MORSE multigroup Monte Carlo code. The next two sections document both the steel-styrofoam model and the Sprint missile model respectively. Data for the steel-styrofoam sample was supplied by IRT and the Sprint was modeled from data supplied by Martin-Marietta Corp. The final section describes the neutron source and the dosimeter response which were supplied by IRT.

3.1 CROSS SECTIONS

Coupled fine group neutron-gamma cross section sets were produced by processing ENDF/B and DNA cross section libraries with the AMPX[13] system of codes which is briefly described below. The fine group structure that was selected is described in Tables 3 and 4. These in turn were collapsed into broad groups using the code COLIXS and weighting functions produced by XSDRNPM--a module of AMPX. The broad group structure is presented in Table 5 along with the dosimeter response. The elements listed in Table 6 have been processed and are available in both the fine and the broad group structure.

24

TABLE 3. NEUTRON FINE GROUP STRUCTURE

Group	Energy Range	Lethargy Range
1	1.5000E+07 - 1.7000E+07	-.531 - -.405
2	1.3500E+07 - 1.5000E+07	-.405 - -.300
3	1.2210E+07 - 1.3500E+07	-.300 - -.200
4	1.1050E+07 - 1.2210E+07	-.200 - -.100
5	1.0000E+07 - 1.1050E+07	-.100 - 0.
6	9.0480E+06 - 1.0000E+07	0. - .100
7	8.1870E+06 - 9.0480E+06	.100 - .200
8	7.4080E+06 - 8.1870E+06	.200 - .300
9	7.0000E+06 - 7.4080E+06	.300 - .357
10	6.7030E+06 - 7.0000E+06	.357 - .400
11	6.3600E+06 - 6.7030E+06	.400 - .453
12	6.0650E+06 - 6.3600E+06	.453 - .500
13	5.4880E+06 - 6.0650E+06	.500 - .600
14	4.9660E+06 - 5.4880E+06	.600 - .700
15	4.7500E+06 - 4.9660E+06	.700 - .744
16	4.4930E+06 - 4.7500E+06	.744 - .800
17	4.0660E+06 - 4.4930E+06	.800 - .900
18	3.6790E+06 - 4.0660E+06	.900 - 1.000
19	3.3290E+06 - 3.6790E+06	1.000 - 1.100
20	3.0120E+06 - 3.3290E+06	1.100 - 1.200
21	2.7250E+06 - 3.0120E+06	1.200 - 1.300
22	2.4660E+06 - 2.7250E+06	1.300 - 1.400
23	2.4100E+06 - 2.4660E+06	1.400 - 1.423
24	2.3000E+06 - 2.4100E+06	1.423 - 1.470
25	2.2310E+06 - 2.3000E+06	1.470 - 1.500
26	2.0190E+06 - 2.2310E+06	1.500 - 1.600
27	1.8270E+06 - 2.0190E+06	1.600 - 1.700
28	1.6530E+06 - 1.8270E+06	1.700 - 1.800
29	1.4960E+06 - 1.6530E+06	1.800 - 1.900
30	1.3530E+06 - 1.4960E+06	1.900 - 2.000
31	1.2250E+06 - 1.3530E+06	2.000 - 2.100
32	1.1080E+06 - 1.2250E+06	2.100 - 2.200
33	1.0030E+06 - 1.1080E+06	2.200 - 2.300
34	9.0720E+05 - 1.0030E+06	2.300 - 2.400
35	8.2080E+05 - 9.0720E+05	2.400 - 2.500
36	7.4270E+05 - 8.2080E+05	2.500 - 2.600
37	6.7210E+05 - 7.4270E+05	2.600 - 2.700
38	6.0810E+05 - 6.7210E+05	2.700 - 2.800
39	5.5020E+05 - 6.0810E+05	2.800 - 2.900
40	4.9790E+05 - 5.5020E+05	2.900 - 3.000
41	4.5050E+05 - 4.9790E+05	3.000 - 3.100
42	4.0760E+05 - 4.5050E+05	3.100 - 3.200
43	3.6880E+05 - 4.0760E+05	3.200 - 3.300
44	3.3370E+05 - 3.6880E+05	3.300 - 3.400
45	3.0200E+05 - 3.3370E+05	3.400 - 3.500
46	2.7320E+05 - 3.0200E+05	3.500 - 3.600
47	2.4720E+05 - 2.7320E+05	3.600 - 3.700
48	2.2370E+05 - 2.4720E+05	3.700 - 3.800
49	2.0240E+05 - 2.2370E+05	3.800 - 3.900
50	1.8320E+05 - 2.0240E+05	3.900 - 4.000
51	1.6570E+05 - 1.8320E+05	4.000 - 4.100
52	1.5000E+05 - 1.6570E+05	4.100 - 4.200
53	1.3570E+05 - 1.5000E+05	4.200 - 4.300

TABLE 3. (Cont'd.)

Group	Energy Range	Lethargy Range
54	1.2280E+05 - 1.3570E+05	4.300 - 4.400
55	1.1110E+05 - 1.2280E+05	4.400 - 4.500
56	8.6520E+04 - 1.1110E+05	4.500 - 4.750
57	6.7380E+04 - 8.6520E+04	4.750 - 5.000
58	5.2480E+04 - 6.7380E+04	5.000 - 5.250
59	4.0870E+04 - 5.2480E+04	5.250 - 5.500
60	3.1830E+04 - 4.0870E+04	5.500 - 5.750
61	2.4790E+04 - 3.1830E+04	5.750 - 6.000
62	1.9300E+04 - 2.4790E+04	6.000 - 6.250
63	1.5030E+04 - 1.9300E+04	6.250 - 6.500
64	1.1710E+04 - 1.5030E+04	6.500 - 6.750
65	9.1190E+03 - 1.1710E+04	6.750 - 7.000
66	7.1020E+03 - 9.1190E+03	7.000 - 7.250
67	5.5310E+03 - 7.1020E+03	7.250 - 7.500
68	4.3070E+03 - 5.5310E+03	7.500 - 7.750
69	3.3550E+03 - 4.3070E+03	7.750 - 8.000
70	2.6130E+03 - 3.3550E+03	8.000 - 8.250
71	2.0350E+03 - 2.6130E+03	8.250 - 8.500
72	1.5850E+03 - 2.0350E+03	8.500 - 8.750
73	1.2340E+03 - 1.5850E+03	8.750 - 9.000
74	9.6110E+02 - 1.2340E+03	9.000 - 9.250
75	7.4850E+02 - 9.6110E+02	9.250 - 9.500
76	5.8290E+02 - 7.4850E+02	9.500 - 9.750
77	4.5400E+02 - 5.8290E+02	9.750 - 10.000
78	3.5360E+02 - 4.5400E+02	10.000 - 10.250
79	2.7540E+02 - 3.5360E+02	10.250 - 10.500
80	2.1450E+02 - 2.7540E+02	10.500 - 10.750
81	1.6700E+02 - 2.1450E+02	10.750 - 11.000
82	1.3010E+02 - 1.6700E+02	11.000 - 11.250
83	1.0130E+02 - 1.3010E+02	11.250 - 11.500
84	7.8890E+01 - 1.0130E+02	11.500 - 11.750
85	6.1440E+01 - 7.8890E+01	11.750 - 12.000
86	4.7850E+01 - 6.1440E+01	12.000 - 12.250
87	3.7270E+01 - 4.7850E+01	12.250 - 12.500
88	2.9020E+01 - 3.7270E+01	12.500 - 12.750
89	2.2600E+01 - 2.9020E+01	12.750 - 13.000
90	1.7600E+01 - 2.2600E+01	13.000 - 13.250
91	1.3710E+01 - 1.7600E+01	13.250 - 13.500
92	1.0680E+01 - 1.3710E+01	13.500 - 13.750
93	8.3150E+00 - 1.0680E+01	13.750 - 14.000
94	6.4760E+00 - 8.3150E+00	14.000 - 14.250
95	5.0430E+00 - 6.4760E+00	14.250 - 14.500
96	3.9280E+00 - 5.0430E+00	14.500 - 14.750
97	3.0590E+00 - 3.9280E+00	14.750 - 15.000
98	2.3820E+00 - 3.0590E+00	15.000 - 15.250
99	1.8550E+00 - 2.3820E+00	15.250 - 15.500
100	1.4450E+00 - 1.8550E+00	15.500 - 15.750
101	1.1250E+00 - 1.4450E+00	15.750 - 16.000
102	8.7640E-01 - 1.1250E+00	16.000 - 16.250
103	6.8260E-01 - 8.7640E-01	16.250 - 16.500
104	5.3160E-01 - 6.8260E-01	16.500 - 16.750
105	4.1400E-01 - 5.3160E-01	16.750 - 17.000
106	1.0000E-05 - 4.1400E-01	17.000 - 27.631

TABLE 4. GAMMA-RAY FINE GROUP STRUCTURE

Group	Energy Range
1	1.000 E + 07 - 1.200 E + 07
2	9.000 E + 06 - 1.000 E + 07
3	8.000 E + 06 - 9.000 E + 06
4	7.500 E + 06 - 8.000 E + 06
5	7.000 E + 06 - 7.500 E + 06
6	6.500 E + 06 - 7.000 E + 06
7	6.000 E + 06 - 6.500 E + 06
8	5.500 E + 06 - 6.000 E + 06
9	5.000 E + 06 - 5.500 E + 06
10	4.500 E + 06 - 5.000 E + 06
11	4.000 E + 06 - 4.500 E + 06
12	3.500 E + 06 - 4.000 E + 06
13	3.000 E + 06 - 3.500 E + 06
14	2.500 E + 06 - 3.000 E + 06
15	2.000 E + 06 - 2.500 E + 06
16	1.660 E + 06 - 2.000 E + 06
17	1.500 E + 06 - 1.660 E + 06
18	1.330 E + 06 - 1.500 E + 06
19	1.000 E + 06 - 1.330 E + 06
20	8.000 E + 05 - 1.000 E + 06
21	7.000 E + 05 - 8.000 E + 05
22	6.000 E + 05 - 7.000 E + 05
23	5.000 E + 05 - 6.000 E + 05
24	4.000 E + 05 - 5.000 E + 05
25	3.000 E + 05 - 4.000 E + 05
26	2.000 E + 05 - 3.000 E + 05
27	1.000 E + 05 - 2.000 E + 05
28	7.500 E + 04 - 1.000 E + 05
29	5.000 E + 04 - 7.500 E + 04
30	3.000 E + 04 - 5.000 E + 04
31	1.000 E + 04 - 3.000 E + 04

TABLE 5. BROAD GROUP COUPLED NEUTRON AND
GAMMA RAY ENERGY BOUNDS AND SILICON
DOSIMETER RESPONSE

Group	Upper Energy Bound (eV)	Silicon Dosimeter Response rad(Si)/(n or γ/cm^2)
1	1.50(+7)	1.15(-9)
2	1.35(+7)	1.02(-9)
3	1.11(+7)	8.65(-10)
4	9.05(+6)	6.17(-10)
5	7.00(+6)	2.77(-10)
6	5.45(+6)	1.36(-10)
7	4.10(+6)	7.40(-11)
8	3.01(+6)	4.70(-11)
9	2.41(+6)	3.90(-11)
10	2.30(+6)	2.71(-11)
11	1.85(+6)	1.23(-11)
12	1.11(+6)	0.
13	5.50(+5)	0.
14	1.60(+5)	0.
15	1.11(+5)	0.
16	2.50(+4)	0.
17	1.20(+4)	0.
18	3.40(+3)	0.
19	5.90(+2)	0.
20	1.01(+2)	0.
21	1.80(+1)	0.
22	3.10	0.
23	4.14(-1)	0.
24	1.20(+7)	2.40(-9)
25	8.00(+6)	1.90(-9)
26	6.50(+6)	1.60(-9)
27	5.00(+6)	1.30(-9)
28	3.50(+6)	9.70(-9)
29	2.50(+6)	6.90(-10)
30	1.50(+6)	4.60(-10)
31	1.00(+6)	4.60(-10)
32	7.00(+5)	3.40(-10)
33	4.00(+5)	2.20(-10)
34	2.00(+5)	8.70(-11)
35	7.50(+4)	0.
36	5.00(+4)	0.

28

TABLE 6. MATERIALS PROCESSED BY AMPX FOR USE IN THE SPRINT CALCULATIONS

Material	Source of Cross Section (x/s) Data
H-1	DNA 4184 Mod 2 - thermal x/s adjusted for bound H
H-3	DNA 4169 Mod 1 - no gamma production
He-4	DNA 4504 Mod 0 - no gamma production
Be-9	DNA 4154 Mod 2
B-10	ENDF/B 1155 - gamma production x/s added for n, $\alpha\gamma$ only
C	DNA 4274 Mod 0
N	DNA 4133 Mod 4
O	DNA 4134 Mod 2
F	ENDF/B 919 for neutron x/s, DNA 4509 for gamma production
Na	DNA 4156 Mod 1
Mg	DNA 4512 Mod 1
Ai	DNA 4135 Mod 3
Si	DNA 4151 Mod 3
Cl	ENDF/B 1149
Ca	DNA 4152 Mod 3
Ti	ENDF/B 1286
Cr	ENDF/B 1191
Fe	DNA 4180 Mod 2
Ni	ENDF/B 1190
Cu	DNA 4529 Mod 1
Zn	DNA 4529 Mod 1 (Cu) for neutron x/s, DNA 4530 (Zn) for gamma production
Zircaloy	ENDF/B 1284 for neutron x/s, ENDF/B 1189 (Nb) for gamma production

TABLE 6. (Cont'd.)

Material	Source of Cross Section (x/s) Data
Nb	ENDF/B 1189
Ag-107	ENDF/B 1138 for neutron x/s, DNA 4547 for gamma production
Ag-109	ENDF/B 1139 for neutron x/s, DNA 4547 for gamma production
Cd-NAT	ENDF/B 1281 for neutron x/s, ENDF/B 1287 (Mo) for gamma production
Sn	ENDF/B 1138 (Ag-107) for neutron x/s, DNA 4550 (Sn) for gamma production
Gd-NAT	ENDF/B 1030 for neutron x/s, ENDF/B 1291 (Eu) for gamma production
Ta-181	DNA 4179 Mod 3
W-182	DNA 4582 Mod 2
W-183	DNA 4583 Mod 3
W-184	DNA 4584 Mod 3
W-186	DNA 4586 Mod 2
Au-197	DNA 4283 Mod 0
Pb	DNA 4136 Mod 5
U-235	DNA 4188 Mod 1
U-238	DNA 4187 Mod 1
Pu-239	DNA 4539 Mod 0
Pu-240	DNA 4540 Mod 0

Cross sections for the Cs 137 calculations were processed with the SMUG module of the AMPX code for the elements shown in Table 7 into a fine group structure and collapsed to the broad groups shown in Table 8. The source of the x-ray cross sections is the Radiation Shielding Information Center DLC-7 library.

AMPX is a modular system for producing coupled multigroup neutron-gamma cross section sets. Basic cross section data for AMPX are obtained from ENDF/B like libraries. Most commonly used operations required to generate and collapse multigroup cross section sets are provided in the system. AMPX was assembled at ORNL by N. M. Greene, et al. for use on the IBM 360 series machines. SAI has converted the code for use on CDC 7600 and 6600 machines.

The basic processes provided will (1) generate multigroup neutron cross-sections; (2) generate multigroup gamma cross sections; (3) generate gamma yields for gamma-producing neutron interactions; (4) combine neutron cross sections, gamma cross sections, and gamma yields into final "coupled sets"; (5) perform one-dimensional discrete ordinates transport or diffusion theory calculations for neutrons and gammas and, an option, collapse the cross sections to a broad-group structure, using the one-dimensional results as weighting functions; and (6) output multigroup cross sections in convenient formats for other codes.

AMPX includes the following modules.

1. DRIVER - The AMPX module manager.

2. XLACS - Produces weighted multigroup neutron cross sections from ENDF/B.

3. LAPHNGAS - Generates multigroup secondary gamma-ray production cross sections.

31

TABLE 7. ELEMENTS PROCESSED INTO THE X-RAY GROUP STRUCTURE FOR THE CS 137 CALCULATION

Atomic Number	Element
1	H
2	He
3	Li
4	Be
5	B
6	C
7	N
8	O
9	F
11	Na
12	Mg
13	Al
14	Si
17	Cl
18	Ar
20	Ca
22	Ti
24	Cr
26	Fe
28	Ni
29	Cu
30	Zn
42	Mo
47	Ag
50	Sn
56	Ba
73	Ta
74	W
79	Au
82	Pb
92	U
94	Pu

TABLE 8.   X-RAY GROUP STRUCTURE FOR THE CS 137
CALCULATIONS AND THE ASSUMED DOSIMETER
RESPONSE

Group	Upper Energy (keV)	Silicon Dose rad(Si)/(x/cm^2)
1	662.	2.95 (-10)
2	600.	2.69 (-10)
3	500.	2.20 (-10)
4	425.	1.83 (-10)
5	350.	1.47 (-10)
6	275.	1.16 (-10)
7	220.	8.93 (-11)
8	160.	7.22 (-11)
9	120.	7.22 (-11)
10	90.	9.8 (-11)
11	65.	0
12	45.	0
	10.	

4. **CHOX** - Performs cross section interface management.

5. **SMUG** - Generates multigroup photon cross sections.

6. **NITAWL** - Provides for resonance self-shielding and work-
    ing library production.

7. **XSDRNPM** - Provides one-dimensional S_n capability for
    spatial weighting.

3.2   STEEL STYROFOAM MODEL

The steel styrofoam experiment was modeled by six regions, three
of which modeled the dosimeter and were used in the Sprint model as well.
Figure 4 shows the six regions of the steel styrofoam experiment which
are as follows:

1. surface barrier detector
2. surrounding silicon and Al can
3. attaching wires and connectors
4. styrofoam
5. front and back steel plates
6. steel cylinder

Table 9 lists the computer input necessary to model the steel styrofoam
experiment with the combinatorial geometry. Combinatorial geometry is
a ray tracing modual of MORSE that includes all space as intersections and
unions of simple body types such as spheres, cylinders, rectangles, cones
and others. The first section of the table defines the necessary bodies,
and the following cards describe the intersections and unions of the bodies.
Table 10 lists the elemental compositions of each of the six regions used
in our calculation.

ALL DIMENSIONS IN CM
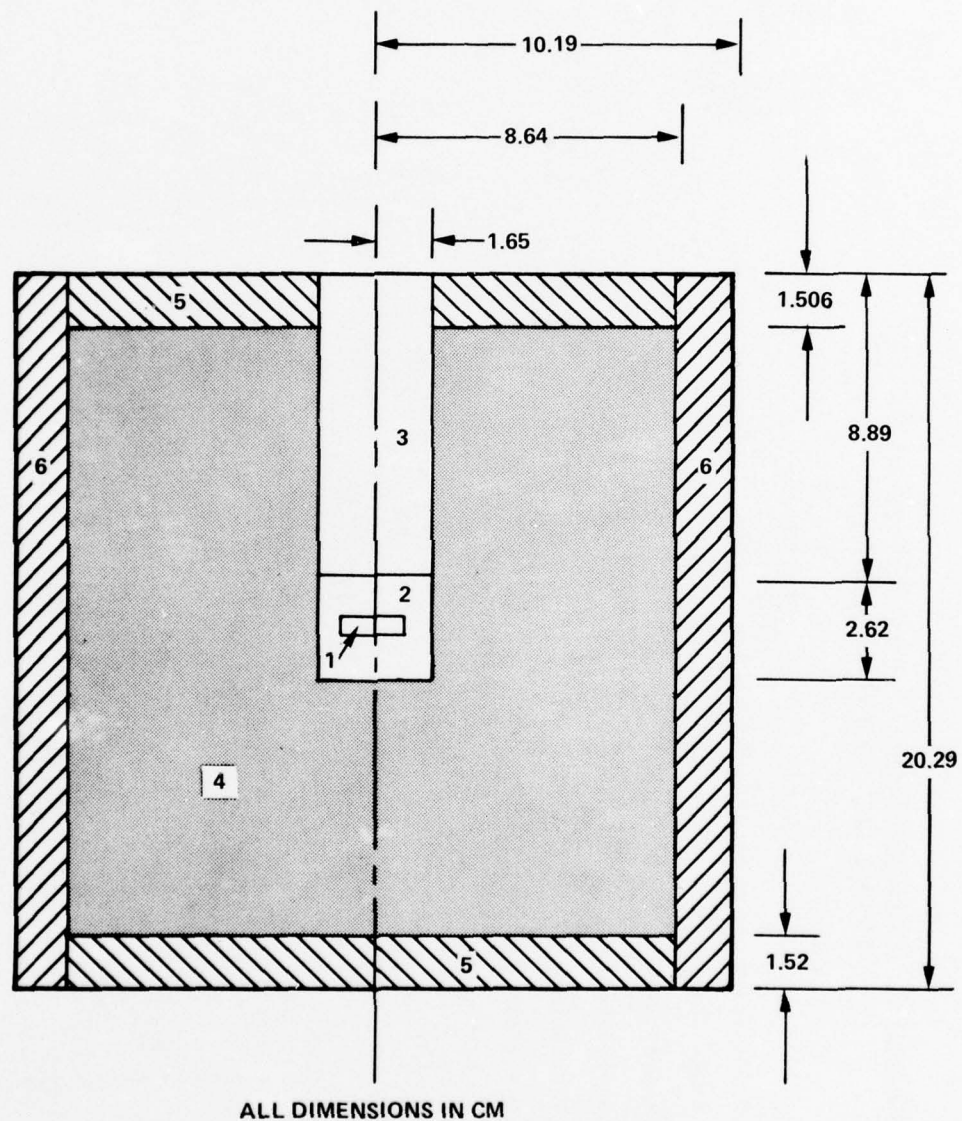
Figure 4. Six Region Combinatorial Geometry Model
of the Steel Styrofoam Sample

TABLE 9. COMBINATORIAL GEOMETRY MODEL FOR THE STEEL-STYROFOAM SAMPLE

BODY DATA

RCC	1	0.	.8300000E+00	0.	-.2350000E+00	0.	0.	.4700000E+00	
RCC	2	0.	.1580000E+01	0.	-.1365000E+01	0.	0.	.2620000E+01	
RCC	3	0.	.1650000E+01	0.	.1255000E+01	0.	0.	.8690000E+01	
RCC	4	0.	.8640000E+01	0.	-.8625000E+01	0.	0.	.1725000E+02	
RCC	5	0.	.8640000E+01	0.	.8625000E+01	0.	0.	.1506000E+01	
RCC	6	0.	.8640000E+01	0.	-.1014500E+02	0.	0.	.1520000E+01	
RCC	7	0.	.1019000E+02	0.	-.1014500E+02	0.	0.	.2029000E+02	
SPH	8	0.	0.	0.	.1760000E+04	-0.	0.		
SPH	9	0.	0.	-0.	.2000000E+04	-0.	0.		
END	10	-0.	-0.	-0.					

INPUT ZONE DATA

DET	0	0	0	0	0	1	0	0	0	0
HOU	0	0	1	0	0	2	0	0	0	0
WJH	0	0	2	0	3	3	0	0	0	0
FOM	0	0	3	0	4	4	0	0	0	0
TOP	0	0	4	0	5	5	0	0	0	0
ROT	0	0	5	0	6	6	0	0	0	0
SID	0	0	6	0	7	7	0	0	0	0
VAC	0	0	7	0	8	8	0	0	0	0
OUT	0	0	8	0	9	9	0	0	0	0
END	-0	-0	0	-0	0	0	0	0	0	0

36

TABLE 10. ELEMENTAL COMPOSITIONS USED FOR STEEL STYROFOAM CALCULATIONS
(units are atoms/barn-cm)

Element	Region 1 Active Detector Region	Region 2 Dosimeter	Region 3 Wires
Cu	.443-3	.296-4	.170-4
Al	.128-1	.179-1	.331-2
C	.465-2	.935-5	.122-4
H	.225-3		
O	.277-1		
N	.228-5		
Mg	.924-2	.203-3	.375-4
Si	.430-3	.382-1	.195-4
Zn			
Cr	.891-2	.189-4	.351-5
F	.301-5	.189-4	.247-4
An		.324-5	

Element	Region 4 CH	Region 5 Steel Front and Back	Region 6 Steel Sides
C	.153-1	.708-3	.609-3
H	.153-1		
Si		.400-3	.409-3
Ni		.934-4	.159-3
Cr		.111-3	.159-3
Fe		.840-1	.823-1
Cl		.177-4	.173-4

3.3   SPRINT MISSILE MODEL

The Sprint missile model is considerably more detailed using 127 bodies to generate 69 zones, 66 of which have different elemental compositions. The model is the result of an evolution which began in 1969 with an eight region model generated by Martin Marietta and through various programs at Martin and SAI has progressed in detail to the existing model. Of the sixty-nine regions, 46 are used to model the Autopilot (A/P), 11 model the Missile Guidance Set (MGS), 5 model the ballast container and antenna, and the remainder model the dosimeter and the skin. Final data for the model was supplied by Ted Bohm of Martin Marietta in the form of a letter report[14] and several blueprints. The letter report included their model to date, plus component lists and compositions of all regions in the vicinity of the detectors. Included with the component lists were the elemental compositions of each of the components.

In order to place the dosimeter into the Autopilot and the MGS, a 3.41 cm diameter hole was drilled into each, from the bottom of the Autopilot and to the side of the MGS. The exact position of these holes showing the material removed is detailed in the Martin letter report. Upon investigating these holes, it was determined that the material removed was representative of the homogenization, containing no significant components with different atomic densities. Therefore the Martin Marietta elemental densities were retained for the regions surrounding the detector holes.

The Sprint missile model used in our calculations is documented in the next three tables. Table 11 lists the zones with a brief description, the volume and the mass. Table 12 presents the combinatorial geometry computer input of the model and Table 13 presents the elemental composition of each region.

38

TABLE 11. SPRINT MISSILE MODEL

Zone	Missile Section	Contents of Region	Volume (cm^3)	Weight (gm)
1	A/P	Squibs	242.700	354.39
2	A/P	Squibs	93.547	71.98
3	A/P	Accel. Summing Ampl. & Rate Summing Ampl.	63.732	70.77
4	A/P	Outer Loop Shaping Ampl.	82.744	94.14
5	A/P	Rate Feedback Modulator	190.628	207.07
6	A/P	Inner Loop Shaping Ampl.	89.833	96.31
7	A/P	Inner Loop Shaping Ampl.	81.940	95.68
8	A/P	Outer Loop Shaping Ampl. & Resistor	85.707	93.48
9	A/P	Structural Filter	218.698	238.54
10	A/P	Roll Filter Amplifier	98.949	132.10
11	A/P	Accel. Summing Ampl. & Rate Summing Ampl. & Resistors	78.708	80.99
12	A/P	Dynamic Pressure Gain Changer	52.161	48.21
13	A/P	T3 Timer	59.344	62.91
14	A/P	Pulse Width Modulator and Resistor	69.547	51.41
15	A/P	Area Gain Changer & Roll Tachometer Ampl.	74.111	82.16
16	A/P	Connector	51.576	127.00
17	A/P	Frame (Areas not covered by Regions 1-16)	524.772	891.37

TABLE 11. (Cont'd.)

Zone	Missile Section	Contents of Region	Volume (cm^3)	Weight (gm)
18	A/P	2nd Stage Servo Ampl.	37.605	58.40
19	A/P	Adaptive Sig. Inverter, 2nd Stage Act. Sum. Ampl., 2nd Stage Servo Ampl., Servo Pwr Ampl., 1st Stage Act. Sum. Ampl., 1st Stage Servo Ampl.	219.508	305.77
20	A/P	1st Stage Act. Sum. Ampl. & 1st Stage Servo Ampl. & Jumper	55.005	76.12
21	A/P	Comparator	25.439	33.90
22	A/P	Adaptive Gain Change Amplifier	38.343	48.86
23	A/P	Roll Modulator, Low Pass Filter, Adaptive Sig. Inverter, 2nd Stage Servo Ampl.	138.650	182.81
24	A/P	High-Pass, Low-Pass Filter, Comparator, 1st Stage Servo Ampl.	169.891	211.33
25	A/P	Adaptive Integrator & Jumper	39.690	44.18
26	A/P	Adaptive Gain Change Amplifier	36.561	53.48
27	A/P	Signal Control Mod., 2nd Stage Act. Sum. Ampl., 2nd Stage Servo Ampl., Servo Pwr Ampl., 1st Stage Act. Sum. Ampl., 1st Stage Servo Ampl.	166.679	249.37

TABLE 11. (Cont'd.)

Zone	Missile Section	Contents of Region	Volume (cm^3)	Weight (gm)
28	A/P	Adaptive Integrator	32.624	49.36
29	A/P	2nd Stage Act. Sum. Ampl., 2nd Stage Servo Ampl., Servo Pwr Ampl.	102.253	140.25
30	A/P	Low Pass Filter, Servo Pwr Ampl.	101.571	120.96
31	A/P	Convertor	110.451	128.65
32	A/P	Frame (Areas not covered by Regions 18-32)	439.55	937.10
33	A/P	Electrical Linear Accelerometer	134.06	113.24
34	A/P	Rate Integrating Gyroscope	212.14	343.07
35	A/P	Electrical Linear Accelerometer	237.16	194.79
36	A/P	Rate Integrating Gyroscope	303.03	324.45
37	A/P	Primary Wet Battery	1728.1	2920.94
38	A/P	Rate Control Elec. Ampl.	207.221	170.71
39	A/P	Elec. Control Ampl. Platform	524.802	765.85
40	A/P	Static Pwr Inverter Subassay.	468.359	366.87
41	A/P	Power Ampl. Inverter Subassay.	781.724	608.58
42	A/P	Single Axis Platform	892.65	2300.64
43	A/P	Electrical Control Rate Ampl.	231.769	317.78

TABLE 11. (Cont'd.)

Zone	Missile Section	Contents of Region	Volume (cm^3)	Weight (gm)
44	A/P	Capacitor Assembly	44.647	8.70
45	A/P	DC Voltage Regulator	307.269	1037.56
46	A/P	Interconnecting Box	1300.937	1650.38
47	A/P MGS	Dosimeter (2)	20.548	52.91
48	A/P MGS	Dosimeter Wires (2)	76.04	11.68
49	Nose	Adjustible Ballast Holder	456.14	907.2
50	MGS	Signal Data Converter & Pulse Decoder	3367.0	4326.
51	MGS	Radio Frequency Detector	1642.0	1788.
52	MGS	Electrical Frequency Converter	4305.0	4018.
53	MGS	Transmitter	2423.0	2581.
54	MGS	Transmitter	1452.0	799.
55	MGS	Electrical Frequency Converter	117.7	220.
56	MGS	Power Supply & P.S. Sub-Assembly	598.8	539.
57	MGS	Power Supply	1825.0	2699.
58	MGS	"S" Band Cable Trough	444.5	101.
59	MGS	"L" Band Cable Trough	444.5	156.
60	MGS	Cover & Housing	1334.0	4147.

TABLE 11. (Cont'd.)

Zone	Missile Section	Contents of Region	Volume (cm^3)	Weight (gm)
61	Skin	Aluminum	5480.	5035.
62	Skin	Phenolic	4455.	6577.
63	Nose	Ballast Container	268.1	2172.2
64	Nose	Ballast	370.36	3079.9
65	Nose	Antenna	443.6	1367.2
66	Nose	Nose Structure	3810.79	7307.5

TABLE 12. COMPUTER INPUT FOR THE 66 REGION SPRINT COMBINATORIAL GEOMETRY MISSILE MODEL

BODY DATA

	No.						
RPP	1	-.2108200E+01	.4902200E+01	-.8102600E+01	.1303020E+02	.1484503E+03	3
RPP	2	-.3505200E+01	.2108200E+01	-.7620000E+01	-.1303020E+02	.1484503E+03	11
RPP	3	-.2108200E+01	.3733800E+01	-.5207000E+01	-.8102000E+01	.1575624E+03	19
RPP	4	-.7380600E+01	.8382000E+01	-.1092200E+02	.1092200E+02	.1525626E+03	27
RPP	5	-.3733800E+01	.7289800E+01	-.5842000E+01	.8102600E+01	.1525626E+03	35
RPP	6	-.4902200E+01	.7289800E+01	-.8102600E+01	.1122680E+02	.1525626E+03	43
RPP	7	-.4953000E+01	.7340600E+01	-.2768600E+01	.5842000E+01	.1525626E+03	51
RPP	8	-.9347400E+01	.4953000E+01	-.1176020E+02	.2768600E+01	.1525626E+03	59
RPP	9	-.2142200E+01	.4953000E+01	-.1176020E+02	.3810000E+01	.1525626E+03	67
RPP	10	-.3734000E+01	.4343400E+01	-.1277620E+02	.3810000E+01	.1525626E+03	75
RPP	11	-.3733800E+01	.4953000E+01	-.5842000E+01	.3810000E+01	.1525626E+03	83
RPP	12	-.2616200E+01	.3733800E+01	-.3810000E+01	.5207000E+01	.1525626E+03	91
RPP	13	-.1905000E+00	.2616200E+01	-.3810000E+01	.5207000E+01	.1525626E+03	99
RPP	14	-.3581400E+01	.4064000E+00	-.3810000E+01	.5207000E+01	.1575624E+03	107
RPP	15	-.3581400E+01	.2142200E+01	-.1315720E+02	.3810000E+01	.1525626E+03	115
RPP	16	-.4749800E+01	.4292600E+01	-.6934200E+01	.4648200E+02	.1525626E+03	123
RPP	17	-.7620000E+01	.4292600E+01	-.1155700E+02	.1155700E+02	.1525624E+03	131
RPP	18	-.7182200E+01	.1905000E+01	-.9347200E+01	.9347200E+01	.1525248E+03	139
RPP	19	-.7182200E+01	.4292600E+01	-.6934200E+01	.5207000E+01	.1525626E+03	147
RPP	20	-.7182200E+01	.1905000E+01	-.4648200E+01	.7620000E+01	.1525626E+03	155
RPP	21	-.3505200E+01	.2142200E+01	-.5207000E+01	.6934200E+01	.1525626E+03	163
RPP	22	-.7182200E+01	.3505200E+01	-.5207000E+01	.4648200E+01	.1525626E+03	171
RPP	23	-.7182200E+01	.4749800E+01	-.4648200E+01	.3810000E+01	.1525626E+03	179
RPP	24	-.4749800E+01	.7581400E+01	-.1270000E+01	.1270000E+01	.1525626E+03	187
RPP	25	-.7182200E+01	.4749800E+01	-.6781800E+01	.6781800E+01	.1525626E+03	195
RPP	26	-.7797800E+01	.3581400E+01	-.1137920E+02	.9017000E+01	.1525626E+03	203
RPP	27	-.7182200E+01	.3581400E+01	-.9017000E+01	.6781800E+01	.1525626E+03	211
RPP	28	-.7797800E+01	.7182200E+01	-.9017000E+01	.1155700E+02	.1525626E+03	219
RPP	29	-.9652000E+01	.9652000E+01	-.1473200E+02	.1473200E+02	.1525626E+02	227
RCC	30	0.	0.	-.1484503E+03	0.	.4112260E+01	235
RPP	31	-.1473200E+02	.2246000E+01	-.1130960E+02	.1109980E+02	.1558648E+03	244
RPP	32	-.2495600E+01	.7569200E+01	-.9144000E+02	.6680200E+01	.1558648E+03	252
RPP	33	-.7038600E+01	.7569200E+01	-.1109980E+02	.9144000E+02	.1558648E+03	260
RPP	34	-.4851400E+01	.4851400E+01	-.1143000E+02	.9144000E+01	.1558648E+03	268
RPP	35	-.7721600E+01	.7569200E+01	-.6680200E+01	.4450000E+01	.1558648E+03	276
RPP	36	-.7620000E+01	.4064000E+01	-.4450000E+01	.2235200E+01	.1558648E+03	284
RPP	37	-.1219200E+01	.7569200E+01	-.4450000E+01	-.2235200E+01	.1558648E+03	292
RPP	38	-.1524000E+01	.7569200E+01	-.2235200E+01	0.	.1558648E+03	300
RPP	39	-.2336600E+01	.7564200E+01	0.	.2209800E+01	.1558648E+03	308

TABLE 12. (Cont'd.)

RPP	40	0.-3937000E+01	.7569200E+01	.2209800E+01	.6705400E+01	.1558468E+03	316
RPP	41	.1905000E+01	.7569200E+01	.6705600E+01	.8639200E+01	.1558468E+03	324
RCC	42	.2413000E+01	.7569200E+01	.8639200E+01	.1098800E+02	.1558468E+03	332
RPP	43	.3937000E+01	.1905000E+01	.6705600E+01	.8639200E+01	.1558468E+03	340
RPP	44	.7420000E+01	.3175000E+01	.8639200E+01	.1155866E+02	.1558468E+03	348
RPP	45	.3175000E+01	.2413000E+01	.8639200E+01	.1099800E+02	.1558468E+03	356
RPP	46	.3175000E+01	.3302000E+01	.1099800E+02	.1335500E+02	.1558468E+03	364
RPP	47	.4368000E+01	.7620000E+01	-.6680200E+01	.4445000E+01	.1558468E+03	372
RPP	48	.7035800E+01	.4368800E+01	.6680200E+01	.4445000E+01	.1558468E+03	380
RCC	49	.7035800E+01	.1219200E+01	.4445000E+01	.2255200E+01	.1558468E+03	388
RPP	50	-.7035800E+01	.1524000E+01	.2235200E+01	0.	.1558468E+03	396
RPP	51	.7035800E+01	.2376800E+01	.2209800E+01	.8639200E+01	.1558468E+03	404
MED	52	.7035800E+01	.3937000E+01	.9144000E+01	.8639200E+01	.1558468E+03	412
RPP	53	.8763000E+01	.7035800E+01	.1473200E+02	.1473200E+02	.1541186E+03	420
RPP	54	-.9525000E+01	.9525000E+01	.1525626E+03	0.	.1558468E+03	428
RFD	55	0.	0.	0.	0.	.3242220E+01	436
RPP	56	0.	.5433720E+01	-.8331200E+01	-.8331200E+01	.1484757E+03	445
RCC	57	0.	.1823720E+01	.1434008E+03	0.	.5074920E+01	453
RPP	58	-.1519936E+02	.4246800E+01	-.3332480E+01	-.3332480E+01	.1484757E+03	462
RPP	59	-.4268800E+01	.9603740E+01	.1405128E+02	.3332480E+01	.1484757E+03	470
RPP	60	-.9987280E+01	.9603740E+01	.8331200E+01	.3324800E+01	.1484757E+03	478
RPP	61	.5433720E+01	.5951220E+01	.1793494E+02	.8331200E+01	.1434008E+03	486
RPP	62	.5135800E+01	.9603740E+01	.3332480E+01	.1662400E+01	.1434008E+03	494
RPP	63	.9999940E+01	.9603740E+01	.1476248E+02	.3332480E+01	.1434008E+03	502
RCC	64	0.	.4775200E+00	.1434008E+03	0.	.7840980E+01	510
RPP	65	.1524000E+02	.8337400E+01	-.3332480E+01	.1112520E+01	.1356868E+03	519
RPP	66	.5951220E+01	.8337400E+01	.1112500E+01	.1230618E+02	.1356868E+03	527
MED	67	.5951220E+01	.1533861E+02	.1445058E+03	.3652520E+01	0.	535
MPP	68	.5135800E+01	.2758400E+01	0.	.8100000E+01	.1356868E+03	549
RPP	69	-.1000252E+02	.5951220E+01	.1662400E+01	.10A7628E+02	.1484503E+03	557
MFD	70	.5135800E+01	.10A762BE+02	.3987800E+01	.4866640E+01	0.	565
RPP	71	-.1000252E+02	.2956400E+01	.8732520E+01	.1087628E+02	.1276350E+02	579
RCC	72	.4090000E+00	.5135800E+01	.1356868E+01	0.	.1484503E+03	587
HPP	73	-.1000252E+02	.5135800E+01	-.3332480E+01	.3987800E+00	.1484503E+03	596
RCC	74	.4090000E+00	.9017000E+01	.1003274E+03	0.	.6007520E+01	604

45

TABLE 12. (Cont'd.)

RPP	75	-.5135800E+01	0.	.5951220E+01	-.3332400E+01	.2128520E+01	.1484008E+03	.1484757E+03 613
HCC	76	0.	.9652000E+01	0.	.1554668E+03	0.		.4445000E+01 621
SPH	77	0.	0.	0.		.5320000E+04	-0.	-0. 630
HCC	78	.4090000E+00	.9017000E+01	.1463349E+03	0.		.1168400E+01 638
RCC	79	.3823000E+01 / .4090000E+00	.9017000E+01	.1475033E+03	0.		.2082800E+01 647
SPH	80	.3239000E+01	0.	0.	.5500000E+04	-0.	0. 656
HCU	81	-.5135800E+01	.1087628E+02	.1459103E+03	-.4866640E+01	0.	0. 664
RCC	82	0.	.2936240E+01	.1484503E+03	0.		.2540000E+01 678
								.2620000E+01
RCC	83	.1705000E+01	0.	.1510703E+03	0.		.9221480E+01 687
RPP	84	-.1186000E+02	-.7810000E+01	-.3733000E+01	.8799800E+02	-.1249530E+03 696
RPP	85	.7810000E+01	.1186000E+02	-.3733000E+01	.8799800E+02	.1249530E+03 704
RCC	86	0.	.5218900E+02	0.		-.6832000E+01 712
TRC	87	.4610000E+01	0.	.1249530E+03	0.		-.3695500E+02 721
TRC	88	.1060000E+02	.7708000E+01	.9007100E+02	0.		-.2073000E+01 731
HCC	89	.9439000E+01	.7366000E+01	.1002380E+03	0.		-.1224000E+02 741
RCC	90	.1400000E+02	0.	.1053980E+03	0.		-.5160000E+01 750
RCC	91	.1400000E+02	0.	.1241580E+03	0.		-.1185000E+02 759
HCC	92	.1400000E+02	0.	.1272790E+03	0.		-.5121000E+01 768
RCC	93	.1400000E+02	0.	.1299400E+03	0.		.2669000E+01 777
RCC	94	.1078500E+02	0.	.1308120E+03	0.		-.8600000E+00 786
RCC	95	.1079500E+02	.7770000E+01	.1308120E+03	0.		.9650000E+00 795
TRC	96	.9005000E+01	0.	.1338570E+03	0.		-.2080000E+01 805
RCC	97	.7770000E+01	0.	.1145780E+03	0.		-.1830000E+01 814
RCC	98	.8965000E+01	0.	.1123080E+03	0.		-.1630000E+01 823
RCC	99	.1400000E+02	0.	.1106780E+03	0.		-.5280000E+01 832

46

TABLE 12. (Cont'd.)

Type No.							Card
RCC 100	0.		0.	.1296690E+03	0.	-.2390000E+01	841
TRC 101	0.	.1399000E+02	.8090000E+01	.8900000E+02	0.	-.1362000E+01	850
TRC 102	0.	.9622000E+01	.8000000E+01	.8900000E+02	0.	-.1159000E+01	860
TRC 103	0.	.9355000E+01	.9465000E+01	.8000000E+01	0.	-.3948400E+02	870
TRC 104	0.	.1255500E+02	.9278000E+01	.1272790E+03	0.	-.3928100E+02	880
TRC 105	0.	.1235200E+02	.8100000E+01	.1272790E+03	0.	.4910000E+01	890
TRC 106	0.	.1265000E+02	.7987000E+01	.1296690E+03	0.	.4710000E+01	900
RCC 107	-.1235200E+02	.1310000E+01		.1296690E+03	.2620000E+01	0.	9..
RCC 108	.1705000E+01	.1310000E+01	.1705000E+01	.1009150E+03	.9390000E+01	0.	5.
RCC 109	0.	.8217000E+01		.1009150E+03	0.	-.1746000E+01	928
TRC 110	0.	.1977900E+02	.1046200E+02	.8625400E+02	0.	-.8559800E+02	937
TRC 111	0.	.1429100E+02	.1024000E+02	.1554660E+03	0.	-.4006300E+02	947
TRC 112	0.	.1926000E+02	.1491000E+02	.1099310E+03	0.	-.4553500E+02	957
TRC 113	0.	.1896600E+02	.1464700E+02	.1554660E+03	0.	.4054600E+02	967
TRC 114	0.	.1341400E+02	.9704000E+01	.1554660E+03	0.	.3483100E+02	977
RCC 115	0.	.1341400E+02		.1046990E+03	0.	.8697000E+01	987
RPP 116	-.9525000E+01	.9525000E+01	-.2000000E+02	.2000000E+02	.1535610E+03	.1525630E+03	996
TRC 117	0.	.9517000E+01	.6985000E+01	.6986800E+02	0.	.1767900E+02	1004
TRC 118	0.	.1080000E+02	.1072100E+02	.8010700E+02	0.	.7370000E+00	1014
RCC 119	0.	.6949000E+01	.2223000E+01	.7513200E+02	.2925000E+01	-.3110000E+00	1024
RCC 120	.9274000E+01	.2223000E+01		.7482100E+02	.1894000E+01	-.2020000E+00	1033
RCC 121	0.	.2223000E+01		.7513200E+02	.2925000E+01	-.3110000E+00	1042
RCC 122	0.	.3302000E+01	.9274000E+01	.7482100E+02	0.	-.2020000E+00	1051

47

TABLE 12. (Cont'd.)

```
RCC  123 -.6349000E+01  0.           .7513200E+02  .2925000E+01  0.           -.3110000E+00 1060
RCC  124 -.2225000E+01  -.9274000E+01 .7482100E+02  .1894630E+01  0.           -.2020000E+00 1069
RCC  125  0.           -.6349000E+01  .7513200E+02  0.           -.2925000E+01 -.3110000E+00 1078
RCC  126  0.           -.2225000E+01  .7482100E+02  0.            .1940000E+01 -.2020000E+00 1087
RCC  127  0.            .3302000E+01  .1249530E+03  0.            0.            .3695500E+02 1096
END  128 -0.            .1400000E+02 -0.           -0.           -0.           -0.           1105
```

INPUT ZONE DATA

TABLE 12. (Cont'd.)

TABLE 12. (Cont'd.)

TABLE 13. SPRINT MODEL ELEMENTAL DENSITIES
(Atoms/Barn-cm)

ELEMENT	ZONE 1	ZONE 2	ZONE 3	ZONE 4	ZONE 5	ZONE 6
HYDROGEN	4.1820E-03	2.2320E-03	1.4650E-03	1.6970E-03	1.7420E-03	1.5700E-03
HELIUM	9.4090E-04	7.7530E-04	5.9960E-04	4.0410E-04	1.4470E-04	1.9160E-04
LITHIUM	1.0450E-02	7.2930E-03	3.9150E-04	3.7760E-04	3.0960E-04	3.0250E-04
BERYLLIUM	1.9900E-02	8.3640E-04	1.0400E-02	9.2350E-03	1.0090E-02	8.1500E-03
BORON	4.3170E-03	3.2150E-04	1.1740E-02	9.9160E-03	1.1760E-02	8.1740E-03
CARBON	4.3170E-03	5.2220E-03	5.2220E-03	5.1150E-03	4.4340E-03	4.5730E-03
NITROGEN	1.8880E-03	7.1960E-04	4.9200E-04	4.9370E-04	5.7170E-04	4.2710E-04
OXYGEN	1.1130E-04	7.4120E-05	5.2940E-05	1.0520E-05	1.4620E-05	6.5400E-04
FLUORINE	3.0410E-05	1.3370E-05	1.5590E-04	1.0500E-04	1.2100E-05	1.5250E-05
SODIUM			1.0660E-05	1.5240E-05	4.4950E-06	1.5200E-05
ALUMINUM	3.2400E-05	2.3490E-05	6.8200E-06	7.5720E-06	3.5110E-06	4.5710E-06
CHLORINE	1.8774E-03	2.0940E-06	8.9470E-05	4.5720E-06	6.2370E-06	4.9900E-04
IRON	5.2730E-04	6.8140E-04	2.0160E-04	1.2160E-05	1.1100E-03	1.7500E-03
NICKEL	8.6850E-05	3.2850E-04	6.8940E-04	2.0050E-04	1.5670E-03	6.7700E-04
COPPER	7.7730E-05	4.9190E-06	3.9220E-05	6.9400E-04	1.0940E-05	1.2490E-04
ZINC	5.9900E-05	1.4250E-04	2.5842E-04	5.2400E-05	1.0340E-03	3.1012E-04
MOLYBDENUM	3.7030E-03	4.6880E-05	5.4600E-04	4.5020E-05	2.2570E-04	5.0400E-04
SILVER	3.5470E-05	1.4140E-03	6.2350E-05	5.7400E-06		
TIN		2.9200E-05	3.9519E-04	4.0090E-04	1.6130E-03	6.0120E-04
BARIUM			5.8860E-04	9.0690E-05	3.9750E-05	2.7840E-05
TANTALUM			1.0340E-05	1.1740E-05	1.9920E-06	9.4930E-06
TUNGSTEN						

ELEMENT	ZONE 7	ZONE 8	ZONE 9	ZONE 10	ZONE 11	ZONE 12
HYDROGEN	1.7270E-03	1.6630E-03	1.5350E-03	2.0100E-03	1.4020E-03	1.3250E-03
HELIUM	6.6730E-04	3.9900E-04	1.1550E-04	9.7760E-05	5.1320E-04	2.1800E-04
LITHIUM	3.4150E-04	3.0840E-04	3.0850E-04	5.2340E-04	4.9690E-04	4.1330E-04
BERYLLIUM	9.1210E-03	8.4120E-03	1.0260E-02	2.7720E-02	1.1130E-02	8.5720E-03
BORON	5.0820E-03	9.4550E-03	1.2620E-02	1.4220E-02	2.1130E-02	8.3200E-03
CARBON	5.6820E-03	4.9330E-03	4.5020E-03	5.6100E-03	5.2700E-03	5.0810E-03
NITROGEN	7.0670E-04	4.8290E-04	6.0120E-04	1.1090E-04	6.3170E-04	4.7590E-04
OXYGEN	1.2770E-04	5.6490E-04	1.4730E-05	1.9940E-04	6.5530E-04	3.1650E-05
FLUORINE	1.0760E-05	1.5340E-04	3.6220E-05	1.7600E-05	1.5860E-04	1.5440E-04
SODIUM	4.7940E-05	1.0490E-04	9.5200E-06	6.1500E-06	1.2510E-06	9.4530E-05
ALUMINUM	4.5680E-04	7.4650E-05	2.3600E-06	5.1500E-05	5.4730E-04	1.0240E-06
CHLORINE		4.3710E-04	2.5570E-03	1.9400E-03	5.4730E-05	1.0240E-06
CALCIUM					1.7920E-04	3.2000E-05
IRON	9.6550E-06	1.1890E-05	2.9430E-06	1.4997E-05	1.2561E-05	8.2607E-05
NICKEL	1.9360E-03	1.9110E-03	1.2390E-04	1.2390E-04	1.2510E-03	1.6190E-03
COPPER	7.4290E-04	8.4510E-04	1.6200E-03	1.9450E-03	5.1740E-04	1.6940E-03
ZINC	4.6470E-05	5.6670E-05	1.4700E-04	3.0700E-05	5.5470E-04	2.6120E-05
MOLYBDENUM	2.9270E-04	3.5830E-04	1.0690E-04	2.0450E-04	2.6420E-04	2.3120E-04
SILVER	5.5320E-04	5.4720E-04	1.4820E-04	1.7290E-04	1.7300E-05	5.0730E-04
TIN		5.5450E-06	5.5450E-06		6.5730E-05	
BARIUM	6.5910E-04	7.5350E-04	1.6510E-05	2.0190E-03	5.3820E-04	4.0210E-05
TANTALUM	3.0520E-05	3.7060E-05	1.9180E-05	7.0900E-05	5.0300E-05	1.1177E-04
TUNGSTEN	1.0760E-05	1.1340E-05	1.8880E-06	1.8750E-06	1.2190E-05	5.4040E-05

51

TABLE 13. (Cont'd.)

ELEMENT	ZONE 1	ZONE 14	ZONE 15	ZONE 16	ZONE 17	ZONE 18
HYDROGEN	7.0980E-04	1.1770E-03	1.5700E-03	4.9170E-03	5.4360E-05	2.2310E-03
HELIUM	4.0180E-04	1.7050E-04	3.3530E-04	5.6540E-04		2.0450E-04
LITHIUM	4.6610E-02	4.6430E-04	4.0570E-04	4.0400E-02	3.1890E-02	2.0960E-02
BERYLLIUM	1.4720E-02	7.9570E-03	9.0690E-03	4.4900E-02	1.0490E-02	1.7940E-02
BORON	8.4830E-03	7.0570E-02	9.1970E-03	1.4710E-02	1.4440E-03	4.8370E-04
CARBON	4.6350E-04	4.1160E-03	5.4150E-03	6.9950E-04	7.0310E-04	4.3720E-04
NITROGEN	5.6160E-06	4.7720E-04	4.6340E-04			6.6530E-04
OXYGEN	3.6040E-05	2.6720E-05	4.6410E-05			1.9910E-04
FLUORINE	1.1740E-05	5.1940E-05	1.3770E-04	6.4990E-05		1.7270E-05
SODIUM	6.1720E-07	1.0290E-04	1.4410E-05			1.2360E-05
ALUMINUM	9.0720E-06	4.0290E-06	1.5340E-05	1.7540E-05	1.4550E-04	4.2040E-04
CHLORINE	4.0450E-05	9.3470E-06	9.0680E-06	2.6450E-04		
CALCIUM		2.6350E-04				
CHROMIUM	1.1300E-04	1.3170E-05	1.8271E-05	1.0200E-03	1.6070E-03	1.5900E-05
IRON	9.2440E-03	1.2260E-03	2.1640E-03			2.1490E-03
NICKEL	9.1470E-06	2.5100E-05	4.5560E-04			1.1990E-05
COPPER	6.9410E-04	2.5690E-05	6.5290E-05	1.7370E-04	2.0430E-06	3.6240E-05
ZINC	2.1830E-05	3.4290E-04	4.0520E-04	4.1270E-04	1.6330E-04	2.0760E-04
MOLYBDENUM	2.6320E-04	3.0490E-04	1.0960E-05	3.3225E-03	7.1920E-04	
SILVER	7.0650E-04	2.4490E-04	7.5411E-04			1.0297E-03
TIN	1.2130E-05	4.0990E-05	1.0020E-04			1.0300E-03
BARIUM		2.0210E-05	1.5870E-05			6.5900E-06

ELEMENT	ZONE 19	ZONE 20	ZONE 21	ZONE 22	ZONE 23	ZONE 24
HYDROGEN	2.0063E-03	1.8340E-03	2.1000E-03	1.7230E-03	1.7250E-03	1.6500E-03
HELIUM	2.7330E-04	4.0490E-04	3.1250E-04	1.5440E-04	4.8540E-04	4.0070E-04
LITHIUM	3.3500E-05	5.2040E-04	4.0570E-04	4.1730E-04	4.1730E-04	6.2540E-04
BERYLLIUM	1.3500E-02	1.4400E-02	1.1970E-02	1.2240E-02	1.5730E-02	1.2340E-02
BORON	1.3470E-02	7.4710E-03	1.1900E-02	7.3560E-02	1.4490E-02	1.4290E-02
CARBON	6.5970E-03	4.4360E-04	6.8390E-05	6.0220E-04	2.1490E-03	4.3200E-03
NITROGEN	6.8450E-04	2.5790E-05	2.5660E-05	6.4050E-03	8.5910E-04	4.3050E-04
OXYGEN	5.0123E-05	6.0430E-04	6.9290E-04	6.9160E-04	5.6020E-05	4.3210E-05
FLUORINE	1.3550E-04	9.0430E-04	1.9400E-04	6.4720E-05	5.0710E-04	1.5270E-05
SODIUM	3.5327E-05	7.5940E-04	6.7900E-05	1.7960E-04	1.2340E-06	1.2460E-05
ALUMINUM	1.0166E-04	2.8167E-04	6.7390E-05	1.4711E-05	9.2790E-06	1.2460E-05
CHLORINE	4.5174E-05	7.5900E-04	6.4330E-04	1.4960E-05	7.7700E-04	4.1900E-05
CALCIUM	2.7160E-05		3.7440E-05	1.4960E-05	1.2340E-04	6.0510E-05
CHROMIUM			4.3210E-04	3.5150E-04	2.2740E-05	2.6490E-05
IRON			2.0390E-05	2.1790E-04	2.7470E-05	2.0190E-05
NICKEL				2.4050E-03	2.1490E-04	2.0490E-05
COPPER				1.0050E-03	8.5910E-04	7.4720E-05
ZINC				4.4320E-04	5.3520E-05	5.1040E-05
MOLYBDENUM				5.4660E-04	4.8240E-04	5.0760E-06
SILVER				3.7440E-05	3.5590E-06	5.5950E-06
BARIUM	7.5070E-04	7.0530E-04	8.6110E-04	8.5560E-04	3.5210E-04	7.4410E-05
TANTALUM	7.1660E-05	1.0500E-04	8.2610E-05	1.4190E-04	1.2150E-04	9.7400E-05
TUNGSTEN	6.4190E-06	8.9730E-06	5.0980E-06	8.3510E-06	6.8710E-06	1.0950E-05

TABLE 13. (Cont'd.)

ELEMENT	ZONE 25	ZONE 26	ZONE 27	ZONE 28	ZONE 29	ZONE 30
HYDROGEN	1.8670E-03	1.8080E-03	1.5740E-03	1.1716E-03	1.5890E-03	1.7130E-03
HELIUM	2.9550E-04	1.0200E-04	4.5000E-04	2.9470E-04	2.2680E-04	2.1750E-03
LITHIUM	4.8520E-04	5.2150E-04	1.1720E-03	7.1743E-04	2.5450E-03	4.5800E-03
BERYLLIUM	1.0400E-02	1.7060E-02	1.7190E-02	1.9991E-02	1.5760E-02	1.0730E-02
BORON	1.0910E-02	1.7170E-02	1.4480E-02	1.4675E-02	1.3670E-02	5.3270E-02
CARBON	5.8430E-03	8.4760E-03	7.4830E-03	8.5920E-03	6.0720E-05	6.7190E-04
NITROGEN	6.9180E-04	7.2420E-04	7.0310E-04	1.1521E-05	6.0250E-03	5.7430E-04
OXYGEN	5.8830E-05	6.7720E-05	6.9930E-04	6.0742E-05	5.0210E-03	5.3490E-05
FLUORINE	1.1040E-04	1.2770E-04	1.5890E-04	1.5010E-04	1.2940E-03	1.0310E-05
SODIUM	1.5310E-05	1.9220E-05	1.7540E-05	1.4620E-05	1.7740E-05	1.5570E-05
ALUMINUM	1.5260E-05	1.5390E-05	1.1890E-05	1.8500E-05	9.0210E-06	5.7180E-06
CALCIUM	1.2860E-05	1.3450E-05	2.7440E-05	2.1390E-05	5.0100E-05	1.9470E-04
IRON	1.0530E-05	3.6070E-04	3.2900E-04	5.0440E-04	3.5510E-04	1.9470E-05
NICKEL	2.9430E-03	2.8500E-05	3.8410E-05	1.2800E-05	2.6710E-05	1.6040E-04
COPPER	9.5450E-04	2.9460E-03	2.5490E-03	3.1970E-03	2.3000E-04	3.5000E-03
ZINC	7.6660E-05	1.1210E-05	4.3500E-04	1.1610E-03	1.9570E-04	3.5030E-04
MOLYBDENUM	2.9420E-04	9.6490E-05	7.5250E-05	9.3303E-05	8.7330E-05	2.5560E-05
SILVER	3.9500E-04	3.9690E-04	5.5940E-04	5.7674E-04	3.5553E-04	2.4170E-05
BARIUM	8.9590E-04	5.9210E-04	7.2090E-04	4.3520E-04	7.3700E-04	6.0800E-04
TANTALUM	6.8590E-05	9.9170E-04	7.9972E-04	1.0300E-03	6.9170E-04	5.0210E-04
TUNGSTEN	6.3160E-06	1.0890E-04	1.1420E-04	8.3490E-05	7.5700E-05	5.7700E-05
		8.9720E-06	9.1140E-06	7.6860E-06	7.5080E-06	5.0660E-06

ELEMENT	ZONE 31	ZONE 32	ZONE 33	ZONE 34	ZONE 35	ZONE 36
HYDROGEN	6.3040E-03	8.2430E-06	6.8092E-06	1.9005E-04	7.1062E-05	6.0906E-04
LITHIUM	3.8600E-04	4.8002E-02	7.8439E-03	2.4319E-02	1.1274E-02	1.4565E-02
BERYLLIUM	2.6236E-02	4.6214E-04	1.8867E-03	1.5046E-03	1.5196E-03	1.1890E-03
BORON	2.5170E-02	4.7962E-04	1.3217E-05	8.4052E-04	2.0006E-04	6.0930E-04
CARBON	8.2120E-03	1.6865E-04	4.4094E-06	8.2099E-04	7.0164E-05	4.0463E-04
NITROGEN	8.5150E-04	4.8959E-05	7.9590E-07	5.6511E-06	1.2050E-05	8.8010E-04
FLUORINE	3.0350E-05			3.8694E-06		4.1170E-04
CHLORINE	1.1880E-05	2.3826E-04	8.7628E-06	1.4790E-03	4.9571E-06	1.0550E-03
CALCIUM				6.2700E-04		4.5920E-04
TITANIUM	1.2530E-04		2.9490E-04		1.6910E-04	
CHROMIUM				5.4800E-05		5.8410E-05
IRON	5.5770E-04	1.8131E-03	5.5540E-04	1.3070E-03	8.0810E-04	1.0470E-04
NICKEL			3.0800E-03	1.4450E-04	1.7310E-03	1.1130E-05
MOLYBDENUM	8.1170E-05	5.2760E-07	7.3000E-06	1.4920E-04	4.1000E-04	2.4330E-04
SILVER	9.0990E-06	8.9221E-05	8.7030E-05	5.6530E-04	4.9930E-05	4.9220E-03
BARIUM	5.6800E-04	4.2457E-04	3.1900E-04	1.9420E-03	1.0090E-04	1.5590E-03
TANTALUM				1.6930E-05		1.1140E-05

TABLE 13. (Cont'd.)

ELEMENT	ZONE 37	ZONE 38	ZONE 39	ZONE 40	ZONE 41	ZONE 42
HYDROGEN	3.111E-03	1.385E-03	1.124E-03	2.149E-03	7.233E-04	1.140E-02
HELIUM	1.5825E-01	6.010E-05	1.297E-04	5.545E-05	5.024E-05	1.120E-02
LITHIUM	1.5960E-02	6.750E-03	1.312E-02	5.341E-05	6.350E-03	4.674E-03
BERYLLIUM	2.2453E-02	1.872E-03	1.166E-02	5.390E-03	5.370E-04	5.335E-03
BORON	4.732E-03	2.490E-03	1.313E-02	5.3A0E-04	5.170E-03	1.816E-03
CARBON	4.3A1E-04	1.2670E-04	6.527E-04	1.450E-03	1.74E-03	2.545E-04
NITROGEN		3.791E-04	1.067E-05	1.7A0E-04	1.361E-04	
OXYGEN	7.062E-05	1.2570E-05	2.201E-06	4.055E-06	1.361E-05	
FLUORINE	A.396E-04	8.190E-06	1.406E-05	2.711E-05	1.761E-05	7.181E-06
SODIUM				6.2A1E-06	1.78E-05	
ALUMINUM	2.651E-06	2.651E-06	1.170E-06	2.216E-06	5.667E-06	1.505E-02
CHLORINE	4.396E-04	4.897E-04	1.9300E-04	1.4950E-06	3.024E-04	5.181E-03
CALCIUM				1.413E-04	1.063E-04	1.960E-03
IRON	3.712E-04	1.0136E-05	1.0916E-05	1.041E-05	1.170E-05	
NICKEL	2.807E-03	1.049E-04	2.950E-03	7.181E-04	2.102E-03	
COPPER	2.489E-04	5.170E-04	5.11A0E-04	9.490E-04	3.849E-03	1.427E-03
ZINC	6.007E-04	2.15A0E-05	1.280E-05	4.695E-06	1.490E-05	
MOLYBDENUM	6.470E-04	5.260E-04	5.700E-04	6.012E-05	1.227E-04	1.41E-05
SILVER	1.124E-04	1.143E-04	6.257E-05	1.135E-05	1.155E-04	1.531E-04
TIN	3.563E-04	2.2020E-05	2.1A40E-05	1.7A40E-05	7.630E-06	5.077E-04
BARIUM	2.392E-03	1.3671E-03	7.A461E-05	6.3340E-04	6.050E-04	6.452E-03
TANTALUM		4.9230E-05	4.610E-05	3.817E-06	6.097E-06	6.040E-05
TUNGSTEN	8.519E-06	7.4610E-06	5.3500E-06	1.0800E-05	6.170E-06	6.040E-05

ELEMENT	ZONE 43	ZONE 44	ZONE 45	ZONE 46	ZONE 47	ZONE 48
HYDROGEN	1.5030E-03	3.0550E-04	1.4090E-03	7.6300E-04	4.3092E-05	2.3141E-05
HELIUM	5.5160E-05		7.7150E-04			
LITHIUM	4.5120E-05	2.2330E-04	1.0100E-02	1.8910E-02	1.5452E-02	5.0202E-03
BERYLLIUM	1.1630E-02	1.6330E-03	2.6330E-05	4.9490E-03	1.947E-04	
BORON	1.5610E-02	1.6310E-03	2.7670E-03	5.6310E-03		
CARBON	6.2A00E-03	8.7A50E-04	1.5400E-03	2.3310E-03	2.5117E-03	
NITROGEN	4.5A00E-05	1.9560E-05	1.5A00E-05	2.7650E-04		
OXYGEN	1.1250E-05		5.5140E-05			
FLUORINE	8.410E-06	1.4530E-05	5.9510E-05	2.1470E-05	2.5A1AE-06	4.6451E-05
SODIUM			9.7800E-06			
ALUMINUM	2.370E-06		2.9720E-06		1.6531E-04	
CHLORINE	4.3790E-06		1.2060E-05		5.7A45E-04	
CALCIUM	5.A470E-05		1.5560E-04	4.6060E-04		
IRON		1.2900E-06	1.6360E-05	9.1740E-06		
NICKEL	9.7020E-06		7.3540E-16	1.6A00E-03	3.1705E-02	2.4096E-05
COPPER	7.1200E-03	6.19A0E-05	1.1340E-03	2.A1A0E-05		
ZINC	1.2200E-05	3.6030E-05	1.0360E-03	4.3500E-07		
MOLYBDENUM	5.6270E-05		6.0600E-16			
SILVER	1.0220E-05	1.0170E-04	1.6154E-03	2.3310E-05	3.3640E-05	4.5103E-06
TIN	5.5450E-05	4.0390E-04	9.9000E-04	4.1A70E-05	1.4A70E-05	4.33A8E-06
BARIUM	1.2452E-03	8.3350E-05	3.0240E-05	1.057E-04	6.4917E-07	1.1A55E-04
TANTALUM	4.4020E-05	3.0721E-04	4.6673E-07	5.7729E-04		3.5287E-06
TUNGSTEN	8.5190E-06	8.4040E-05	1.1750E-05		1.2555E-05	

54

TABLE 13. (Cont'd.)

ELEMENT	ZONE 49	ZONE 50	ZONE 51	ZONE 52	ZONE 53	ZONE 54
HYDROGEN		1.8151E-03	1.9682E-03	4.8821E-04	5.7171E-04	5.1913E-04
HELIUM		1.3929E-05	1.7851E-06	1.0725E-02	2.7294E-06	1.2944E-05
LITHIUM	4.1066E-02	6.3151E-02	6.8665E-03	1.0229E-02	1.945E-03	1.0068E-03
BERYLLIUM		1.3361E-02	9.9706E-03	1.1742E-02	1.0035E-02	8.1969E-03
BORON		1.3687E-02	1.1108E-02	3.4067E-03	1.2294E-02	8.9423E-03
CARBON		4.4304E-03	4.2002E-04	1.6710E-03	9.2475E-04	3.5035E-03
NITROGEN		1.3056E-03	1.1216E-03	4.4554E-04	9.1846E-07	1.5557E-06
OXYGEN		1.3466E-05	3.0225E-06	2.5175E-05	1.6761E-05	6.7425E-06
FLUORINE		2.8494E-04	1.6129E-04		2.6692E-09	1.0217E-04
SODIUM				1.0160E-04	2.0442E-03	6.5536E-07
ALUMINUM	2.0670E-04	2.2805E-06	1.6237E-06	9.1724E-05	1.04661E-03	1.6556E-07
CHLORINE		7.1547E-05	2.2945E-05	4.8915E-05	1.8911E-07	4.1756E-04
CALCIUM		4.5284E-06	1.3404E-05		1.1822E-07	5.0152E-05
TITANIUM	6.5950E-05			3.5294E-07		
CHROMIUM		8.3492E-06	1.4304E-05	4.7444E-04	3.0476E-05	2.5030E-05
IRON		6.6678E-04	4.4225E-04	5.5907E-04	3.0434E-05	4.0406E-04
NICKEL	2.9860E-03	1.6367E-04	8.6232E-05	7.0132E-07	6.7444E-04	4.7307E-05
COPPER		2.2700E-06	3.6040E-06	5.6244E-07	7.0885E-04	1.0972E-06
ZINC		7.3704E-04	4.7904E-04	6.0637E-05	8.1657E-07	2.4047E-06
MOLYBDENUM		3.8493E-04	8.1065E-05	2.2629E-05	1.1062E-04	1.8549E-05
SILVER		1.4677E-05	1.0966E-05	1.0193E-05	1.0753E-04	2.1900E-04
TIN		1.5511E-04	1.4630E-04	1.8550E-05	1.4516E-05	2.1940E-04
BARIUM		1.7246E-05	2.6891E-05	5.5325E-06	4.0598E-05	1.0062E-05
TANTALUM		6.4025E-06	8.5846E-07	1.4554E-08	4.5606E-04	1.5719E-06
TUNGSTEN					7.3348E-08	

ELEMENT	ZONE 55	ZONE 56	ZONE 57	ZONE 58	ZONE 59	ZONE 60
HYDROGEN	2.5573E-03	9.6460E-04	3.2187E-05	1.3352E-03	2.1849E-03	8.8347E-05
HELIUM		9.0030E-05	5.4016E-05			6.7477E-02
LITHIUM	6.7192E-05	9.0238E-05	4.9173E-06			
BERYLLIUM		4.7544E-03	7.4743E-03			
BORON	3.3184E-03	5.1406E-03	8.7747E-03	1.0652E-03	1.5515E-03	
CARBON	4.0042E-03	2.5126E-03	3.1119E-03			
NITROGEN	3.6405E-04	1.0830E-05	9.4396E-04			
OXYGEN	1.9100E-06	1.7905E-05	1.5948E-06			
FLUORINE	7.2362E-05	1.2256E-04	5.4701E-05			
SODIUM			1.6194E-04			
ALUMINUM	5.0712E-07		8.5200E-04			
CHLORINE	8.3642E-05		1.2653E-04		2.7865E-03	7.6938E-04
CALCIUM	1.2664E-06	3.2878E-05	5.2347E-07	1.9094E-03		
IRON	8.7566E-05	1.7729E-06	8.4127E-04			
NICKEL	5.5457E-05	1.4966E-03	2.5178E-03			4.9904E-04
COPPER	1.4396E-06	2.5632E-05	5.1619E-05	2.2339E-05	3.5010E-05	
ZINC	3.5836E-04	3.1385E-04	2.0029E-04			
MOLYBDENUM	5.8766E-05	1.0309E-04	1.8104E-05			5.7237E-05
SILVER	6.2207E-05	4.5535E-05	1.5154E-05			1.7493E-04
TIN	5.0101E-06	5.9370E-05	6.2477E-04			1.0051E-04
TANTALUM	3.1091E-07	2.2569E-05	1.3664E-05			
TUNGSTEN		3.4260E-06	2.2236E-07			

55

TABLE 13. (Cont'd.)

ELEMENT	ZONE 61	ZONE 62	ZONE 63	ZONE 64	ZONE 65	ZONE 66
LITHIUM	1.4970E-02					
BERYLLIUM		5.3830E-02	3.3680E-03	1.7490E-03	4.7090E-02	3.7640E-02
BORON		4.4430E-02			1.9610E-02	3.5340E-05
CARBON		4.4850E-03				
FLUORINE	1.1310E-04			1.1640E-02	5.7130E-03	
CHLORINE						2.4060E-05
CALCIUM	3.6570E-05				2.8360E-04	
CHROMIUM	1.5780E-03	4.0830E-03	7.8410E-04	4.3470E-04	3.9550E-03	6.1400E-05
NICKEL			8.6335E-02	4.5797E-02	7.8350E-05	2.7610E-03
HAFNIUM					6.2830E-03	9.0015E-04

Our Sprint model differs in several small ways from the Martin Marietta model. First our model includes the ballast, antennas and nose structure which are unique to this experiment. Further, several of our zones have slightly different volumes, sometimes more realistic and sometimes less realistic than the Martin model depending upon the proximity of the detectors and other geometry knowledge gained from other SAI Sprint programs. However in all cases we maintained the masses documented by Martin causing some of our densities to be slightly different.

Of interest in the conclusion is the fact that although 46 regions were used to model the autopilot, only eleven were used for the MGS. A difference in the experimental calculation comparisons might be an indication of the degree of modeling accuracy required for future internal dose calculations, especially if the MGS results agree as well with the experiment as the A/P results.

3.4   NEUTRON SOURCES AND DOSIMETER RESPONSE

This section documents the neutron sources and the dosimeter response which were supplied by IRT and used in our calculations. In order to gain good experimental statistics without swamping the detector's counting ability, it was necessary to perform the experiment at two different flight path positions. With the experiment at 53.095 meters incident neutrons from 20 MeV to .18 MeV were measured. To measure the lower energy neutrons, the experiment was moved to 17.59 meters and the electronics gated so that neutrons from 327 keV to .6 eV were measured.

Tables 14 and 15 present the spectra of source neutrons at 53.095 and 17.59 meters respectively. The 17.59 meter spectrum also includes the high energy component that could have an effect on the results by

TABLE 14. SPECTRUM OF NEUTRONS AT 53.095 METERS
(Supplied by IRT)

LEADING EDGE ENERGY (MEV)	AVERAGE ENERGY (MEV)	NEUTRON FLUX (NEUTRONS/ MEV-SQ CM- SOURCE MONITOR)	FRACTIONAL STD. DEV. OF THE FLUX	NEUTRON FLUX IN BIN (NEUTRONS/ SQ CM- SOURCE MONITOR)	TOTAL NEUTRON FLUX IN AND ABOVE BIN (NEUTRONS/ SQ CM- SOURCE MONITOR)
1.9872+01	1.9163+01	1.3930+05	5.3127-02	1.9764+05	1.9764+05
1.8454+01	1.7818+01	1.5876+05	5.0534-02	2.0176+05	3.9940+05
1.7183+01	1.6611+01	2.0899+05	4.6256-02	2.3885+05	6.3825+05
1.6040+01	1.5524+01	2.6479+05	4.3404-02	2.7311+05	9.1136+05
1.5008+01	1.4541+01	3.3305+05	3.9794-02	3.1127+05	1.2226+06
1.4074+01	1.3649+01	4.1702+05	3.7303-02	3.5421+05	1.5768+06
1.3224+01	1.2837+01	5.0042+05	3.4771-02	3.8745+05	1.9643+06
1.2450+01	1.2096+01	5.4763+05	3.2969-02	3.8762+05	2.3519+06
1.1742+01	1.1418+01	6.3690+05	3.2105-02	4.1321+05	2.7651+06
1.1094+01	1.0795+01	6.7220+05	3.1714-02	4.0076+05	3.1659+06
1.0497+01	1.0223+01	7.6227+05	3.1252-02	4.1860+05	3.5845+06
9.9482+00	9.6947+00	8.0478+05	3.1220-02	4.0797+05	3.9925+06
9.4413+00	9.2068+00	9.7173+05	3.1041-02	4.5574+05	4.4482+06
8.9723+00	8.7549+00	1.0145+06	3.1922-02	4.4104+05	4.8892+06
8.5375+00	8.3356+00	1.1442+06	3.2229-02	4.6199+05	5.3512+06
8.1338+00	7.9459+00	1.1848+06	3.3039-02	4.4511+05	5.7963+06
7.7581+00	7.5930+00	1.1725+06	3.4250-02	4.1053+05	6.2069+06
7.4079+00	7.2445+00	1.2865+06	3.4806-02	4.2052+05	6.6274+06
7.0811+00	6.9282+00	1.3974+06	3.5718-02	4.2710+05	7.0545+06
6.7754+00	6.6323+00	1.3596+06	3.6770-02	3.8910+05	7.4436+06
6.4892+00	6.3550+00	1.5300+06	3.8770-02	4.1064+05	7.8542+06
6.2208+00	6.0948+00	1.6221+06	3.9680-02	4.0879+05	8.2630+06
5.9688+00	5.8504+00	1.6110+06	4.1055-02	3.8175+05	8.6448+06
5.7319+00	5.6203+00	1.6579+06	4.1821-02	3.6986+05	9.0146+06
5.5088+00	5.4036+00	1.7023+06	4.3996-02	3.5795+05	9.3726+06
5.2985+00	5.1993+00	1.8061+06	4.5086-02	3.5839+05	9.7310+06
5.1001+00	5.0063+00	1.8834+06	4.5711-02	3.5305+05	1.0084+07
4.9126+00	4.8240+00	2.0608+06	4.6697-02	3.6536+05	1.0449+07
4.7353+00	4.6514+00	2.3433+06	4.7903-02	3.9330+05	1.0843+07
4.5675+00	4.4880+00	2.2979+06	4.8602-02	3.6551+05	1.1208+07
4.4084+00	4.3330+00	2.3630+06	4.9726-02	3.5648+05	1.1565+07
4.2576+00	4.1859+00	2.4443+06	4.9779-02	3.5013+05	1.1915+07
4.1143+00	4.0463+00	2.4765+06	4.9548-02	3.3709+05	1.2252+07
3.9782+00	3.9135+00	2.5842+06	5.0700-02	3.3456+05	1.2586+07
3.8487+00	3.7871+00	2.6925+06	5.2077-02	3.3177+05	1.2918+07
3.7255+00	3.6668+00	2.7577+06	5.2575-02	3.2374+05	1.3242+07
3.6081+00	3.5522+00	2.8068+06	5.2786-02	3.1414+05	1.3556+07
3.4962+00	3.4428+00	2.7890+06	5.2491-02	2.9778+05	1.3854+07
3.3894+00	3.3385+00	2.9541+06	5.5077-02	3.0118+05	1.4155+07
3.2875+00	3.2388+00	2.8303+06	5.4363-02	2.7576+05	1.4431+07
3.1901+00	3.1435+00	2.9004+06	5.3601-02	2.7012+05	1.4701+07
3.0969+00	3.0524+00	2.9852+06	5.4906-02	2.6603+05	1.4967+07
3.0078+00	2.9651+00	2.9931+06	5.5699-02	2.5537+05	1.5222+07
2.9225+00	2.8816+00	2.8698+06	5.6905-02	2.3457+05	1.5457+07

TABLE 14. (Cont'd.)

LEADING EDGE ENERGY (MEV)	AVERAGE ENERGY (MEV)	NEUTRON FLUX (NEUTRONS/ MEV-SQ CM- SOURCE MONITOR)	FRACTIONAL STD. DEV. OF THE FLUX	NEUTRON FLUX IN BIN (NEUTRONS/ SQ CM- SOURCE MONITOR)	TOTAL NEUTRON FLUX IN AND ABOVE BIN (NEUTRONS/ SQ CM- SOURCE MONITOR)
2.8407+00	2.8016+00	2.8767+06	5.8091-02	2.2538+05	1.5682+07
2.7624+00	2.7248+00	3.0244+06	5.6689-02	2.2726+05	1.5910+07
2.6873+00	2.6512+00	3.9901+06	5.0786-02	2.8776+05	1.6197+07
2.6151+00	2.5805+00	4.6582+06	4.6911-02	3.2257+05	1.6520+07
2.5459+00	2.5126+00	5.1730+06	4.6376-02	3.4409+05	1.6864+07
2.4794+00	2.4474+00	5.1148+06	4.4903-02	3.2719+05	1.7191+07
2.4154+00	2.3847+00	5.5766+06	4.3827-02	3.4291+05	1.7534+07
2.3539+00	2.3243+00	5.6845+06	4.3933-02	3.3649+05	1.7871+07
2.2947+00	2.2662+00	6.4712+06	4.2894-02	3.6866+05	1.8239+07
2.2378+00	2.2103+00	6.8677+06	4.2100-02	3.7692+05	1.8616+07
2.1829+00	2.1564+00	6.9771+06	4.1589-02	3.6895+05	1.8985+07
2.1300+00	2.0515+00	6.7023+06	4.0101-02	1.0515+06	2.0037+07

*************** ABOVE DATA TAKEN WITH NE-213 DETECTOR **************

LEADING EDGE ENERGY (MEV)	AVERAGE ENERGY (MEV)	NEUTRON FLUX (NEUTRONS/ MEV-SQ CM- SOURCE MONITOR)	FRACTIONAL STD. DEV. OF THE FLUX	NEUTRON FLUX IN BIN (NEUTRONS/ SQ CM- SOURCE MONITOR)	TOTAL NEUTRON FLUX IN AND ABOVE BIN (NEUTRONS/ SQ CM- SOURCE MONITOR)
1.9731+00	1.8866+00	8.7712+06	1.5188-02	1.5165+06	2.1553+07
1.8002+00	1.7246+00	1.0256+07	1.4823-02	1.5497+06	2.3103+07
1.6491+00	1.5827+00	1.1758+07	1.4554-02	1.5615+06	2.4664+07
1.5163+00	1.4576+00	1.3079+07	1.4216-02	1.5342+06	2.6198+07
1.3990+00	1.3468+00	1.3496+07	1.4357-02	1.4076+06	2.7606+07
1.2947+00	1.2482+00	1.4371+07	1.4063-02	1.3365+06	2.8943+07
1.2017+00	1.1600+00	1.5251+07	1.3807-02	1.2704+06	3.0213+07
1.1184+00	1.0809+00	1.5743+07	1.3735-02	1.1807+06	3.1394+07
1.0434+00	1.0088+00	1.6176+07	1.3635-02	1.1181+06	3.2512+07
9.7428-01	9.4373-01	1.7006+07	1.3997-02	1.0391+06	3.3551+07
9.1318-01	8.8541-01	1.9681+07	1.3864-02	1.0929+06	3.4644+07
8.5765-01	8.3234-01	2.0423+07	1.4397-02	1.0336+06	3.5677+07
8.0704-01	7.8391-01	2.0256+07	1.4907-02	9.3704+05	3.6614+07
7.6078-01	7.3958-01	1.9660+07	1.5293-02	8.3339+05	3.7448+07
7.1839-01	6.9891-01	2.1250+07	1.4817-02	8.2769+05	3.8275+07
6.7944-01	6.6151-01	2.0165+07	1.5235-02	7.2312+05	3.8999+07
6.4358-01	6.2703-01	1.7720+07	1.6265-02	5.8653+05	3.9585+07
6.1048-01	5.9517-01	1.4309+07	1.8200-02	4.3800+05	4.0023+07
5.7987-01	5.5252-01	1.6988+07	1.1889-02	9.2907+05	4.0952+07
5.2518-01	5.0152-01	1.7795+07	1.1572-02	8.4188+05	4.1794+07
4.7787-01	4.5727-01	1.8058+07	1.1258-02	7.4381+05	4.2538+07
4.3668-01	4.1864-01	1.9128+07	1.1277-02	6.9014+05	4.3228+07
4.0060-01	3.8470-01	2.0979+07	1.1044-02	6.6692+05	4.3895+07
3.6881-01	3.5473-01	2.1531+07	1.1139-02	6.0631+05	4.4501+07
3.4065-01	3.2813-01	2.2053+07	1.1237-02	5.5221+05	4.5053+07
3.1561-01	3.0441-01	2.1237+07	1.1675-02	4.7550+05	4.5529+07
2.9322-01	2.8318-01	2.0234+07	1.2255-02	4.0630+05	4.5935+07
2.7314-01	2.6409-01	2.3913+07	1.1652-02	4.3259+05	4.6368+07
2.5505-01	2.4687-01	2.4112+07	1.2123-02	3.9423+05	4.6762+07
2.3870-01	2.3129-01	2.4621+07	1.2691-02	3.6488+05	4.7127+07
2.2388-01	2.1713-01	2.2373+07	1.4229-02	3.0181+05	4.7429+07
2.1039-01	2.0424-01	2.1205+07	1.5776-02	2.6082+05	4.7690+07

59

TABLE 14. (Cont'd.)

LEADING EDGE ENERGY (MEV)	AVERAGE ENERGY (MEV)	NEUTRON FLUX (NEUTRONS/ MEV-SQ CM- SOURCE MONITOR)	FRACTIONAL STD. DEV. OF THE FLUX	NEUTRON FLUX IN BIN (NEUTRONS/ SQ CM- SOURCE MONITOR)	TOTAL NEUTRON FLUX IN AND ABOVE BIN (NEUTRONS/ SQ CM- SOURCE MONITOR)
1.9809-01	1.9246-01	2.2219+07	1.6541-02	2.5019+05	4.7940+07
1.8683-01	1.8167-01	2.4007+07	1.7031-02	2.4775+05	4.8188+07
1.7651-01	1.7176-01	2.4411+07	1.7984-02	2.3166+05	4.8419+07
1.6702-01	1.6264-01	2.2955+07	1.9669-02	2.0086+05	4.8620+07
1.5827-01	1.5423-01	1.8849+07	2.2857-02	1.5211+05	4.8772+07
1.5020-01	1.4646-01	2.0099+07	2.3157-02	1.5014+05	4.8922+07
1.4273-01	1.3762-01	2.1140+07	1.9436-02	2.1584+05	4.9138+07
1.3252-01	1.2794-01	2.7561+07	1.7746-02	2.5218+05	4.9390+07
1.2337-01	1.1925-01	2.7190+07	1.8670-02	2.2377+05	4.9614+07
1.1514-01	1.1142-01	2.8348+07	1.8900-02	2.1091+05	4.9825+07
1.0770-01	1.0433-01	2.7901+07	1.9651-02	1.8805+05	5.0013+07
1.0096-01	9.7900-02	2.6380+07	2.0850-02	1.6145+05	5.0175+07
9.4840-02	9.2048-02	2.2712+07	2.3310-02	1.2682+05	5.0301+07
8.9256-02	8.6703-02	1.8576+07	2.6671-02	9.4830+04	5.0396+07
8.4151-02	8.1811-02	2.0088+07	2.6398-02	9.3992+04	5.0490+07
7.9472-02	7.7322-02	2.6703+07	2.3529-02	1.1482+05	5.0605+07
7.5172-02	7.3192-02	3.2039+07	2.2109-02	1.2684+05	5.0732+07
7.1213-02	6.9385-02	3.5354+07	2.1661-02	1.2922+05	5.0861+07
6.7558-02	6.5867-02	3.4131+07	2.2712-02	1.1540+05	5.0976+07
6.4177-02	6.2114-02	3.6367+07	1.9728-02	1.5005+05	5.1126+07

TABLE 15. SPECTRUM OF NEUTRONS AT 17.59 METERS
(Supplied by IRT)

UPPER EDGE NEUTRON ENERGY (EV)	LEADING EDGE TIME (MICRO-SECONDS)	AVERAGE NEUTRON ENERGY (EV)	AVERAGE TIME (MICRO-SECONDS)	NEUTRON FLUX (NEUT/MICRO-SECOND-SQ CM-SOURCE MONITOR)	NEUTRON FLUX (NEUT/EV-SQ CM-SOURCE MONITOR)	FRACT-IONAL STD. DEV. OF THE FLUX	NEUTRON FLUX IN BIN (NEUT/SQ CM-SOURCE MONITOR)	TOTAL NEUTRON FLUX IN AND ABOVE BIN (NEUT/SQ CM-SOURCE MONITOR)
1.9900+07	2.8969-01	1.8303+07	3.0555-01	3.85+07	3.82-01	8.68-02	1.22+06	1.22+06
1.6707+07	3.2142-01	1.4685+07	3.4123-01	6.05+07	5.94-01	6.09-02	2.40+06	3.61+06
1.2663+07	3.6103-01	1.1451+07	3.8084-01	7.42+07	1.21+00	5.01-02	2.94+06	6.55+06
1.0240+07	4.0065-01	9.1971+06	4.2447-01	8.52+07	1.94+00	4.39-02	4.05+06	1.06+07
8.1543+06	4.4830-01	7.4012+06	4.7209-01	8.37+07	2.64+00	4.73-02	3.97+06	1.46+07
6.6482+06	4.9587-01	6.0069+06	5.2365-01	7.63+07	3.30+00	5.04-02	4.24+06	1.89+07
5.3657+06	5.5143-01	4.8369+06	5.8311-01	6.45+07	3.86+00	5.50-02	4.09+06	2.30+07
4.3081+06	6.1479-01	3.8809+06	6.5052-01	5.95+07	4.97+00	5.65-02	4.25+06	2.72+07
3.4537+06	6.8624-01	3.1128+06	7.2591-01	4.78+07	5.53+00	5.75-02	3.79+06	3.09+07
2.7720+06	7.6557-01	2.5019+06	8.0918-01	5.74+07	9.27+00	4.73-02	5.02+06	3.59+07
2.2319+06	8.5278-01	2.0184+06	9.0038-01	7.63+07	1.71+01	3.77-02	7.26+06	4.32+07
1.8050+06	9.4798-01	1.6201+06	1.0047+00	8.18+07	2.51+01	3.37-02	9.27+06	5.22+07

```
***************** ABOVE DATA TAKEN WITH NE-213 DETECTOR *****************
```

UPPER EDGE NEUTRON ENERGY (EV)	LEADING EDGE TIME (MICRO-SECONDS)	AVERAGE NEUTRON ENERGY (EV)	AVERAGE TIME (MICRO-SECONDS)	NEUTRON FLUX (NEUT/MICRO-SECOND-SQ CM-SOURCE MONITOR)	NEUTRON FLUX (NEUT/EV-SQ CM-SOURCE MONITOR)	FRACT-IONAL STD. DEV. OF THE FLUX	NEUTRON FLUX IN BIN (NEUT/SQ CM-SOURCE MONITOR)	TOTAL NEUTRON FLUX IN AND ABOVE BIN (NEUT/SQ CM-SOURCE MONITOR)
1.4353+06	1.0614+00	1.2899+06	1.1251+00	7.87+07	3.45+01	3.09-02	1.00+07	6.24+07
1.1445+06	1.1886+00	1.0105+06	1.2735+00	6.88+07	4.35+01	3.09-02	1.17+07	7.40+07
8.7654+05	1.3583+00	7.8464+05	1.4430+00	5.64+07	5.22+01	3.09-02	9.59+06	8.37+07
6.9274+05	1.5279+00	6.2698+05	1.6126+00	3.62+07	4.66+01	3.09-02	6.14+06	8.98+07
5.6122+05	1.6975+00	5.0236+05	1.8034+00	3.11+07	5.63+01	3.09-02	6.60+06	9.64+07
4.4351+05	1.9095+00	4.0140+05	2.0154+00	2.79+07	7.04+01	3.09-02	5.94+06	1.02+08
3.5930+05	2.1215+00	3.2288+05	2.2487+00	1.88+07	6.55+01	3.09-02	4.76+06	1.07+08
2.8647+05	2.3758+00	2.6010+05	2.5031+00	1.52+07	7.35+01	3.09-02	3.86+06	1.11+08
2.3373+05	2.6303+00	2.1123+05	2.7786+00	1.08+07	7.11+01	3.09-02	3.20+06	1.14+08
1.8874+05	2.9271+00	1.7015+05	3.0967+00	7.63+06	6.94+01	3.09-02	2.59+06	1.17+08
1.5157+05	3.2663+00	1.3654+05	3.4571+00	5.36+06	6.80+01	3.09-02	2.05+06	1.19+08
1.2152+05	3.6479+00	1.0952+05	3.8599+00	4.28+06	7.55+01	3.18-02	1.81+06	1.21+08
9.7527+04	4.0719+00	8.8019+04	4.3052+00	2.61+06	6.39+01	3.62-02	1.22+06	1.22+08
7.8511+04	4.5384+00	7.0995+04	4.7927+00	2.34+06	7.91+01	3.49-02	1.19+06	1.23+08
6.3479+04	5.0472+00	5.7536+04	5.3228+00	2.31+06	1.07+02	3.24-02	1.27+06	1.24+08
5.1594+04	5.5984+00	4.6885+04	5.8952+00	1.68+06	1.06+02	3.55-02	1.00+06	1.25+08
4.2176+04	6.1920+00	3.8217+04	6.5312+00	1.08+06	9.23+01	3.49-02	7.30+05	1.26+08
3.4258+04	6.8704+00	3.1004+04	7.2520+00	1.10+06	1.29+02	3.65-02	8.42+05	1.27+08
2.7750+04	7.6336+00	2.5114+04	8.0577+00	1.10+06	1.77+02	3.37-02	9.39+05	1.28+08
2.2478+04	8.4817+00	2.0361+04	8.9481+00	9.67+05	2.12+02	3.37-02	8.98+05	1.29+08
1.8244+04	9.4146+00	1.6551+04	9.9234+00	7.42+05	2.23+02	3.58-02	7.55+05	1.29+08
1.4859+04	1.0432+01	1.3462+04	1.1005+01	6.24+05	2.56+02	3.62-02	7.16+05	1.30+08
1.2065+04	1.1577+01	1.0962+04	1.2191+01	5.31+05	2.95+02	3.68-02	6.55+05	1.31+08
9.8595+03	1.2807+01	8.9602+03	1.3485+01	4.23+05	3.18+02	3.86-02	5.73+05	1.31+08
8.0609+03	1.4164+01	7.3149+03	1.4927+01	3.67+05	3.76+02	3.83-02	5.58+05	1.32+08
6.5688+03	1.5690+01	5.9592+03	1.6538+01	2.92+05	4.05+02	3.99-02	4.96+05	1.32+08
5.3497+03	1.7386+01	4.8564+03	1.8319+01	2.58+05	4.89+02	3.99-02	4.81+05	1.33+08

TABLE 15. (Cont'd.)

UPPER EDGE NEUTRON ENERGY (EV)	LEADING EDGE TIME (MICRO-SECONDS)	AVERAGE NEUTRON ENERGY (EV)	AVERAGE TIME (MICRO-SECONDS)	NEUTRON FLUX (NEUT/ MICRO-SECOND-SQ CM-SOURCE MONITOR)	NEUTRON FLUX (NEUT/ EV-SQ CM-SOURCE MONITOR)	FRACT-IONAL STD. DEV. OF THE FLUX	NEUTRON FLUX IN BIN (NEUT/ SQ CM-SOURCE MONITOR)	TOTAL NEUTRON FLUX IN AND ABOVE BIN (NEUT/ SQ CM-SOURCE MONITOR)
4.3630+03	1.9251+01	3.9658+03	2.0269+01	2.20+05	5.63+02	4.05-02	4.48+05	1.33+08
3.5686+03	2.1287+01	3.2389+03	2.2432+01	1.84+05	6.39+02	4.11-02	4.20+05	1.34+08
2.9091+03	2.3576+01	2.6435+03	2.4827+01	1.54+05	7.26+02	4.23-02	3.86+05	1.34+08
2.3778+03	2.6078+01	2.1500+03	2.7541+01	1.32+05	8.47+02	4.29-02	3.86+05	1.35+08
1.9223+03	2.9003+01	1.7216+03	3.0806+01	1.09+05	9.73+02	4.20-02	3.92+05	1.35+08
1.5208+03	3.2608+01	1.3770+03	3.4410+01	9.46+04	1.18+03	4.42-02	3.40+05	1.35+08
1.2332+03	3.6212+01	1.1086+03	3.8375+01	8.03+04	1.39+03	4.33-02	3.46+05	1.36+08
9.8405+02	4.0538+01	8.9376+02	4.2700+01	6.64+04	1.59+03	4.70-02	2.87+05	1.36+08
8.0346+02	4.4863+01	7.2633+02	4.7385+01	5.74+04	1.89+03	4.60-02	2.91+05	1.36+08
6.4921+02	4.9908+01	5.8545+02	5.2792+01	5.10+04	2.31+03	4.51-02	2.95+05	1.36+08
5.2169+02	5.5674+01	4.7008+02	5.8918+01	4.19+04	2.63+03	4.70-02	2.71+05	1.37+08
4.1848+02	6.2162+01	3.7726+02	6.5766+01	3.70+04	3.25+03	3.18-02	2.68+05	1.37+08
3.3603+02	6.9370+01	3.0333+02	7.3335+01	3.35+04	4.07+03	3.09-02	2.66+05	1.37+08
2.7063+02	7.7299+01	2.4476+02	8.1624+01	2.85+04	4.76+03	3.09-02	2.46+05	1.37+08
2.1890+02	8.5949+01	1.9844+02	9.0634+01	2.49+04	5.68+03	3.09-02	2.33+05	1.38+08
1.7798+02	9.5318+01	1.6077+02	1.0072+02	1.95+04	6.14+03	3.09-02	2.10+05	1.38+08
1.4356+02	1.0613+02	1.3018+02	1.1189+02	1.60+04	6.89+03	3.24-02	1.84+05	1.39+08
1.1680+02	1.1767+02	1.0577+02	1.2416+02	1.47+04	8.62+03	3.12-02	1.90+05	1.39+08
9.4748+01	1.3064+02	8.5800+01	1.3785+02	1.23+04	9.90+03	3.12-02	1.77+05	1.39+08
7.6851+01	1.4506+02	6.9651+01	1.5298+02	1.04+04	1.15+04	3.15-02	1.66+05	1.39+08
6.2450+01	1.6091+02	5.6682+01	1.6956+02	9.86+03	1.48+04	3.09-02	1.71+05	1.39+08
5.0914+01	1.7821+02	4.6148+01	1.8795+02	8.23+03	1.67+04	3.09-02	1.60+05	1.39+08
4.1382+01	1.9767+02	3.7614+01	2.0812+02	7.54+03	2.08+04	3.09-02	1.57+05	1.40+08
3.3846+01	2.1858+02	3.0687+01	2.3047+02	5.45+03	2.05+04	3.43-02	1.30+05	1.40+08
2.7528+01	2.4236+02	2.5538+01	2.5221+02	5.00+03	2.48+04	3.37-02	9.90+04	1.40+08

********** ABOVE DATA TAKEN WITH LI-6 GLASS SCINTILLATOR DETECTOR ***********

2.3547+01	2.6206+02	2.1290+01	2.7677+02	3.24+03	2.12+04	4.51-02	9.54+04	1.40+08
1.9034+01	2.9147+02	1.7240+01	3.0752+02	3.50+03	3.14+04	3.92-02	1.12+05	1.40+08
1.5446+01	3.2356+02	1.4020+01	3.4094+02	3.01+03	3.68+04	3.86-02	1.05+05	1.40+08
1.2594+01	3.5833+02	1.1390+01	3.7838+02	3.24+03	5.43+04	3.34-02	1.30+05	1.40+08
1.0186+01	3.9844+02	9.2462+00	4.1983+02	2.76+03	6.29+04	3.37-02	1.18+05	1.40+08
8.3064+00	4.4122+02	7.5295+00	4.6529+02	2.12+03	6.55+04	3.46-02	1.02+05	1.40+08
6.7527+00	4.8936+02	6.1202+00	5.1609+02	7.28+02	3.09+04	5.59-02	3.89+04	1.41+08
5.4877+00	5.4283+02	4.9773+00	5.7225+02	1.51+03	8.72+04	3.43-02	8.88+04	1.41+08
4.4670+00	6.0167+02	4.0572+00	6.3375+02	1.42+03	1.11+05	3.21-02	9.08+04	1.41+08
3.6474+00	6.6584+02	3.3081+00	7.0194+02	1.24+03	1.32+05	3.09-02	8.93+04	1.41+08
2.9687+00	7.3804+02	2.6919+00	7.7815+02	1.11+03	1.62+05	3.00-02	8.98+04	1.41+08
2.4151+00	8.1827+02	2.1914+00	8.6239+02	9.67+02	1.90+05	3.03-02	8.52+04	1.41+08
1.9678+00	9.0650+02	1.7880+00	9.5465+02	8.37+02	2.23+05	3.00-02	8.06+04	1.41+08
1.6081+00	1.0028+03	1.4606+00	1.0563+03	7.18+02	2.61+05	2.97-02	7.67+04	1.41+08
1.3131+00	1.1097+03	1.1933+00	1.1686+03	6.19+02	3.04+05	2.97-02	7.30+04	1.41+08
1.0734+00	1.2274+03	9.7485-01	1.2929+03	5.31+02	3.53+05	3.00-02	6.94+04	1.41+08
8.7630-01	1.3585+03	7.9614-01	1.4306+03	4.36+02	3.92+05	3.06-02	6.29+04	1.41+08

TABLE 15. (Cont'd.)

UPPER EDGE NEUTRON ENERGY (EV)	LEADING EDGE TIME (MICRO-SECONDS)	AVERAGE NEUTRON ENERGY (EV)	AVERAGE TIME (MICRO-SECONDS)	NEUTRON FLUX (NEUT/ MICRO-SECOND-SQ CM-SOURCE MONITOR)	NEUTRON FLUX (NEUT/ EV-SQ CM-SOURCE MONITOR)	FRACT-IONAL STD. DEV. OF THE FLUX	NEUTRON FLUX IN BIN (NEUT/ SQ CM-SOURCE MONITOR)	TOTAL NEUTRON FLUX IN AND ABOVE BIN (NEUT/ SQ CM-SOURCE MONITOR)
7.1599-01	1.5028+03	6.5026-01	1.5830+03	3.42+02	4.15+05	3.28-02	5.48+04	1.41+08
5.8452-01	1.6633+03	5.3114-01	1.7515+03	2.55+02	4.22+05	3.62-02	4.50+04	1.41+08
4.7776-01	1.8398+03	4.3413-01	1.9373+03	1.55+02	3.45+05	4.60-02	3.02+04	1.41+08

************** ABOVE DATA TAKEN WITH BF3 PROPORTIONAL COUNTER ***************

63

thermalizing in the experiment and residing until later times. For this reason our calculations at 17.53 meters included the entire spectrum and results were also calculated at times earlier than the experimental times. This source data was supplied by IRT on computer cards which were used as input to our source routines (described in the next section). The beam profile measured by IRT was also included in our calculations.

The IRT silicon dosimeter is a silicon surface barrier detector surrounded by silicon and encased in an aluminum can. The silicon surface barrier detector measures ionizing energy deposition above 200 keV, so that the entire silicon dosimeter has a response much like a free field ionizing silicon response which has been attenuated through the surrounding silicon and aluminum can.

The response of the dosimeter to neutrons and to gamma rays was supplied to us by IRT. The response to neutrons was measured, and the response to gamma rays was calculated with the SANDYL code and verified by measurement. Our approach was to use the IRT response at the outside of the dosimeter and also to include the dosimeter in our calculations. This required a special treatment of the dosimeter. For all adjoint calculations, the adjoint particles were initialized isotropically at the center of the dosimeter sampling the IRT response to determine the energy and particle type. For the particle's first flight, the dosimeter was assumed void so that the dosimeter response would be maintained to the surface of the dosimeter. For the remainder of the adjoint random walk, the dosimeter material was included.

For the forward calculations, which used a next flight estimator, the detector was assumed void for all estimations and the material was included for all transport. Also no estimation was performed for scatterings within the dosimeter. These treatments assured that the dosimeter

64

response would apply to the surface of the dosimeter and that the dosimeter be included in the transport calculation.

Our dosimeter response was presented in the previous section, see Table 5, in our 36 energy group.

4. STEEL-STYROFOAM CALCULATIONS

Before attempting the more complex Sprint missile experiment, IRT fabricated and measured the steel-styrofoam cylindrical sample which was designed to have characteristics similar to the real Sprint experiment. Using the same procedures later used for the Sprint experiment, the cylinder response was measured at both the 17 meter and the 53 meter stations of the flight path. The 17 meter measurement observed the response to the lower energy neutrons from .25 MeV to .4 eV, and the 53 meter experiment measured the higher count rates of the high energy neutrons from 100 keV to 20 MeV. In this section details and results of three time dependent Monte Carlo calculations of these two experiments are presented. The 17 meter experiment was calculated with both forward and adjoint techniques while the 50 meter experiment was calculated only with the adjoint method.

4.1 FORWARD MONTE CARLO TECHNIQUES

The forward Monte Carlo calculations of the cylinder experiment was performed with the standard version of MORSE which was modified slightly to treat the time dependent nature of the source. The scoring technique used was the next flight estimator (subroutine RELCOL). A track length per volume estimator was also included as a check. The LINAC source as measured by IRT was previously presented in Tables 14 and 15. Description of the Monte Carlo techniques for both the forward and adjoint calculations follow. These same techniques were also employed for the missile calculations which are described in the next section.

Our actual sampling scheme was to select a continuous energy off a uniform lethargy distribution and adjust the source weight to agree with the IRT source. The energy was selected from

$$E = E_{min}\left(\frac{E_{max}}{E_{min}}\right)^{\xi}$$

where ξ is a uniform random number between 0 and 1 and E_{min} and E_{max} are the lowest and highest energies respectively. The source weight was then calculated by

$$SW = A \cdot E \cdot f(E) \, \ell n\left(\frac{E_{max}}{E_{min}}\right)$$

which assures a fair game. Here $f(E)$ is the Intelcom source in units neutrons$/(eV$-cm^2-source monitor$)$ and A is the area of the beam. Rather than setting the source particle's weight to SW, the weight was set to 1.0 and SW was carried with the particle and all its secondaries to be included later as a factor in all scores. In this manner transport importance parameters were independent of a particle's initial energy.

The actual steps taken in the forward MORSE calculation are listed below:

1. A continuous energy E was sampled from a uniform lethargy distribution and a source weight was calculated as a function of E and the Intelcom supplied source.

2. The time of arrival t at the front of the cylinder was calculated from E and the flight path length.

3. The energy group IG corresponding to E was determined.

4. An uncollided contribution was scored in the time bin corresponding to the time of arrival at the detector center. The score was

$$\frac{SW}{A} \ F(IG) \ R(IG)$$

where the $F(IG)$ are pre-calculated attenuation factors for each energy group through the centerline of the sample to the detector point and $R(IG)$ is the detector response (Table 5).

5. A source position was sampled on the front surface of the cylinder from the beam shape.

6. From here a standard MORSE calculation with WATE = 1.0 and using the next flight estimator was initiated with the initial values calculated in steps 1-5 above.

7. For each score the source weight factor was also included.

4.2   TIME DEPENDENT ADJOINT CALCULATION

In Section 2 the adjoint next flight estimator to a beam was discussed for the calculation of the steady state energy response. The extension of this technique to calculate the time dependent deposition should be straightforward, especially since the time a particle takes to travel from its source to the detector will be the same as an adjoint history traveling the reverse trajectory from the detector to the source. In a time dependent adjoint calculation the next flight estimator knows a particle's weight (WATE), an energy group (IG), and the time from the detector (AGE) when the particle is entering the beam at the front of the cylinder. It only remains to determine the correct time bin (or time bins) and source intensity for the score. A misconception at this point of how to fold the adjoint fluence with the time and energy dependent source caused considerable consternation and as such is worth explaining in detail.

68

The weight of the adjoint particle upon entering the source beam represents a total dose in the detector per incident particle per unit area from a source neutron with energy group IG [the units of weight are rad(Si)/(n/cm^2)]. The time AGE represents a random estimate of time elapsed between entry of the neutron into the sample and deposition of the dose. The three plots of Fig. 5 schematically depict the correct procedure for scoring the time dependence.

Plots a and b define the source; a) giving the energy-time correlation which in this case is defined by the flight path, and b) depicting the time dependence of the source. In our case of energy and time correlation these two curves exactly define the source. More complicated energy and time dependent sources would be represented by a surface in time-energy-source intensity space. The adjoint radiation transport results are contained in the three quantities, AGE (transport time), WATE (adjoint particle weight), and IG (the energy group number). The third plot c) then defines the correct transformation required to fold the transport results with the time dependent source. The energy group IG on plot a) defines a time domain on plot b) which encloses a portion of the time dependent source rate. It is this portion of the time dependent source rate that should be multiplied by WATE and scored as a dose rate at the times AGE later than the source times. Notice that the shape of the neutron source rate should be preserved when scoring it into the dose rate results.

For actual computer implementation the process is complicated by the existance of three sets of time bins associated with each of the three curves. The energy group boundaries define broad time boundaries TIG corresponding to the times of arrival of the energy group edges. The source rate actually exists as a fine histogram with times TSØR and average count rates RSØR. The final count rate then is to be scored into

69
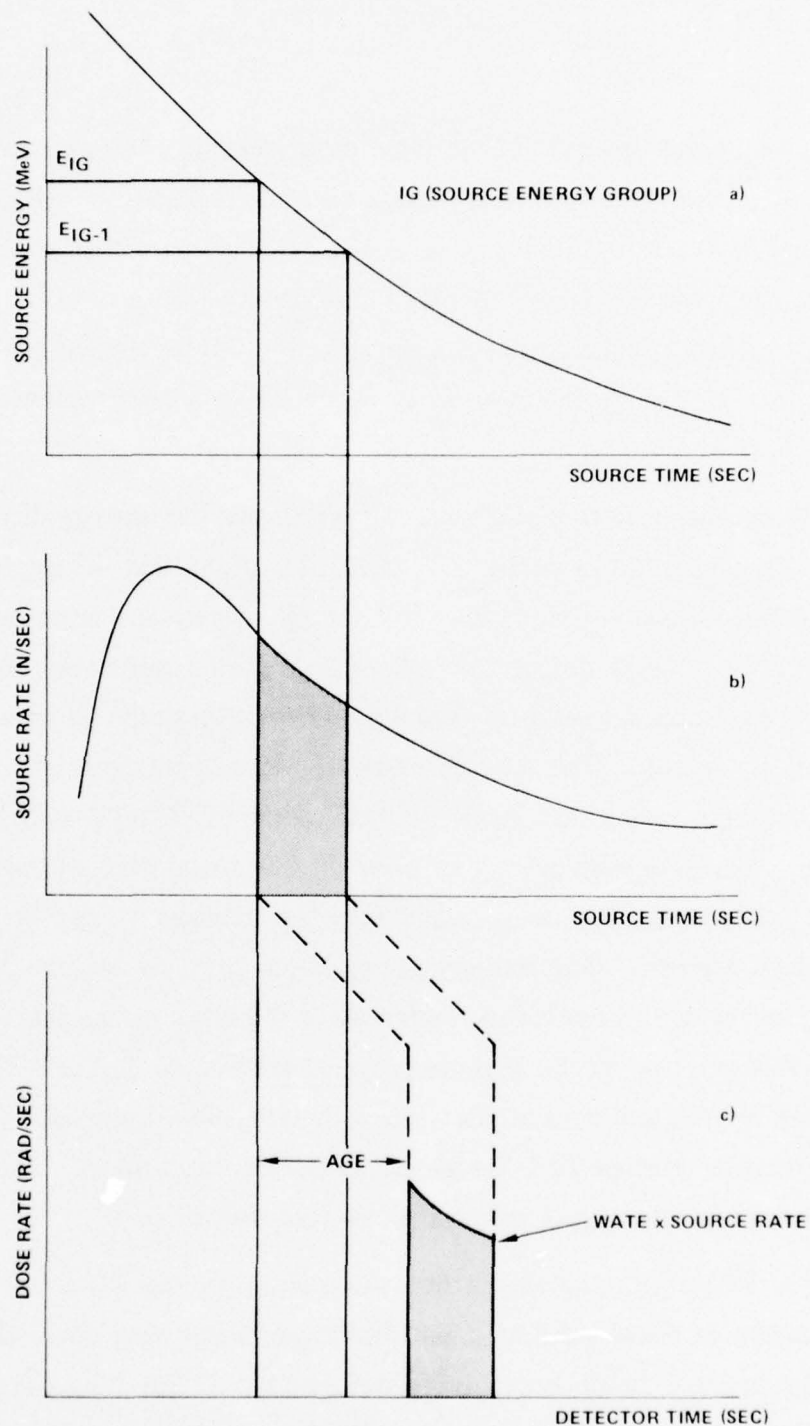
Figure 5. Graphical Depiction of Adjoint Time Dependent Scoring.
(a) Source Energy-Time Correlation, (b) Time Dependence
of the Source, and (c) Procedure for Scoring a Time
Dependent dose rate

70

time bins TBIN decided by the code user. Figure 6 depicts these three time bins and demonstrates our algorithm for scoring the dose rate. Before any transport is performed the source rate histogram (TSØR, RSØR) is represented by TSAV(IG, I) and SØR(IG, I) where the TSAV's are the centers of the smallest time bins bounded either by the TSØR's or the TIG's. The SØR's then are the total number of neutrons represented at times TSAV which are the product of the corresponding RSØR and time product of the corresponding RSØR and time bin widths. Let NIS(IG) be the number of times TSAV that lie between TIG(IG) and TIG (IG-1). For each adjoint estimate to the beam, NIS(IG) scores are made at times AGE + TSAV (IG, I). Each scoring value is WATE*SØR(IG, I). The scoring routine determines which time bin TBIN contains AGE +TSAV (IG, I) and sums the scoring value in the appropriate bin. At the conclusion of the Monte Carlo calculation, each value in the TBIN's array is divided by the time bin widths TBIN(I) - TBIN(I + 1) to change the units back to a dose rate (rads/sec). This procedure performs the transformation indicated in the three curves of Fig. 5 within the resolution of the user defined time bins TBIN.

When first attempting the time dependent adjoint calculation we unfortunately discovered that other more intuitive scoring algorithms can in fact given the wrong answer. It is essential that the shape of the time dependent source rate possible with group IG be scored in the analysis time bins with the same shape but with time delayed by AGE. We maintained the shape by scoring several times for each estimate. A single time could be sampled and the entire source enclosed by TIG(IG) and TIG(IG + 1) scored at this time, but of course this would increase the variance.

71
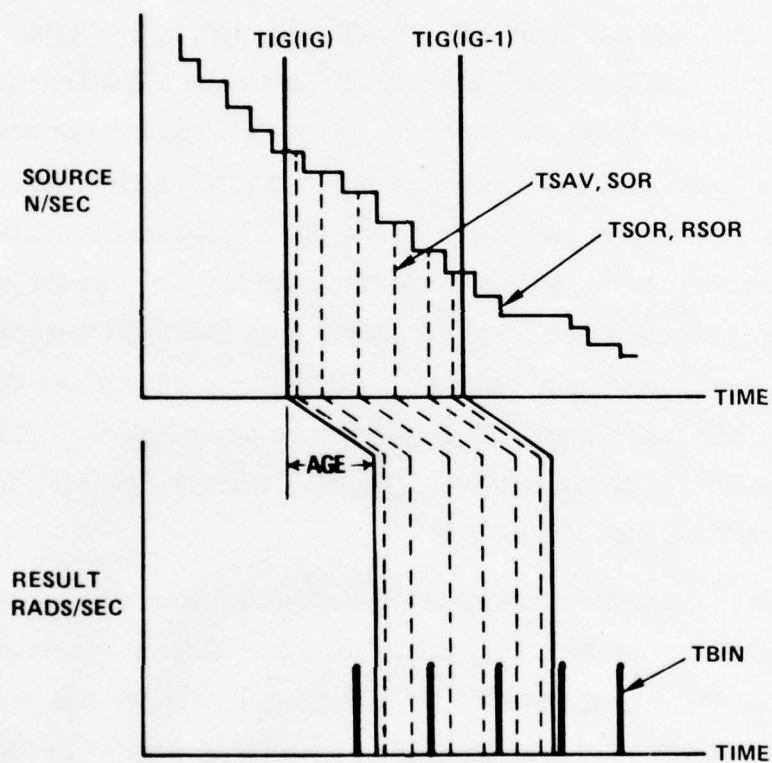
Figure 6.   Three Sets of Time Bins Used for Adjoint
Time Dependent Scoring

72

This adjoint technique was used to calculate the steel-styrofoam and Sprint missile time dependent response for both the 17 and 53 meter experiments.

4.3 COMPARISONS OF THE STEEL-STYROFOAM RESULTS - FORWARD, ADJOINT, AND EXPERIMENT

The steel-styrofoam 17 meter experiment was calculated with both forward and adjoint Monte Carlo while the 53 meter experiment was calculated with the adjoint technique only. Figure 7 compares the adjoint steel-styrofoam calculation at 53.59 meters to the IRT experiment. The results are plotted as dose with the units rad(Si)/(μsec $\cdot$ source monitor) versus time (μsec). The verticle bars represent a standard deviation. The 53 meter adjoint calculation tracked 40,000 histories in 5.77 minutes on a CDC 7600 computer. Splitting and Russian roulette parameters were set so that 10% of the particles split and 50% were killed by Russian roulette.

The agreement with the experiment appears to be excellent up to 4 microseconds where the calculation drops 40% below the experiment. Times after 4 microseconds corresponds to incident neutron energies from 1 to .1 MeV. These neutrons contribute small amounts of neutron ionization, almost no inelastic gamma rays, and must loose considerable energy before they generate capture gamma rays. Therefore, this component of the dose is both small and difficult to calculate. The excellent agreement above 1 MeV demonstrates that the fast neutron effects in iron, polystyrene and silicon are well understood and can be accurately calculated.

The 17 meter steel-styrofoam experiment was calculated with both the forward and adjoint methods. As such, it represents not only a good
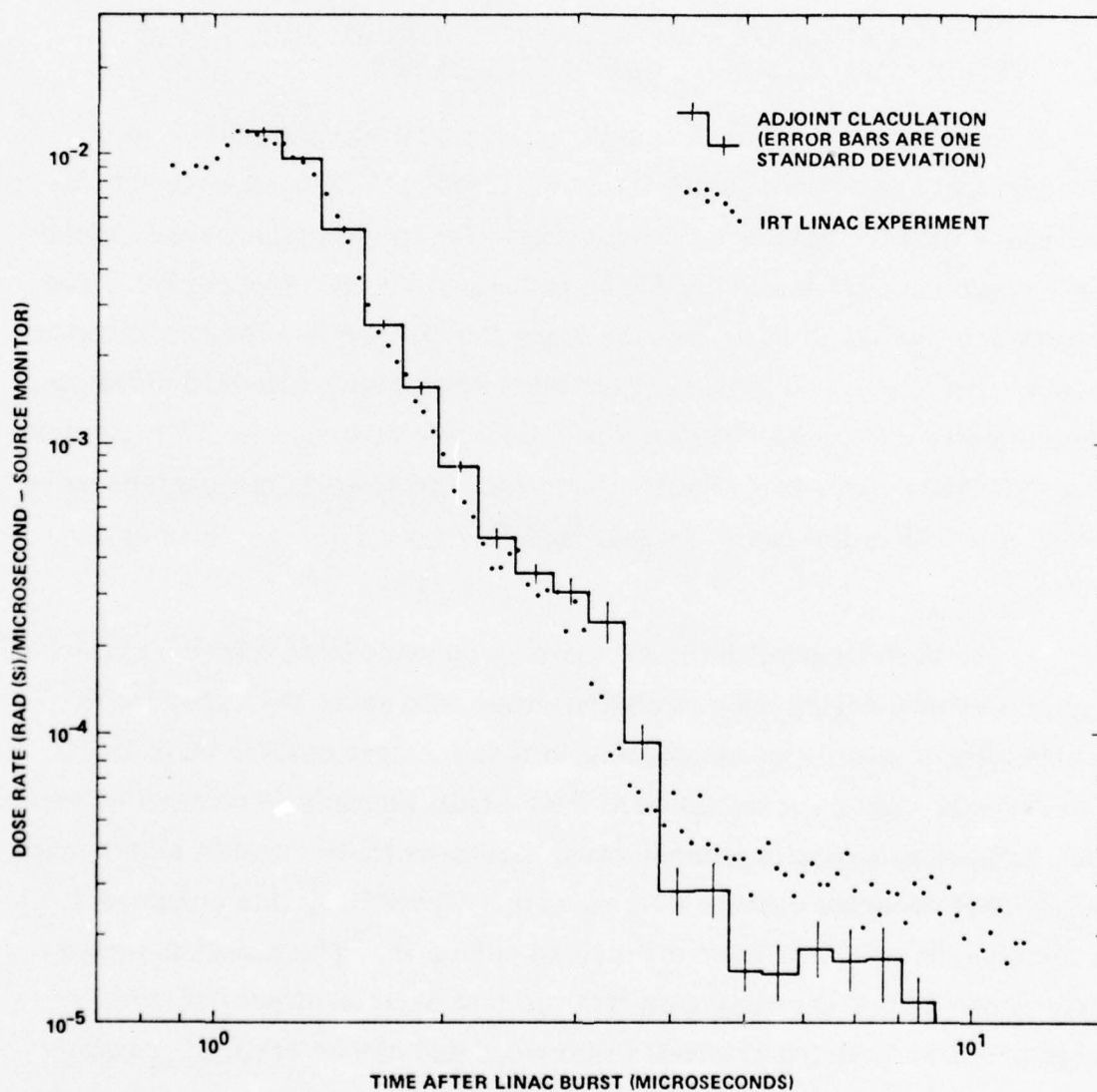
Figure 7. Comparison of the 53 Meter Steel-Styrofoam Adjoint
Calculation With the IRT Linac Experiment

74

compairson between experiment and calculation but also an excellent comparison of two calculational techniques. Both calculations used very little Russian roulette or splitting as the primary history termination was escape. For the forward calculation 48,000 histories were tracked in 8.73 minutes on a CDC 7600 computer with an average of eleven scatterings per history. The adjoint calculation tracked 80,000 histories in 12.15 minutes on the same computer with splitting and Russian roulette parameter set so that 10% of the particles split and 50% were killed by Russian roulette.

Figure 8 compares the forward and adjoint 17 meter calculations with the experiment. Usually comparisons of forward and adjoint Monte Carlo calculations are not time dependent. As such, the only possible comparison is between the two total doses, two single numbers that may be dominated by special aspects of the transport and therefore not representative of the entire calculations. The time dependent results presented here show the entire character of the two calculations. For instance dose before 1.3 μsec is from fast neutrons and inelastic gamma rays while the dose after 500 μsec is due to thermal capture. Between these times epithermal capture and thermal capture are both contributing dose.

Returning to the forward adjoint comparison, first notice that the forward calculation is generally lower than the adjoint results, at spots as much as 50%. This probably represents the nature of the next flight estimator in the forward calculation which tends to undersample collisions close to the dose point. In this steel-styrofoam calculation, most of the collision density occurs in the steel shell, and except for low energy neutrons, there is little scattering in the styrofoam or the dosimeter. Therefore the next flight estimator generates resonable statistics with no infinite
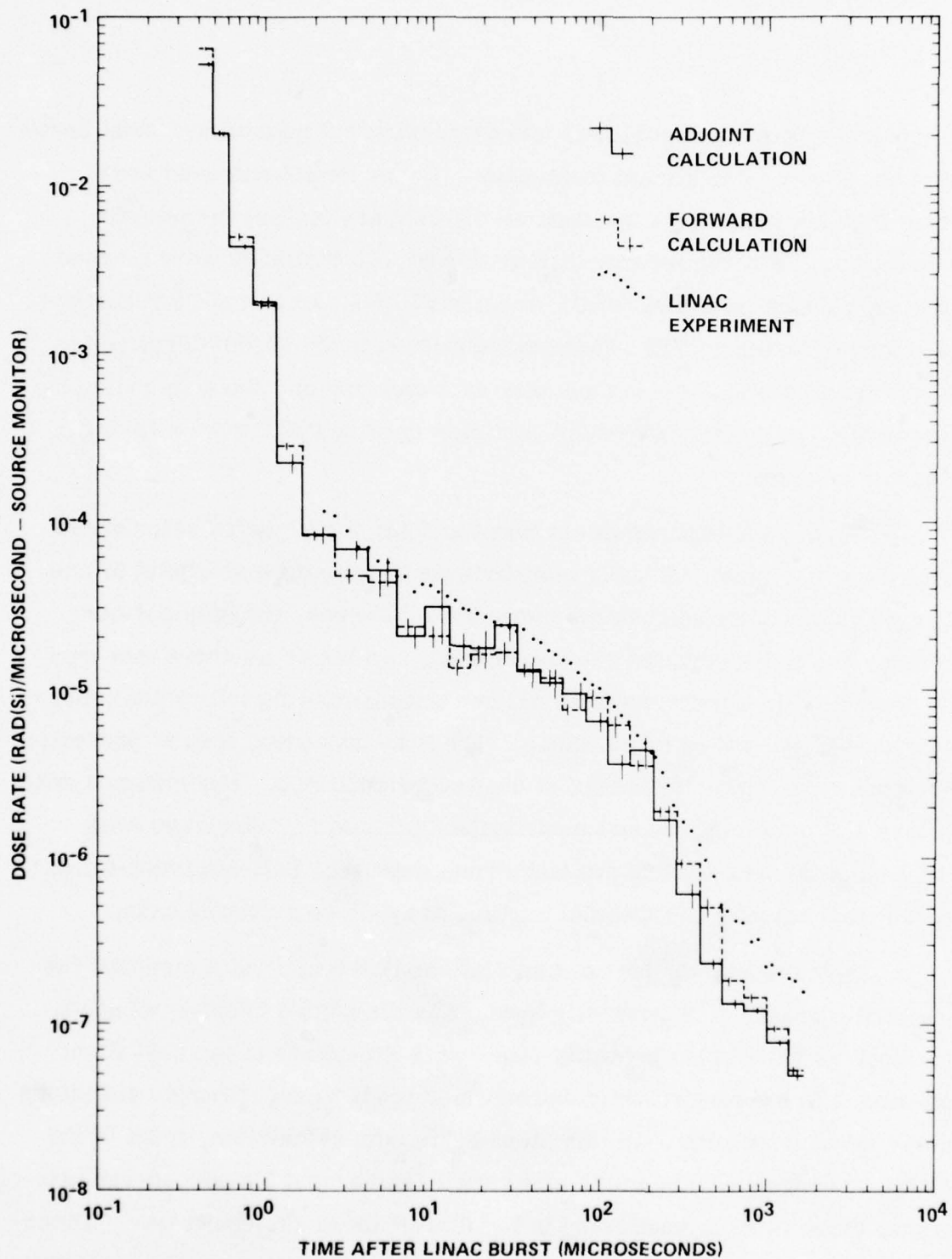
Figure 8. Comparison of the 17 Meter Steel-Styrofoam Forward
and Adjoint Calculations with the Linac Experiment

variance signs, but may still be underestimating the contribution of collisions near the dosimeter.

It is also of interest to notice the relative efficiencies of the forward and adjoint calculations. In general it is expected that a forward calculation will be more efficient when the source is small and the detector is large, and an adjoint calculation will be more efficient when the detector is small and the source is large. Thus, for the steel-styrofoam calculation, the adjoint technique might be expected to be more efficient. However, Fig. 7 shows that at times around 250 μsec the adjoint fractional standard deviation is 0.270 for 12.15 minutes of computing while the forward fsd is 0.128 for 8.73 minutes of computing. Defining a relative efficiency as $t_1(\text{fsd}_1)^2/t_2(\text{fsd}_2)^2$, the adjoint calculation would require 6.19 more computing time to calculate the same variance as the forward calculation. The explanation of this startling result lies in the estimates that are made during thermal scattering. In the forward random walk, estimates of capture gamma ray dose contributions are made from many of the thermal neutron collision sites. Since thermal collision each occurs at a different time, estimates are made to several of the time bins from a single random walk. However, in the adjoint random walk meaningful estimates cannot be made from the thermal collisions. The upscatter probabilities are such that the next flight estimation can only be made to the energy group immediately above the thermal group. Since there is no source in either this group or the thermal group, next flight estimation gives no score. The only information gained from the thermal random walk is the location and time of the eventual upscatter or escape. Once a single upscatter from the thermal group has occurred, the time will not change significantly for the rest of the history. Thus a single thermal random walk (perhaps 50 collisions) will only generate a few

scores in a few adjacent time bins (or no score at all if leakage occurs before upscattering). Clearly the general feeling regarding detector sizes and forward versus adjoint calculation efficiencies is not always true for time dependent calculations. In this case the ability of the forward next flight estimator to generate more estimates over longer times makes the forward calculation more efficient than the adjoint.

Returning to Fig. 8, notice that both the forward and the adjoint calculations are lower than the experiment. In general, the calculations are 30% lower than the experiment but at a few times they are as much as 70% lower than the experiment. Also the spectral shapes agree approximately within the statistics of the calculations.

Possible sources of this difference between experiments and calculations could result from any of the following effects:

1. Experimental normalization
2. Too much absorption or leakage in the calculations
3. Incorrect detector response to low energy neutrons
4. Incorrect capture gamma ray yields or energy spectra
5. Other calculational difficulties

Another forward calculation with slightly less absorption and a slightly harder capture gamma ray spectrum showed very little difference from the forward calculation of Fig. 8, therefore, eliminating reasons 2 and 4. Reasons 1 and 5 would be difficult to verify, but both IRT and SAI used considerable care in our procedures to eliminate such errors. The normalization of the experimental results depends on an accurate determination of the dosimeter's active volume which did prove to be a difficult experimental task. The good experiment-calculation agreement at high

energies indicates that the experimental normalization is correct. The difference was found to be reason 3), incorrect detector response to low energy neutrons. Unfortunately this fact was not found until after the Sprint missile calculations were completed and the dosimeter treatment already described was used in all the missile calculations.

4.4   IMPROVED DOSIMETER TREATMENT

The 17 meter calculations of the steel-styrofoam sample (Fig. 8) and the Sprint missile indicated that the dosimeter treatment described in Section 3.4 and tabulated in Table 5 was generating low results at late times by ignoring capture in the detector. Originally it was planned to include all effects of the detector by including it in the calculations and using a free field silicon dose response at the detector's center. This free field response was to be corrected for low energy gamma ray attenuation in the detector, thus allowing the detector to be treated as a point. This technique proved inaccurate for neutrons from 0.5 to 2 MeV where the 95 keV detector bias prevented accurate determination of a neutron ionizing response. Because of this we elected to use the measured dosimeter response at all times. In measuring the detector response to low energy neutrons IRT found no response to neutrons below 300 keV with the single exception of a gold line between 4.44 and 5.36 eV. For this reason we assumed that the 17 meter results would be dominated by capture in the steel and the styrofoam.

To test the effect of capture in the detector, a simple modification to a forward 17 meter calculation was made. As discussed in Section 4.1, scatterings inside the detector were ignored because their effect was already included in the next flight estimator contributions which assumed the dosimeter response. The modification to include capture in

the detector was to perform the next flight estimation of a capture gamma ray to the detector center for each neutron scattering in the detector which had an energy below 300 keV. In this manner the detector response to low energy neutrons was estimated in the calculations. To avoid infinite variance results, scattering within one centimeter of the detector center scored with the average value of $1/r^2$ over the sphere (in this case 3) rather than with $1/r^2$ which could be very large. The random walk of the forward 17 meter calculation was maintained so that the effect of capture in the detector would not be clouded by statistics. Figure 9 compares the two forward 17 meter steel/styrofoam calculations with and without capture in the detector with the experiment. Notice that within statistics the differences between the experiment and the calculation have vanished, the calculation and experiment agree. Thus, it appears that for the steel styrofoam sample, capture in the detector accounts for 30 to 40 percent of the late time dose. For budgeting reasons it was not possible to repeat the other calculations, including the Sprint missile calculation, but it appears this effect will explain why the calculated late time results are usually lower than the experiments.

Because the detector is thin to all energy neutrons it is possible to estimate the dosimeter low energy neutron response from the multigroup homogenized detector cross sections. The necessary equation is derived as follows: Because the detector is thin,

$$\overline{A} \, \varphi_i \, \Sigma_i^t \, \overline{\ell} \, G_i$$

is the number of gamma rays generated in the detector volume assuming φ_i is the neutron flux in group i at the detector. $\overline{A}$ and $\overline{\ell}$ are the mean projection and the mean chord length of the detector respectively so that $\overline{A} \, \overline{\ell} \equiv V$, the detector volume. Σ_i^t is the neutron macroscopic total cross section in units cm^{-1} and G_i is gamma ray generation probability given a
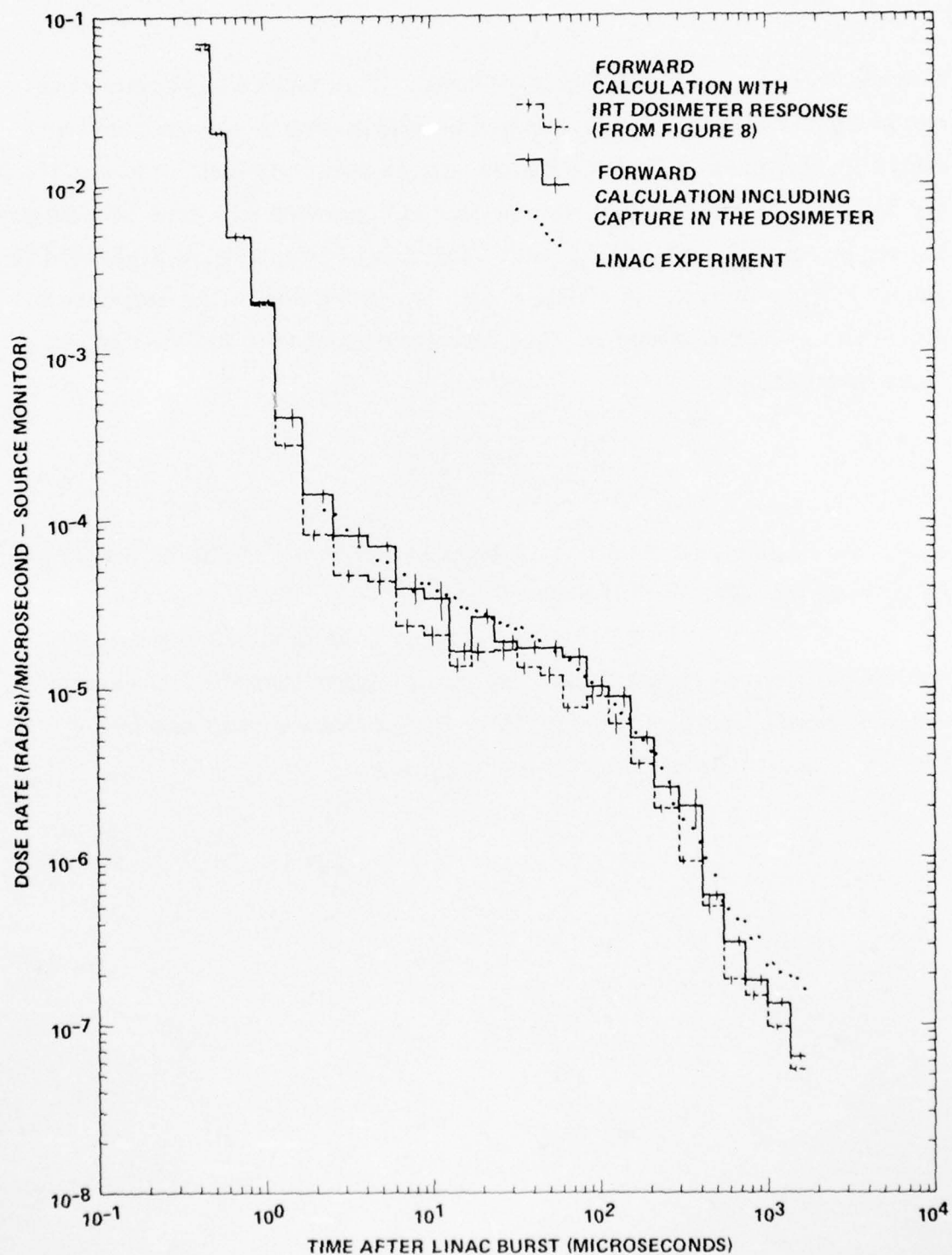
80

Figure 9. Effect of Neutron Capture in the Dosimeter. Comparison of 17 Meter Steel Styrofoam Forward Calculations with and without Neutron Capture in the Dosimeter.

81

neutron event (G_i is GAMGEN in MORSE). This source of gamma rays can be converted to a gamma ray flux by multiplying by the average track length (in this case $\bar{\ell}/2$ because the gamma source is inside the detector) divided by the volume. This gamma flux is converted to a dose by multiplying by $\bar{D}_i = \sum_j f_{ij} D_j$ where f_{ij} is the fraction of gamma rays generated in group j from neutrons in group i and D_j is the dosimeter response to a gamma ray flux in group j. The detector response to low energy neutrons thus becomes

$$R_i = \Sigma_i^t \; G_i \; \frac{\bar{\ell}}{2} \; \bar{D}_i$$

where the mean chord length $\bar{\ell}$ is given by $4V/A = 2RL/(R+L) = 1.77$ cm (A here is the total surface area of the detector). Table 16 presents Σ_i^t, G_i, $\bar{D}_i$, and R_i for all low energy neutron groups. Notice that the epithermal neutron response is considerably lower than the fast neutron response which was presented in Table 5, but that the response in the bottom three groups certainly is not negligible.

82

TABLE 16. CALCULATION OF THE DETECTOR RESPONSE TO LOW ENERGY NEUTRONS

Adjoint Neutron Group Number	Σ_i^t Total Cross Section (cm^{-1})	G_i Probability of Gamma Generation	$\bar{D}_i$ Average Dose Response of Gamma $(rad(Si)/(\gamma/cm^2))$	R_i Detector Response $(rad(Si)/(n/cm^2))$
23	.1159	1.617-1	1.136-9	1.888-11
22	.1090	3.389-2	1.132-9	3.709-12
21	.1109	6.782-2	.9130-9	6.091-12
20	.1076	6.796-2	1.085-9	7.038-13
19	.1075	3.896-3	1.058-9	3.930-13
18	.1076	2.001-3	1.00-9	1.910-13
17	.1099	4.104-3	1.00-9	4.001-13
16	.08026	2.428-3	1.251-9	2.162-13
15	.1717	3.073-3	1.163-9	5.443-13
14	.1384	1.137-3	1.076-9	1.502-13
13	.2771	4.819-4	.7545-9	8.937-14
12	.2100	7.655-4	.6432-9	9.171-14

5. CALCULATION OF THE SPRINT MISSILE EXPERIMENTS

In this chapter the real purpose of the program, that is to verify our ability to calculate internal doses in complicated three dimensional missiles, is addressed. To gain confidence in our geometry model a preliminary experiment on the autopilot was performed with the dosimeter in place and a Cs^{137} source located at eight positions around the autopilot. The first section of this chapter discusses an adjoint calculation of this experiment which shows that with one exception the geometry model of the autopilot is as accurate as was hoped. The last two sections of the chapter discusses our calculations of the Sprint missile in the linac source with the detector in the MGS and the autopilot respectively. Eight measurements of the missile were performed which were composed of two detector positions (autopilot and MGS), two flight path lengths (53.095 meters and 17.59 meters), and two missile orientations (90° and 30° off the nose). Because of budgetary consideration only five of these were calculated; these were the four high energy experiments at 53.095 meters, and only the 90° MGS experiment at 17.59 meters.

5.1 CALCULATION OF THE Cs^{137} AUTOPILOT EXPERIMENT

The Cs^{137} experiment is depicted in Fig. 10 which was supplied by IRT. The response of dosimeter inside the autopilot to a 0.662 MeV isotropic gamma ray source (Cs^{137}) was measured at each of the eight positions shown in the figure. The experimental results have fractional standard deviations less than 0.4%.
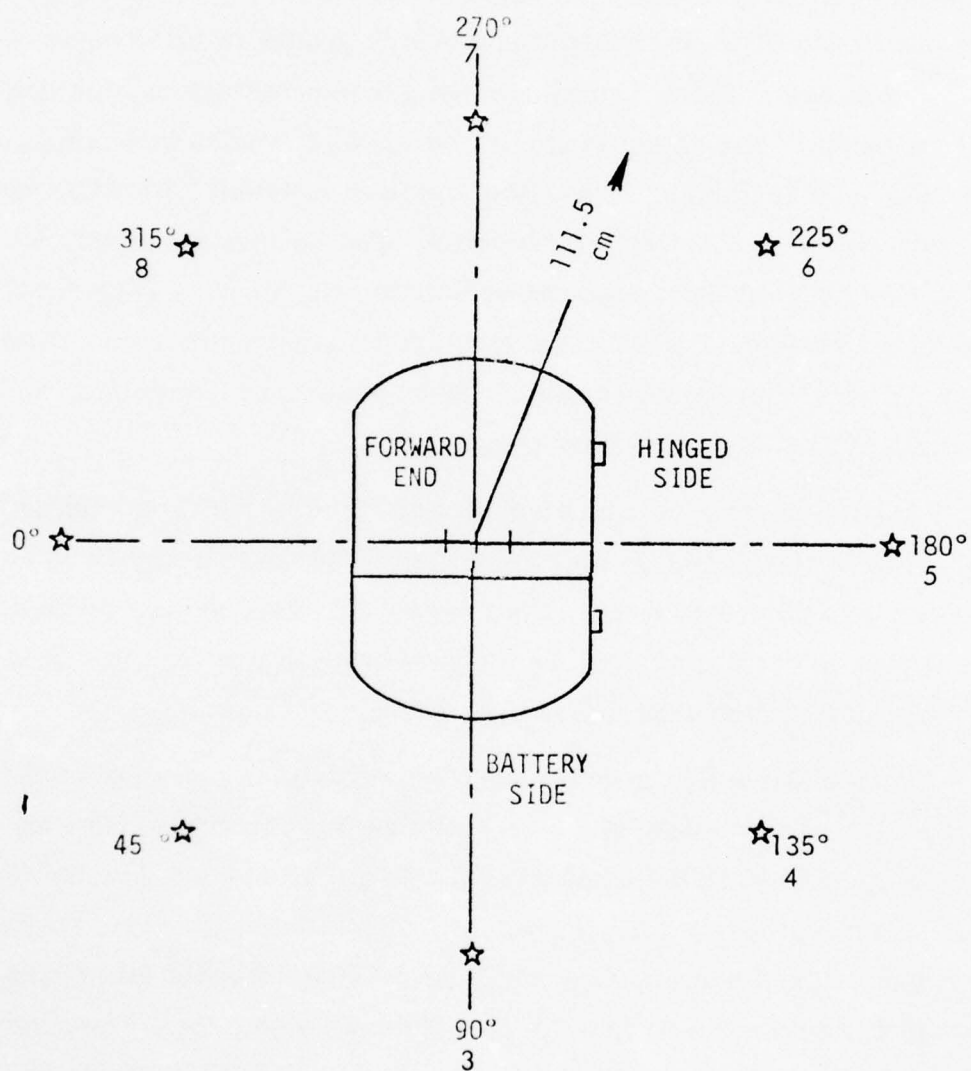
Figure 10. Configuration of the Calculation of the Sprint A/P Response to 137 Cs Gamma Rays (Not to Scale).

We were able to calculate the experiment with a single adjoint calculation which employed a next flight estimator to each of the eight source positions. The calculation used twelve groups tailored especially for Cs^{137} sources. Table 8 presents the group structure and the dosimeter response. The calculation tracked 2,000 histories in 4 minutes on the CDC 7600 computer. This slow run time resulted from eight next flight estimations in a 46 region geometry. The calculation generated 7,400 scatterings and estimated the scattered component to 10 percent fractional standard deviation. The uncollided component has no variance because both the source and dosimeter were assumed to be points, and the source energy was all in the first energy group.

Table 17 compares our calculation to the experiments. Notice that except for detectors 2 and 3, the calculation is systematically 15 to 35 percent lower than the experiment. This is probably because our homogenized model allows no streaming between components which certainly will happen with x-rays incident on real missile hardware.

Another effect that could cause the calculations to be low is that the IRT, Cs^{137} source was held in a lead shield which could cause an additional component to the source from lead backscattered gamma rays. The IRT source strength included only the 667 keV gamma rays. However, these backscattered gamma rays would have a considerably lower energy and probably could not significantly penetrate the Autopilot. The large difference between the experiment and calculation for the second source position (-y axis) indicates a mass error in one of the regions, probably region 9 (the Structural Filter). This discrepancy however was not resolved, and the geometry model as presented in Chapter 3 was used for the rest of the missile calculations.

TABLE 17. COMPARISON OF Cs 137 CALCULATION WITH EXPERIMENT

Source Position	Rad (Si)			IRT Experiment	% Difference $\frac{\text{Calc-Exp}}{\text{Exp}}$
	Uncollided**	Scattered	Total*		
1	6.71 (-16)	5.76 (-16)	12.47 (-16)	10.95 (-16)	+14
2	4.39	5.22	9.61	6.235	+54
3	4.25	5.23	9.48	4.090	+131
4	4.33	4.75	9.08	7.776	+17
5	5.86	5.34	11.20	10.78	+4
6	3.94	4.10	8.01	9.061	-11
7	3.51	3.46	6.97	7.328	-5
8	4.63	4.42	9.05	7.972	+13

*Statistics are 10-15% on the scattered contribution.
**Uncollided with no A/P present would be 1.888 (-15)

The conclusions of the Cs^{137} experiments are that within a 10 to 30 percent range caused by x-ray streaming between components, the autopilot model is accurate except for one direction. This discrepancy could be corrected with the addition of mass and/or high atomic number elements to the model in region 9. The effect of streaming between components should not affect our ability to calculate neutron and gamma ray doses as this radiation will easily penetrate individual components.

5.2   CALCULATIONS OF THE SPRINT MISSILE EXPERIMENT

Most of the details pertinent to the Sprint missile calculations have already been presented. The calculational technique was essentially the adjoint time dependent method discussed in Section 4.2. The geometry model was documented in Section 3.3 and the source and dosimeter treatments were discussed in Section 3.4. The only remaining detail is to define the source beam orientations for each of the calculations which are presented in Table 18. The adjoint next flight estimation to the beam assumed that the beam began at a point at the location to the Be photoneutron target. Rather than rotating the missile for each calculation, it was much simpler to rotate the beam. Therefore, Table 18 gives the coordinate of the source point and the z intercept of the beam center with the missile coordinates for each of the five missile calculations we performed.

Table 19 presents some of the Monte Carlo details of these calculations which were all performed on a CDC 7600 computer. Notice that each of the runs were about 10 minutes for 20,000 adjoint histories. Also notice that the 90° and 30° calculations of the same detector used exactly the same random walk, but because of estimation to different beam orientations, results and run times are different.

88

TABLE 18.   COORDINATES OF THE SOURCE BEAM
FOR THE SPRINT CALCULATION

Calculation	Source Coordinates (cm)			Z Intercept (cm)
	x	y	z	
53 AP 90°	-5309.5	0.0	136.8	136.8
53 MGS 90°	-5309.5	0.0	100.91	100.91
53 AP 30°	-2654.7	0.0	-4457.6	128.5
53 MGS 30°	-2666.7	0.0	-4490.4	128.5
17 MGS 90°	-1759.0	0.0	100.91	100.91

89

TABLE 19. MONTE CARLO DETAILS OF SPRINT MISSILE CALCULATION

Calculations	Histories	Run Time (sec)	Scatterings	Boundary Crossings	Secondaries Generated	Russian Roulette	Splittings
53 AP 90°	20,000	724	70276	230812	8876	6978	3280
53 MGS 90°	20,000	534	50477	195348	8452	6708	1516
53 AP 30°	17,000	759	59882	198305	7691	6000	2764
53 MGS 30°	20,000	567	50477	195348	8452	6708	1516
17 MGS 90°	20,000	618	57845	206564	8960	6904	2228

90

The time dependent results of these calculations are compared with the IRT experimental results in figures 11 through 15 where the vertical error bars represent one standard deviation of the calculation. Figures 11 and 12 show the 53 meter MGS results at the 90° and 30° orientations. The agreement shown here is remarkable, strongly demonstrating our ability to calculate the high energy neutron and secondary gamma ray silicon doses in missile electronics. This also demonstrates that the eleven region MGS model is certainly an accurate enough geometrical representation for missile n, γ calculations.

Figure 13 shows the results of the 17 meter MGS calculation at 90°. The results here are dominated by neutron thermalization in the missile generating secondary gamma rays from neutron capture. The results shown are consistently low in the same manner that the steel-styrofoam 17 meter calculations were low. We have already discussed that this effect is due to using a dosimeter response that neglected neutron capture in the dosimeter.

Figures 14 and 15 show the 53 meter autopilot results at the 90° and 30° orientations respectively. Here there appears to be a systematic difference. Before 2.8 μ seconds the agreement is very good, but from 2.8 μ seconds to 10 μ seconds the calculations are nearly a factor of two higher than the experiment. The cause of this discrepancy has not been determined, but it certainly could be caused by an error in the cross section mixtures. A preliminary examination of the cross section mixtures showed that an order of magnitude error in the copper density in region 45 had always existed in the model and we hoped that it was causing this difference. However, a recalculation of the autopilot at 53 meters and 90° showed nearly the same results. Therefore at this time, the source of this
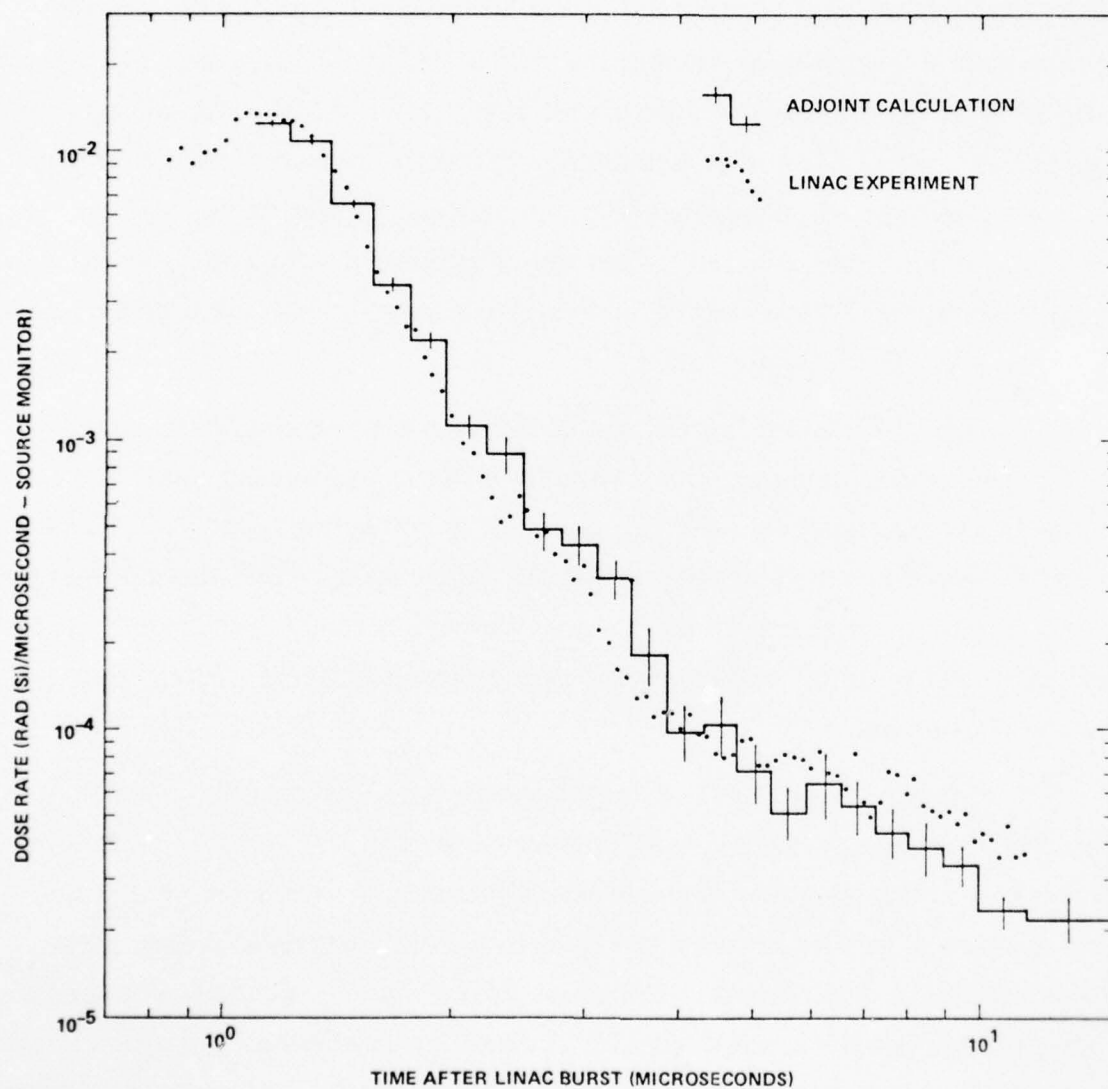
Figure 11. Comparison of the 53 Meter Missile Guidance Set Adjoint Calculation at 90° With the Linac Experiment
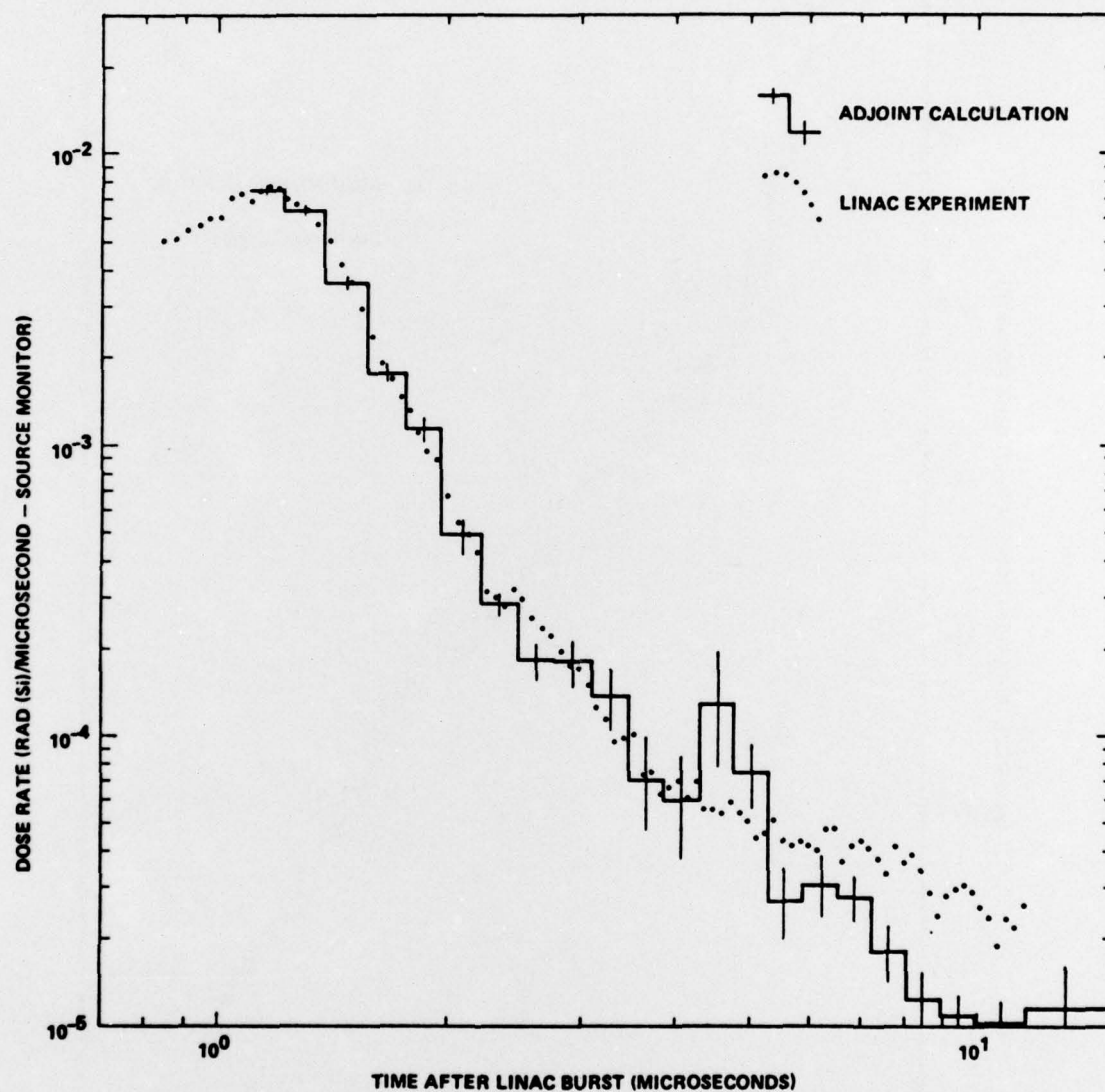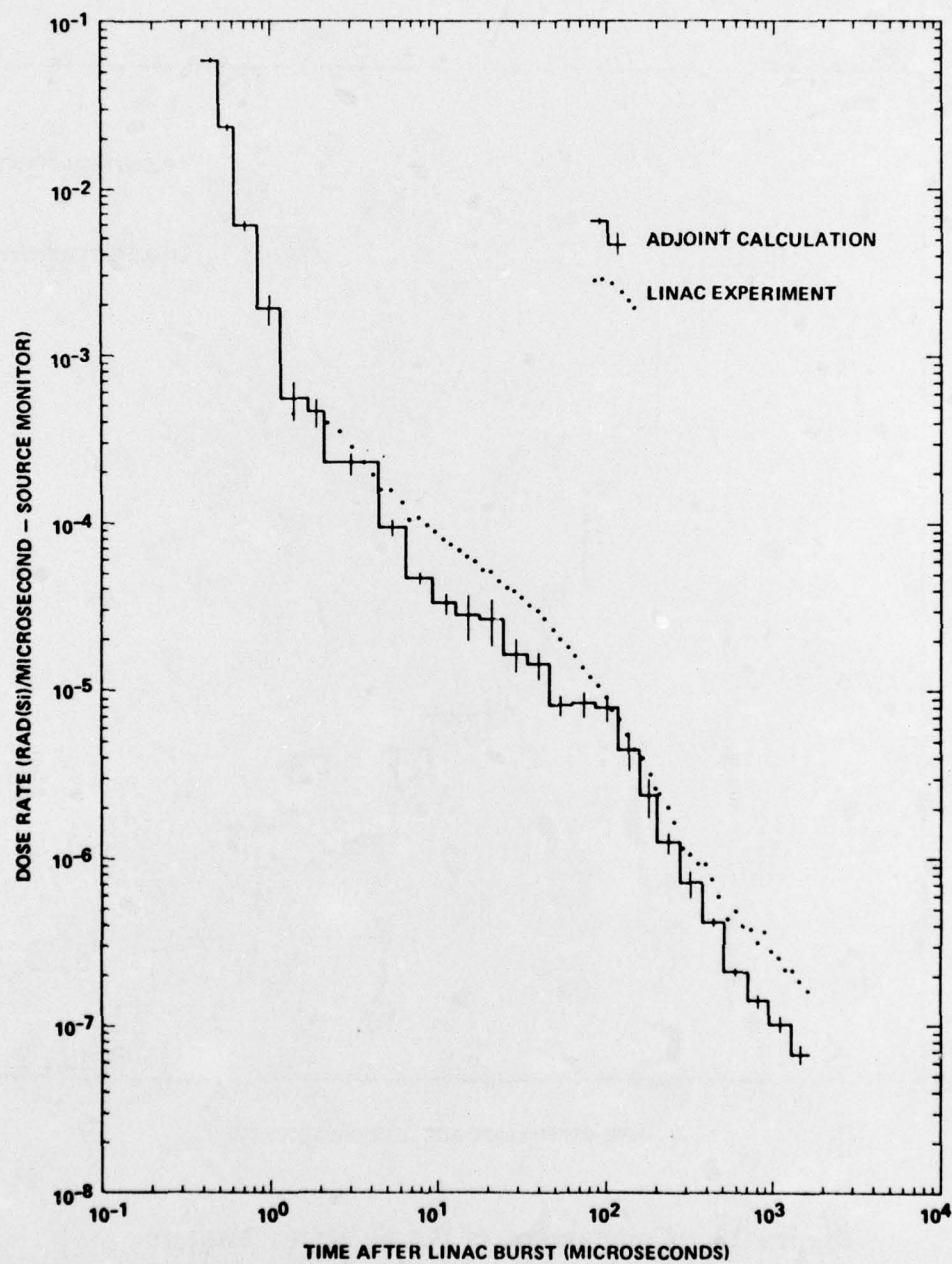
Figure 12. Comparison of the 53 Meter Missile Guidance Set Adjoint Calculation at 30° With the Linac Experiment

Figure 13. Comparison of the 17.59 Meter Missile Guidance Set
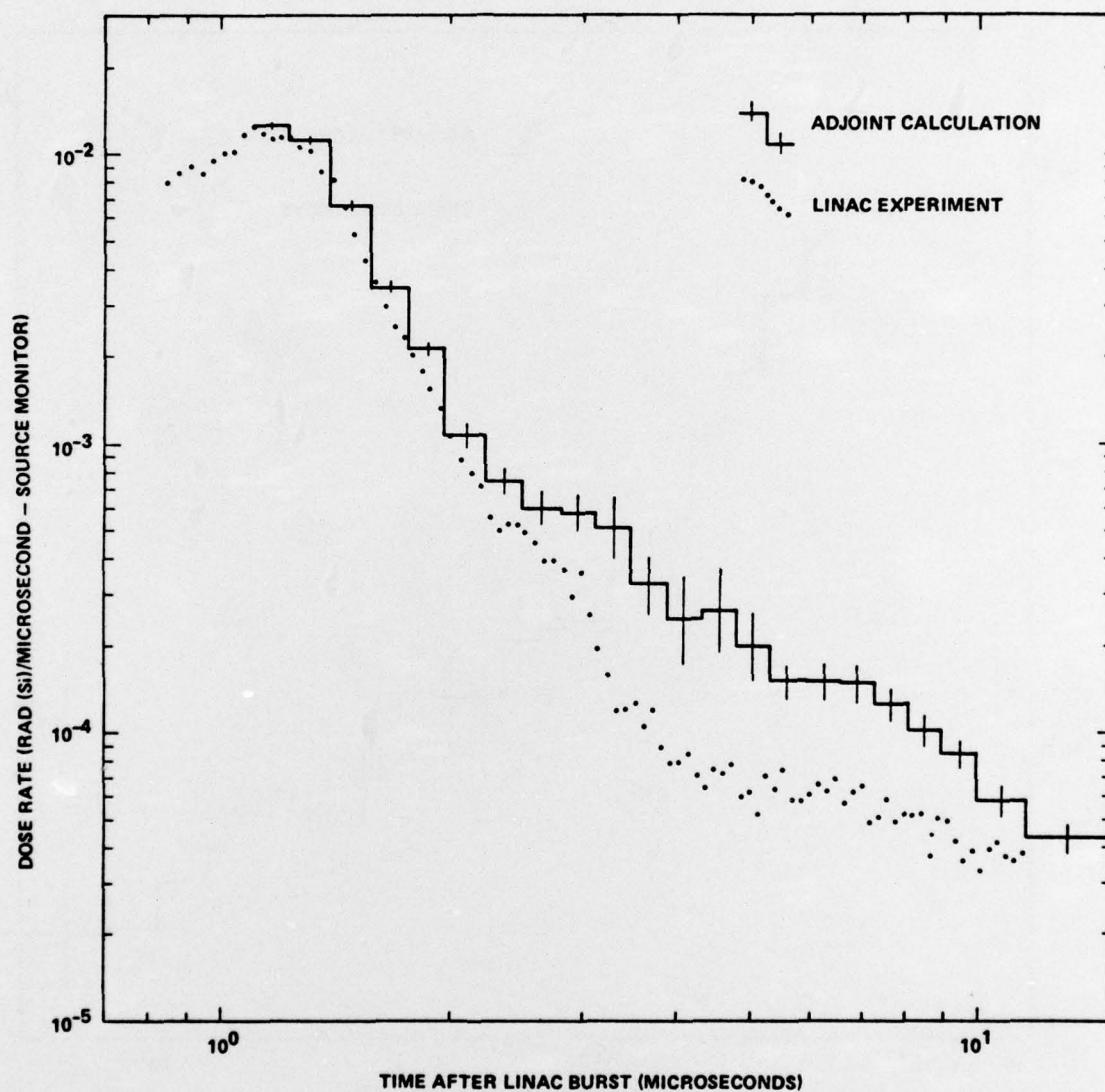Adjoint Calculation at 90° With the Linac Experiment.

94

Figure 14. Comparison of the 53 Meter Autopilot
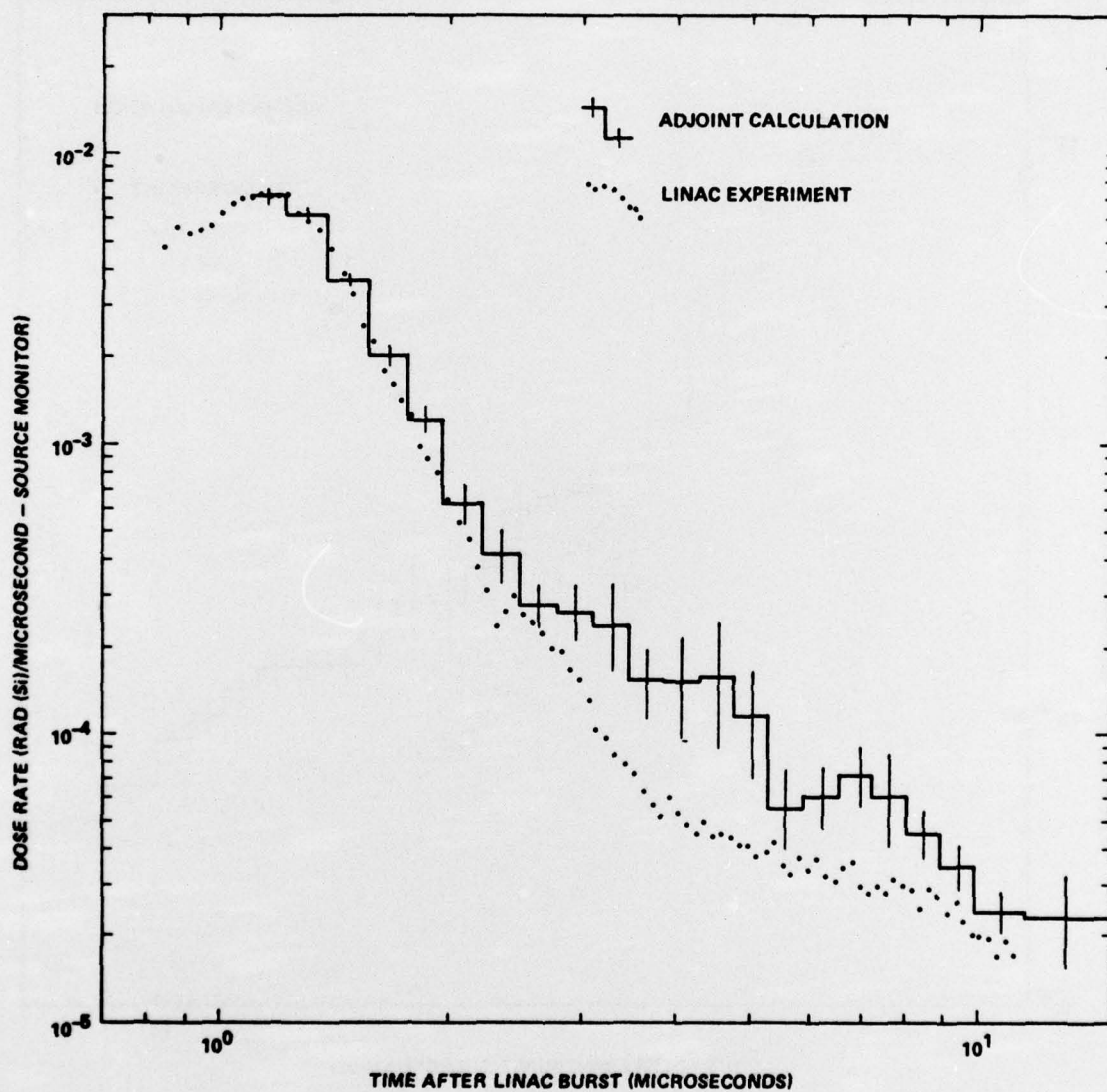Adjoint Calculation at 90° with the
Linac Experiment

Figure 15. Comparison of the 53 Meter Autopilot
Adjoint Calculation at 30° with the
Linac Experiment

difference is not known. However it is clear that this difference would only make a small change in any calculation of the total neutron induced missile dose which is dominated by both high and low energy neutrons. Neutrons in the range from 10 keV to 1 MeV which are causing this difference have the least affect on total dose.

Several conclusions can be drawn from these calculations. First, the silicon dose for high energy neutrons is accurately calculated in all cases. Second, the eleven region MGS model gives better agreement with experiment than the 46 region autopilot model. This indicates that the eleven regions are certainly adequate and that perhaps by going to greater detail we have introduced errors in the model. Third, both the MGS and autopilot results are similar, both in magnitude and shape of the time dependent results. This could mean that the effects of the various elements average out and that in fact reasonable estimates of internal doses could be made without as detailed geometrical modeling. These conclusions will be discussed further in the final chapter.

6. CONCLUSIONS

Overall this joint experimental-calculational program has been successful in demonstrating that missile doses generated by incident neutrons including the effects of inelastic and capture gamma rays can be accurately calculated with existing Monte Carlo techniques, cross sections and missile models. Also many of the trends shown in the program indicate that these same doses may be reasonably estimated with simpler, less expensive techniques. For example the similarity of the results from the MGS, the autopilot and the steel-styrofoam sample indicate that general sizes and average materials dominate the results rather than individual immediate components which are very different for each calculation or measurement.

The initial stages of this program involved designing the steel-styrofoam sample, processing cross sections into multigroup structure and preparing the 66 region of the Sprint missile. The multigroup cross section processing proved particularly difficult. As we attempted to process new cross section evaluations, modifications had to be made to our version of AMPX to correct errors which had not been previously tested. Newer cross section evaluations caused continual updating of our multigroup library especially as the newer DNA evaluations become available. This constant effort was necessary in order to assure that no differences between experiment and calculation would result from an outdated cross section set or a failure to use an available gamma-ray generation set.

The generation of the 66 region sprint model was greatly simplified by the outstanding job performed by Martin Marietta giving us their present model and documenting in great detail the regions where the experimental and flight configurations of missile differed, particularly where electronics had to be drilled out to allow insertion of the dosimeter. The fact that this program demonstrates that reasonable estimates are possible with coarser modeling could save funds on future assessments of internal missile doses.

The steel-styrofoam sample experiment has proved to be an excellent benchmark experiment. Good agreement between a time dependent experiment and two independent calculational techniques at all times serves to verify not only experimental techniques but also the cross sections and the calculation methods. Previous comparisons of forward and adjoint Monte Carlo calculations have verified that the two methods generate the same total dose, but this single number often is dominated by only one aspect of the transport problem. Agreement from early to late times of the forward and adjoint calculations adds considerable confidence to the relatively new adjoint Monte Carlo method.

Our technique of performing time dependent adjoint calculations discussed in Section 4.2 should be noted, as the inclusion of time and energy dependent sources in an adjoint calculation is not straightforward and involves some rather tricky code modifications. In forward Monte Carlo calculations time and energy dependent sources are generally handled by random sampling both the energy and time from the appropriate distribution. However, in adjoint Monte Carlo, scoring a time and energy dependent source requires a careful mapping of the source time and the scoring times with the source energy. Our discussion in Section 4.2 should aid other code users attempting similar problems.

The late time response of the steel-styrofoam cylinder (Figure 8) shows that the calculations are 30-50% lower than the experiment. However, inclusion in the calculation of neutron capture in the detector (Figure 9) shows excellent agreement with the experiment. Because the remainder of the calculations likewise do not include a dosimeter response to low energy neutrons, they also should be somewhat low at late time. This effect is seen in the MGS calculation at 17 meters (Figure 13).

Calculation of the eight Cs^{137} measurements on the autopilot show that for seven out of the eight orientations, the autopilot model appears accurate. The calculations are somewhat lower than the experiment, but this can be attributed to two effects. First, the autopilot model is a series of homogenizations having no streaming paths between them. In reality the autopilot contains hundreds of discrete components surrounded by low density foam allowing x-rays to scatter around the components avoiding absorption. In this manner a homogenized model will give underestimates of the dose. Second, the calculation did not include any low energy gamma rays that may have been backscattered from the lead source holder. This effect is probably negligible. In one direction the Cs^{137} experiment indicates a mass difference in the autopilot, but this discrepancy was not resolved and may be relative to the differences between the autopilot and Linac comparisons.

The actual missile calculations showed excellent agreement at the MGS for all energy neutrons and for high energy neutrons in the autopilot. For neutrons from 1.8 to .15 MeV in the autopilot, calculations were higher than the experiment. This probably was due to inaccuracies in the geometry model. The good results with the eleven region MGS, and the discrepancies with the 46 region autopilot model seems to indicate that

100

increased modeling effort does not generate more accurate dose calcula-tions, and in fact, increases the changes of an error. In spite of the dif-ference at the autopilot it must be emphasized that calculations of the total dose would still be accurate because neutrons in the range of the differences are the least important for calculating total dose.

Two final conclusions about future missile internal dose calculations can be made. First the problem we found with the dosimeter response indicates that care should be taken in the immediate region of a com-ponent whose dose is to be calculated. The best approach would be a preliminary calculation of a component response that includes its immediate region. This component response could then be used in a coarse missile model. This approach would include the detail where required, yet allow a single missile model for fast and accurate calculations. The component response might include a volume of material whose mean chord length would be approximately .2 mean free paths of 2 MeV neutrons. This is small enough that single scattering would dominate, yet large enough that capture in the immediate area would be accurately determined. The component response could be calculated by adjoint Monte Carlo with a model of the immediate region.

Finally the similarity of all the measurements and calculations of this program (steel-styrofoam, MGS and autopilot) indicate that the internal doses are governed mostly by average effects such as an average homo-genization, average size, and probably average hydrogen content. Then it should be possible to generate reasonably accurate internal neutron and gamma ray doses from the gross parameters of the missile without either generating detailed missile model or performing expensive adjoint Monte Carlo calculations.

REFERENCES

1. Thomas R. Jeter, Arthur D. Coates, and John A. Devanney, "Program 2, Operation HENRE - Part 1, Free-Field Spectral and Dose Determinations," BREL-R-1420, Oct. 1968.

2. R. L. French and L. G. Mooney, "Differential Measurements of Fast-Neutron Air-Ground Interface Effects; Project 9.2 Operation HENRE," TACOM 10590, July 15, 1969.

3. J. H. Thorngate, et al., "Energy and Angular Distribution of Neutrons and Gamma Rays - Operation BREN," CEX-62.12, Feb. 1967.

4. E. A. Straker, "Status of Neutron Transport in the Atmosphere," ORNL-TM-3065, July 29, 1970.

5. W. H. Scott, Jr., J. A. Lonergan and W. A. Woolson, "Adjoint Monte Carlo Generation of Radiation Response Functions for Complex Missiles," DNA 3197F, Aug. 1973.

6. L. Harris, Jr., H. Kendrick, Y. D. Naliboff, S. M. Sperling, "Time-Dependent Fast Neutron and Secondary Gamma Ray Spectrum Measurements in Concrete," DASA 2401 (2 Vols.), Gulf General Atomic, 1969.

7. W. H. Scott, Jr., et al., "Multigroup Analysis of Neutron and Secondary Gamma Ray Transport in Concrete," Science Applications, Inc., DNA 2994F, Dec. 1972.

8. M. O. Cohen, "Analysis of Neutron and Gamma-Ray Transport Using the SAM-CE Code," MAGI, ANS Trans., Vol. 14, No. 2 (Oct. 1971).

9. L. F. Hansen, et al., "Time Spectra from Spheres Pulsed with 14-MeV Neutrons and Their Analysis," UCRL-71124, June 1968.

10. D. K. Steinman, et al., "Time Dependent Measurements of Induced Silicon Dose Rates in a Missile Guidance System," IRT Corp., (to be published).

11.   E. A. Straker, P. N. Stevens, D. C. Irving and V. R. Cain, "The MORSE Code - A Multigroup Neutron and Gamma-Ray Monte Carlo Transport Code," ORNL-4585, Sept. 1970.

12.   E. A. Straker, W. H. Scott, Jr. and N. R. Byrn, "The MORSE Code with Combinatorial Geometry," DNA 2860T, May 1972.

13.   N. M. Greene, et al., "AMPX: A Modular Code System for Generating Coupled Multigroup Neutron-Gamma Libraries from ENDF/B," Oak Ridge National Laboratory, ORNL-TM-3706.

14.   T. Bohm, "Sprint In-Missile Radiation Experiment and Analysis Project Letter Report," Martin Marietta Corp., Orlando, FL, 74-90631-1, Aug. 20, 1974.

DISTRIBUTION LIST

DEPARTMENT OF DEFENSE

Director
Defense Advanced Rsch. Proj. Agency
    ATTN: TIO, Fred A. Koether

Defense Documentation Center
12 cy ATTN: TC

Director
Defense Intelligence Agency
    ATTN: DI-7D, Edward O'Farrell

Director
Defense Nuclear Agency
    ATTN: STSI, Archives
    ATTN: DDST
    ATTN: RATN
3 cy ATTN: STTL, Tech. Library

Commander
Field Command
    ATTN: FCPR

Director
Interservice Nuclear Weapons School
    ATTN: Tech. Lib.

Chief
Livermore Division Fld. Command, DNA
    ATTN: FCPRL

DEPARTMENT OF THE ARMY

Commander
Harry Diamond Laboratories
    ATTN: DRXDO-RBF
    ATTN: DRXDO-EM
    ATTN: DRXDO-NP
    ATTN: DRXDO-RBG

Commander
Picatinny Arsenal
    ATTN: R. Kesselman
    ATTN: ND-C-T
    ATTN: T. De Rosa

Commander
Trasana
    ATTN: R. E. Dekinder, Jr.

Director
U.S. Army Ballistic Research Labs.
    ATTN: DRXBR-AM, W. R. Vanantwerp

DEPARTMENT OF THE NAVY

Superintendent (Code 1424)
Naval Postgraduate School
    ATTN: Code 2124, Tech. Rpts. Librarian

Commander
Naval Surface Weapons Center
    ATTN: Code WX21, Tech. Lib.
    ATTN: Code WA501, Navy Nuc. Prgms. Off.
    ATTN: N. E. Schofield
    ATTN: Code WA50, John H. Malloy

DEPARTMENT OF THE NAVY (Continued)

Commanding Officer
Naval Weapons Evaluation Facility
    ATTN: J. Abbott

DEPARTMENT OF THE AIR FORCE

AF Institute of Technology, AU
    ATTN: Library AFIT, Bldg. 640, Area B
    ATTN: ENP, Charles J. Bridgman

AF Weapons Laboratory, AFSC
    ATTN: ELP, Carl E. Baum
    ATTN: DYT, Capt Ray Shulstad
    ATTN: SAS

SAMSO/DY
    ATTN: DYAE

SAMSO/MN
    ATTN: MNNH

Commander in Chief
Strategic Air Command
    ATTN: XPFS, Maj Brian G. Stephan

U.S. ENERGY RESEARCH AND DEVELOPMENT ADMINISTRATION

University of California
Lawrence Livermore Laboratory
    ATTN: Tech. Info. Dept. L-3
    ATTN: Robert Howerton, L-71
    ATTN: Auston Odell, L-531

Los Alamos Scientific Laboratory
    ATTN: Doc. Control, F. P. Young
    ATTN: Doc. Control for Donald Harris

Sandia Laboratories
Livermore Laboratory
    ATTN: Doc. Control for Tech. Library

U.S. Energy Rsch. & Dev. Admin.
    ATTN: Supervisor, Rm. 13 for Nat. Neu. Cross
        Sec., Sol Pearlstein

U.S. Energy Rsch. & Dev. Admin.
    ATTN: Doc. Control for Lester Price

U.S. Energy Rsch. & Dev. Admin.
    ATTN: Doc. Control for Phil Hemmig

Union Carbide Corporation
    ATTN: Doc. Control for Fred Mynatt
    ATTN: Doc. Con. for Rad. Shielding Ctr.
    ATTN: Doc. Control for C. E. Clifford
    ATTN: Doc. Con. for Tech. Lib.

OTHER GOVERNMENT AGENCIES

Department of Commerce
    ATTN: J. Hubell

DEPARTMENT OF DEFENSE CONTRACTORS

Aerospace Corporation
    ATTN: Library

The BDM Corporation
    ATTN: Joseph V. Braddock

General Electric Company
TEMPO-Center for Advanced Studies
    ATTN: DASIAC

Institute for Defense Analyses
    ATTN: IDA Librarian, Ruth S. Smith

IRT Corporation
    ATTN: Technical Library

Kaman Sciences Corporation
    ATTN: Frank H. Shelton

Lockheed Missiles & Space Co. Inc.
    ATTN: Technical Library

Martin Marietta Aerospace
    ATTN: Carl Napolitano

Mathematical Applications Group Inc.
    ATTN: Herb Steinberg
    ATTN: Malvin H. Kalos
    ATTN: Martin O. Cohen

McDonnell Douglas Corporation
    ATTN: Tech. Library Services

Stanford Research Institute
    ATTN: Philip J. Dolan

Systems, Science and Software, Inc.
    ATTN: Technical Library

University of Wisconsin
    ATTN: Charles W. Maynard, Professor

DEPARTMENT OF DEFENSE CONTRACTORS (Continued)

Mission Research Corporation
    ATTN: Conrad L. Longmire

R & D Associates
    ATTN: Cyrus P. Knowles
    ATTN: Harold L. Brode

Radiation Research Associates, Inc.
    ATTN: Library

Science Applications, Inc.
    ATTN: T. E. Albert

Science Applications, Inc.
    ATTN: W. W. Woolson
    ATTN: E. A. Straker
    ATTN: William H. Scott, Jr.
    ATTN: Phil A. Read
    ATTN: Dean C. Kaul
    ATTN: Ron E. Dietz